DELFT UNIVERSITY OF TECHNOLOGY

MASTER THESIS MARINE TECHNOLOGY
MT54035

Energy Storage Systems for Nuclear-Powered Vessels

Thesis report

Author:
Luuk Hulleman

Supervisors:
Dr.ir. H. Polinder (TU Delft)
ir. A. Steenhuis (Allseas)
ir. G. Berden (TU Delft)

Date of defence:
May 8, 2026

Thesis for the degree of MSc in Marine Technology in the specialization of *Marine Engineering*

Energy Storage Systems for Nuclear-Powered Vessels

By

Luuk Hulleman

Performed at

Allseas Engineering B.V.

This thesis MT.25/26.026.M is classified as confidential in accordance with the general conditions for projects performed by the TUDelft.

8th of May, 2026

Company supervisors
Responsible supervisor: ir. A.L.J. Steenhuis

Thesis exam committee
Chair/Responsible Professor: dr.ir. H. Polinder
Staff Member: Prof.dr. R. Pecnik
Staff Member: ir. G.T.A. Berden
Company Member: ir. A.L.J. Steenhuis

Author Details
Studynumber: 5300304

Abstract

The integration of nuclear propulsion into civilian maritime vessels offers a promising pathway towards low-emission, long-endurance operations, particularly for energy-intensive offshore applications.
High-Temperature Gas-Cooled Reactors (HTGRs) are well suited for such use due to their inherent safety characteristics and high thermal efficiency, but their limited load-following capability restricts their ability to directly meet the highly dynamic power demands of ships. This thesis investigates how a hybrid energy storage system (ESS), combining thermal and electrical storage, can be sized, configured, and integrated to enable safe and efficient HTGR-based maritime propulsion.

A dynamic, system-level model is developed in Python to represent the interaction between an HTGR, an intermediate molten-salt loop, a steam Rankine power cycle, auxiliary diesel generators, and hybrid energy storage. Reactor ramp-rate constraints, thermal inertia, turbine efficiency limits, and storage charge–discharge constraints are modelled. A 14-day operational load profile of the deep-sea mining vessel Hidden Gem is used as a case study to quantify power mismatches and storage requirements. A comprehensive sizing study is performed for a range of thermal and electrical storage capacities, evaluating feasibility based on unmet load, dumped energy, diesel fuel consumption, and operational stability.

The results demonstrate that a hybrid ESS substantially improves operational flexibility, eliminates unmet load across feasible configurations, and reduces diesel fuel consumption compared to a non-storage baseline. Thermal storage primarily buffers medium-timescale reactor ramp limitations, while electrical storage absorbs fast transients and residual mismatches. The findings highlight that optimal ESS sizing strongly depends on the temporal structure of the ship's load profile, rather than peak demand alone, and provide a structured methodology for hybrid ESS integration in future nuclear-powered vessels.

AI Statement
For this report for the course MT MSc Thesis (MT54035) I have used Generative AI to:

- Create (part of) the code in Python for solving the problem
- Obtain inspiration for the overall structure of the report
- Improve the grammar, style, layout, and/or spelling of the text

In all cases I have reviewed and corrected the work and remain fully responsible for the content of the report.

Contents

List of Figures

List of Tables

Nomenclature

ABS American Bureau of Shipping
AC Alternating Current

BESS Battery Energy Storage System
BMS Battery Management System
BOP Balance of Plant

CFP Coated Fuel Particle

DC Direct Current
DG Diesel Generator
DNV Det Norske Veritas
DOE United States Department of Energy
DP Dynamic Positioning

EES Electrical Energy Storage
EMA Exponential Moving Average
EMSA European Maritime Safety Agency
ESS Energy Storage System

FBP Fixed Burnable Poison
FIMA Fissions of Initial Metal Atom

HTF Heat Transfer Fluid
HTGR High-Temperature Gas-Cooled Reactor
HTR-PM High-Temperature Gas-Cooled Reactor Pebble-Bed Module
HVAC Heating, Ventilation and Air Conditioning
HX Heat Exchanger

IAEA International Atomic Energy Agency
IEC International Electrotechnical Commission
IMO International Maritime Organization
INL Idaho National Laboratory

KAIST Korea Advanced Institute of Science and Technology

LP Load Profile

LWR Light Water Reactor

MCR Maximum Continuous Rating
MS Molten Salt
MSR Molten Salt Reactor

NEA Nuclear Energy Agency (OECD)
NFPA National Fire Protection Association
NGNP Next Generation Nuclear Plant
NMC Nickel Manganese Cobalt
NTU Number of Transfer Units

OECD Organisation for Economic Co-operation and Development

PC Power Cycle
PWR Pressurized Water Reactor
PyC Pyrolytic Carbon

ROT Reactor Outlet Temperature

SEM Ship Energy Management
SFC Specific Fuel Consumption
SiC Silicon Carbide
SMA Simple Moving Average
SMR Small Modular Reactor
SOC State of Charge
SOLAS International Convention for the Safety of Life at Sea
SSG-30 IAEA Safety Guide on Structures, Systems and Components
SSG-34 IAEA Safety Guide on Electrical Power Systems

TES Thermal Energy Storage
TRISO TRi-structural ISOtropic

UA Overall Heat Transfer Coefficient

List of Symbols

Symbol	Unit	Description
k	–	Discrete simulation time index
Δt	s	Simulation time step
τ	s	Time constant of exponential moving average HTGR
τ_{trend}	s	Diesel trend filter time constant
P_{load}	kW	Ship electrical load demand
P_{set}	kW	Electrical reactor power setpoint
P_{gross}	kW	Gross electrical power output of power cycle
$P_{\text{pc,out}}$	kW	Net electrical power output of power cycle
P_{DG}	kW	Total diesel generator power output
$P_{\text{DG},i}$	kW	Power output of diesel generator unit i
P_{gap}	kW	Residual power mismatch after generation
$P_{\text{batt,net}}$	kW	Net battery power exchanged with ship grid
P_{unmet}	kW	Unmet electrical power after ESS action
P_{sys}	kW	Auxiliary electrical power consumption of the system
Q_{set}	kW_{th}	Reactor thermal power setpoint
Q_{out}	kW_{th}	Reactor thermal power output
Q_{pc}	kW_{th}	Thermal power delivered to power cycle
Q_{dump}	kW_{th}	Dumped thermal power
Q_{req}	kW_{th}	Requested thermal power
$Q_{\text{c,req}}$, $Q_{\text{d,req}}$	kW_{th}	TES charge and discharge requests
$Q_{\text{c,real}}$, $Q_{\text{d,real}}$	kW_{th}	Actual TES charge and discharge power
$Q_{\text{TES,net}}$	kW_{th}	Net thermal contribution of TES
$E_{\text{cap,e}}$	kWh_{e}	Electrical energy storage capacity
$E_{\text{cap,th}}$	kWh_{th}	Thermal energy storage capacity
E_{del}	kWh_{th}	Deliverable thermal energy in TES
E_k	kWh_{e}	Electrical energy stored at time step k
SOC_{e}	–	Electrical energy storage state of charge
SOC_{th}	–	Thermal energy storage state of charge
SOC_{min}, SOC_{max}	–	Minimum and maximum allowed SOC
η_{thermo}	–	Thermal-to-electric conversion efficiency
η	–	Generic efficiency
η_{base}, η_{diff}	–	Battery efficiency parameters
γ	%/min	Maximum reactor ramp rate
γ_{pc}	%/min	Power-cycle ramp-rate limit
γ_{DG}	%/min	Diesel generator ramp-rate limit
ΔP	kW_{e}	Change in electrical power per time step
ΔQ	kW_{th}	Change in thermal power per time step
T_{hot}, T_{cold}	°C	TES hot and cold tank temperatures
$T_{\text{hot,in}}$, $T_{\text{cold,in}}$	°C	Heat-exchanger inlet temperatures
T_{amb}	°C	Ambient temperature
ΔT_{min}	°C	Minimum pinch temperature difference
$\dot{m}$	kg/s	Mass-flow rate
$\dot{m}_{\text{max}}$	kg/s	Maximum allowable mass-flow rate
m_{hot}, m_{cold}	kg	Hot and cold TES salt inventory
$c_p(T)$	kJ/kgK	Specific heat capacity
$\rho(T)$	kg/m^3	Density
UA	MW/K	Overall heat-transfer conductance

Symbol	Unit	Description
ε	–	Heat-exchanger effectiveness
NTU	–	Number of transfer units
SFC	g/kWh	Specific fuel consumption
$\dot{m}_{\text{fuel}}$	kg/h	Diesel fuel mass-flow rate
Δm_{fuel}	kg	Fuel consumed per time step

1
Introduction

1.1. Background

Maritime transport is undergoing a transformation as the sector seeks to reduce emissions, improve operational efficiency, and meet more strict regulatory demands. Nuclear propulsion has re-emerged as a potential solution for large, energy-intensive vessels due to its capacity to provide long-endurance, zero-emission operation [1]. Among advanced reactor technologies, the High-Temperature Gas-Cooled Reactor (HTGR) is regarded as a promising candidate for maritime deployment. Its passive safety characteristics, high outlet temperatures, compact modular design, and favourable thermodynamic efficiency make it particularly attractive for civilian applications at sea [2].

The HTGR operates with helium coolant and graphite moderation, enabling reactor outlet temperatures above 750 °C and, in advanced designs, approaching 950 °C [3]. Such high temperatures enable efficient electricity generation and support secondary applications such as hydrogen production. Unlike conventional pressurised water reactors, the HTGR benefits from strong negative temperature coefficients and inherently safe fuel forms, such as TRISO-coated particles. These design features reduce the reliance on active safety systems and provide robustness against loss-of-coolant and reactivity transients [4, 5].

Despite these advantages, the integration of HTGRs into marine platforms presents distinctive operational challenges. Ship load profiles are highly dynamic, characterised by rapid power fluctuations driven by propulsion manoeuvres, station-keeping, mission-specific equipment, and environmental variations. These fluctuations often exceed the permissible ramp rates and thermal response capabilities of an HTGR. The reactor's thermal inertia, fuel temperature gradients, and xenon dynamics constrain how quickly its power output may be adjusted without compromising safety. As a result, an HTGR cannot directly follow the fast-varying electrical load of most vessels [6, 7, 8].

Energy storage systems (ESS) offer a solution by decoupling the reactor's stable thermal output from the ship's variable electrical demand. Appropriate storage integration enables the reactor to operate near optimal conditions while the ESS absorbs or supplies power during fast transients [9, 10]. The combination of storage technologies, configured in a hybrid architecture, has the potential to overcome the operational mismatch between the reactor and the maritime load demand. This thesis investigates how such a hybrid ESS can be designed, sized, and integrated with a helium-cooled HTGR to support nuclear propulsion on a deep-sea mining vessel.

Nuclear propulsion at sea is not a new concept. Since the 1950s, nuclear reactors have powered military submarines, aircraft carriers, Russian icebreakers and a hand full of other civilian vessels, demonstrating the operational feasibility and strategic advantages of reactor-based propulsion. Vessels such as the USS *Nautilus* and the Soviet icebreaker *Lenin* illustrated that nuclear energy enables long-endurance missions, high power output, and independence from conventional refuelling, particularly in remote or demanding environments [11, 12].

Civilian applications have also been explored, including the Nuclear Ship (NS) *Savannah*, the NS *Otto Hahn*, and the NS *Mutsu*. Although these ships demonstrated the technical viability of maritime nuclear propulsion, economic and regulatory challenges—such as high capital cost, port-access restrictions, and public concern—limited their commercial success. The use of low-enriched uranium in civilian reactors, required for non-proliferation, further constrained reactor endurance compared with military systems [13, 14].

These historical examples highlight that while nuclear propulsion offers significant operational benefits, its adoption in the commercial sector has been hindered by safety perception, regulatory barriers, and limited

economic competitiveness. Modern reactor concepts, particularly inherently safe Small Modular Reactors such as HTGRs, are being developed to address precisely these obstacles. Their passive safety features, benign coolants, and modular architecture aim to make civilian maritime nuclear propulsion both safer and more economically viable than earlier designs [15].

1.2. Relevance

The relevance of this research is both societal and scientific.

From a societal perspective, large offshore and deep-sea operations increasingly demand reliable, emission-free energy sources [1]. Vessels such as deep-sea mining ships, heavy-lift construction vessels, and specialised offshore platforms operate far from shore for extended periods and exhibit some of the highest power consumption profiles in the maritime sector [15]. For these vessels, conventional fossil-fuel propulsion faces growing environmental, economic, and regulatory pressure [12]. HTGR-based propulsion offers a potential pathway towards sustainable long-duration maritime operations with reduced emissions and enhanced energy autonomy [2].

Scientifically, the integration of HTGRs with hybrid energy storage systems in a marine context remains a largely unexplored domain. Existing literature addresses nuclear–storage integration for land-based power plants, but little work has been done on the specific constraints of shipboard environments, such as limited space, strict safety requirements, sloshing effects, and highly variable load profiles [9, 16, 17]. Furthermore, the dynamic interaction between different types of storage systems, when coupled to a reactor with strong inherent ramp limitations, has not been comprehensively analysed for maritime applications. This thesis therefore contributes new insights to hybrid nuclear–storage energy systems and provides a methodology applicable to future marine propulsion architectures [1, 10].

1.3. Allseas

Allseas is a global offshore engineering contractor specialising in complex marine operations, including heavy-lift construction, subsea installation, and deep-sea mining. The company operates large, highly specialised vessels that require sustained high power over long missions, often far from shore and under strongly variable operating conditions. These characteristics lead to high fuel consumption, complex logistics, and increasing regulatory and economic pressure related to emissions.

As part of its long-term innovation strategy, Allseas is investigating alternative propulsion and power-generation concepts that can deliver reliable, high-capacity energy with reduced emissions and improved operational autonomy. Nuclear propulsion has been identified as a promising option for energy-intensive vessels such as deep-sea mining ships. Within this context, Allseas has selected a High-Temperature Gas-Cooled Reactor (HTGR) as the reference reactor concept for future maritime applications, based on its inherent safety features, high outlet temperature, and suitability for long-duration operation.

Several key architectural choices were defined prior to this research and form fixed boundary conditions for the present study. The HTGR is assumed to operate with an intermediate molten-salt loop to provide radiological separation, prevent water ingress into the primary helium circuit, and introduce thermal buffering. Electrical power is generated using a steam Rankine cycle with load-dependent efficiency and limited ramping capability. Conventional diesel generators are retained as auxiliary power sources for prolonged high-load operation or contingency scenarios.

The case study vessel used in this thesis is the *Hidden Gem*, a deep-sea mining vessel operated by Allseas. A representative 14-day load profile is used to characterise power demand during transit, riser assembly, and mining operations[18]. Within this predefined system architecture, the aim of this thesis is not to redesign the primary power plant, but to investigate how thermal and electrical energy storage systems can be integrated to improve operational flexibility, reduce diesel usage, and enable safe and efficient load following.

1.4. Research questions

The initial literature review led to the formulation of the following main research question:

How can a hybrid energy storage system be sized, configured, and integrated with a high-temperature gas-cooled reactor to enable safe, efficient, and economically viable operation of a nuclear-powered vessel under dynamically varying maritime load conditions?

This question was addressed through the following four literature review sub-questions:

1: What are the main operational characteristics of a helium-cooled HTGR?

2: Which energy storage technologies are most suitable for integration with an HTGR?

3: How can an ESS be integrated with an HTGR within a maritime environment?

4: What improvements arise from combining an ESS with an HTGR in maritime applications?

Based on the outcomes of the literature review and identification of research gaps, the following research questions were formulated for the modelling and analysis phase:

1: How can a dynamic model of ship load profiles and HTGR operational constraints be developed to quantify power mismatches and inform hybrid ESS sizing requirements?

2: Which technical and operational characteristics of hybrid ESS components are required for a feasible system design in HTGR-powered maritime applications?

3: How can thermal and electrical storage subsystems be managed in a hybrid ESS while maintaining HTGR safety and operational stability?

4: Which sizes of hybrid ESS can balance performance, safety, and cost?

5: What is the most effective configuration of different storage layers for maritime nuclear propulsion, based on load demand and operational constraints in the selected case study?

1.5. Methodology

The methodology adopted in this thesis consists of four major components.

First, a comprehensive literature review was conducted to examine the operational behaviour of HTGRs, the characteristics of maritime load profiles, and the suitability of various electrical, thermal, chemical, and mechanical energy storage technologies. This formed the basis for identifying the most promising ESS candidates and defining the core research gaps.

Second, a dynamic system model was developed to represent the interaction between the HTGR, an intermediate molten-salt loop, the power conversion unit, diesel generators, and multiple energy storage subsystems. Physics-based constraints, including reactor ramp-rate limitations, thermal inertia, heat exchanger performance, and ESS charge–discharge limits, were implemented to ensure realistic system behaviour.

Third, hybrid ESS architectures combining thermal and electrical storage were designed and integrated into the model. Control strategies for storage dispatch, state-of-charge management, and reactor setpoint adjusting were implemented to ensure safe and efficient operation under varying load conditions.

Finally, a sizing study was conducted using the case study vessel *Hidden Gem*, applying both the originally created load profile and adjusted profiles representing different operational and weather conditions. Parameter sweeps across TES and EES sizes were performed to determine feasible configurations, assess dumped energy, reduce diesel consumption, and avoid power deficits. The performance of each configuration was evaluated to identify which combination of storages would be effective to meet the load demand.

1.6. Scope and Limitations

This thesis focuses on the integration of a hybrid thermal and electrical energy storage system with a helium-cooled High-Temperature Gas-Cooled Reactor for maritime propulsion. The scope of the research is defined by the specific technical, operational, and modelling boundaries adopted throughout the work.

The analysis is centred on a single case study vessel, the *Hidden Gem*, whose 14-day operational load profile forms the basis for the power-mismatch assessment and subsequent sizing of the hybrid ESS. The reactor model reflects the operational principles and physical constraints of a pebble-bed HTGR but does not represent a fully detailed neutronic or thermo-hydraulic simulation. Instead, it employs lumped-parameter approximations for ramp-rate behaviour, thermal inertia, and reactivity feedback in order to capture system-level dynamics with computational efficiency. Similarly, the intermediate molten-salt loop and thermal storage subsystems are modelled using simplified heat-exchanger formulations, fixed approach temperatures, and constant overall heat-transfer coefficients. These assumptions ensure tractability over long-duration simulations but omit spatial temperature gradients, flow distribution effects, and degradation phenomena such as salt ageing or fouling.

The electrical energy storage system is treated using a first-order energy balance model with simplified voltage–SOC behaviour and linear charge–discharge efficiencies. Battery thermal effects, ageing mechanisms, and cell-level electrochemistry are not considered. Mechanical, chemical, and hydrogen-based storage technologies are included only in the literature review and are not modelled dynamically. Furthermore, the diesel generators are represented using generic specific-fuel-consumption curves rather than manufacturer-specific engine maps.

Operational conditions are constrained to the available load profile and several deterministically scaled variants representing heavier or milder fluctuations. Weather-induced variability, sea-state effects, or stochastic operational uncertainties are not modelled probabilistically. The case study reflects continuous normal operation; emergency scenarios, accident conditions, fault propagation, and nuclear safety case development are outside the scope of this work.

The economic evaluation of the ESS is limited to relative weight, volume, and cost indicators derived from literature values. A full techno-economic optimisation—including lifecycle cost, maintenance, infrastructure, or port-access implications—is beyond the present scope. Regulatory considerations, classification requirements, and licensing aspects are discussed qualitatively but are not formally analysed.

Overall, the thesis provides a system-level investigation of hybrid ESS integration with an HTGR under realistic maritime load conditions, while acknowledging that several detailed physical, economic, and regulatory aspects remain outside the scope due to their complexity or the absence of publicly available data. These limitations define clear opportunities for future research while ensuring that the present work remains focused on the core objective of hybrid ESS sizing and integration for maritime nuclear propulsion.

1.7. Thesis structure

This thesis is structured as follows:

- **Chapter 2** presents an extensive summary of the literature review on HTGR fundamentals, energy storage technologies, and integration considerations for maritime nuclear applications.
- **Chapter 3** introduces the case study vessel, analyses its load profile, and identifies the resulting power-mismatch challenges after discussing the modelled power producing systems.
- **Chapter 4** describes the development of the dynamic system model with the hybrid ESS subsystems.
- **Chapter 5** presents the ESS sizing study, evaluates performance for multiple load profiles, and identifies feasible storage configurations.
- **Chapter 6** discusses the implications of the results, the limitations of the methodology, and the relation of findings to broader system design considerations. It also provides the main conclusions of the research and offers recommendations for future work.

2

Literature review

This chapter discusses the literature relevant for this research. It considers High Temperature Gas-Cooled Reactors, Energy Storage Systems and nuclear powered vessels. The review is aimed to combine these topics and inform on how to use the ESS to support HTGR operation on a ship.

2.1. High Temperature Gas-Cooled Reactors (HTGRs)

To know how HTGRs are operated and what their strong and weak points are, this section looks into the fundamentals of the HTGR and its operational characteristics. The choice for a HTGR is made by Allseas, this section will implicitly explore the reasoning behind this choice by assessing the strong and weak points of this type of reactor.

2.1.1. HTGR fundamentals

High Temperature Gas-Cooled Reactors (HTGRs), a Generation IV design, target higher efficiency, versatile heat applications, and enhanced passive safety. A HTGR, also referred to as a Very High Temperature Reactor (VHTR) in advanced concepts, supplies heat of up to 950 °C for diverse industrial processes[2, 4]. This significantly exceeds the output of common PWRs (approximately 300 °C), thereby improving thermal efficiency and enabling broader industrial applications [19]. These high temperatures are achieved by using a special fuel assembly, helium gas as a coolant, and graphite as a moderator. The VHTR concept aims for an initial reactor outlet temperature (ROT) of 750 °C, increasing to 900–950 °C for subsequent units [3]. Despite this very high potential, the commercial development of HTGRs has proven challenging. Major programs in Germany, the USA, the UK, and France throughout the second half of the 20th century failed to produce a commercially but mainly economically viable design [20].

All currently planned HTGRs utilise unique coated fuel particles (CFPs), which are small kernels of fissile material (e.g., uranium oxide or uranium oxycarbide) coated with four layers: a porous buffer carbon, a dense inner pyrolytic carbon (PyC), silicon carbide (SiC), and a dense outer PyC layer. This multi-layer design is the fundamental reason for the fuel's demonstrated high structural integrity. These so-called TRISO particles can then be processed into hexagonal graphite blocks (prismatic type) or into spherical shells made of graphite called pebbles (pebble-bed type), with each element containing more than 10,000 of these fuel kernels [5]. These packaging materials can withstand temperatures of up to 1600 °C. This robustness enables very high burn-up rates of approximately 120 GWd/t, about three times higher than typical Light Water Reactor (LWR) fuel [2]. Developments under programs like the Next Generation Nuclear Plant (NGNP) in the United States have demonstrated TRISO fuel performing at up to 19% FIMA (Fission of Initial Metal Atoms) burn up [3]. Despite these demonstrated capabilities, operational experience has revealed potential vulnerabilities. For instance, experience from the German AVR prototype reactor suggests that under certain, poorly understood core conditions, fuel temperatures may exceed design limits, potentially leading to fuel failure and significant contamination [20, 21]. This has led to recommendations that future pebble-bed designs require gas-tight containment structures, a significant design consideration that impacts cost and safety philosophy [20].

Two different types of cores can be distinguished: the pebble-bed type and the prismatic type. These use the different variants of fuel assemblies mentioned above. The pebble-bed design allows for continuous online refuelling, reducing shutdown frequency, while the prismatic block design features an annular core configuration that improves passive decay heat conduction to the reactor vessel [3]. This research focuses on the pebble-bed type reactor, but the underlying technology is largely similar to that of the prismatic type

reactor. A key difference lies in the fuel management and heat transfer correlations, which require different modelling approaches [3]. While allowing online refuelling, pebble-bed designs face challenges such as pebble damage, graphite dust, and complex fuel handling [20]. Figure 2.1 illustrates the simplified configuration of a pebble-bed HTGR, highlighting its modular fuel arrangement.

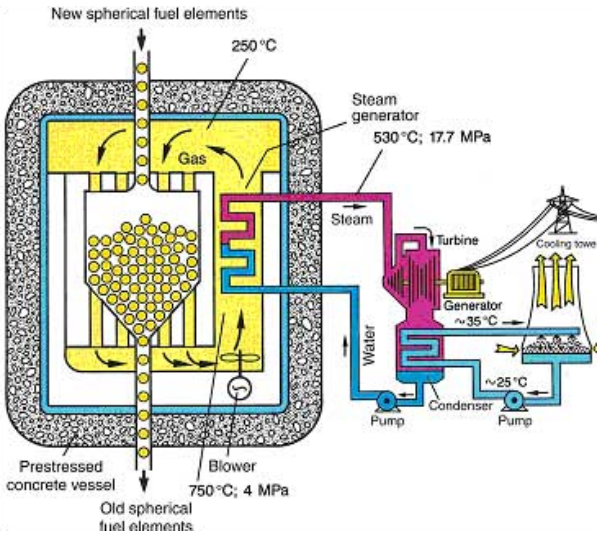

Figure 2.1: Simple version of a pebble bed HTGR [22]

The moderator in these HTGR designs is graphite, which is already included in the fuel assemblies. Graphite is chosen because it provides structural support, has a relatively low neutron absorption cross-section, and can tolerate high temperatures and radiation. This material slows down neutrons, increasing the probability that they will induce further fissions in ^{235}U and thus sustain the chain reaction. The large graphite mass also acts as a significant temporal heat sink during heat fluctuations. A challenge for modern designs is that historical graphite grades are no longer available, necessitating full characterization of new materials [3].

One important passive safety feature of HTGRs is the strong negative temperature coefficient of reactivity. As the core and fuel heat up, physical effects reduce the reactor's reactivity and therefore its power. The primary effect is Doppler broadening, a phenomenon driven by the thermal motion of ^{238}U atoms in the fuel. As the fuel temperature increases, the resonance absorption cross-section for neutrons in ^{238}U broadens, leading to increased neutron absorption and a reduction in reactivity [23]. Simultaneously, the graphite moderator contributes a negative moderator-temperature coefficient; as it heats up, it becomes less dense and less effective at slowing down neutrons, which also reduces reactivity. Together, these feedback mechanisms rapidly reduce the neutron population and thus the power if the coolant is lost or the core temperature increases. In the event of a complete loss of coolant, passive heat transfer through conduction and radiation to the reactor structures and ultimately to the environment is sufficient to remove decay heat without fuel temperatures exceeding design limits [2, 4]. This strategy is feasible due to the reactor's inherently low power density compared to LWRs [2]. The claim of "intrinsic safety" has, however, been debated. While the physics of the negative feedback is sound, the practical implementation must account for risks such as air ingress causing graphite oxidation or the dispersal of radioactive graphite dust in accident scenarios, which has led to calls for robust containment structures [20, 24]. Furthermore, the design requires a very pure helium coolant atmosphere, as the introduction of moisture or other impurities can lead to oxidation of the graphite core and corrosion issues [24].

HTGRs have been proposed as suitable candidates for merchant marine use due to their high efficiency, load-following capabilities, and waste management advantages. Their extended refuelling cycles, a characteristic of high burn up rates, can align well with the maintenance schedules of deep-sea vessels, potentially matching dry-docking with refuelling intervals and thus minimising operational downtime [1].

A critical advantage for maritime integration is the comparatively robust passive safety profile of HTGRs as already described, most important in this feature are the TRISO fuel particles which all basically act as their own containment vessels. This design makes the fuel robust to maintain structural integrity under severe accident conditions [1].

Moreover, the compact nature of HTGRs, particularly as SMRs, is advantageous for marine applications

where space and weight are constrained. Modular design enables mass production of standard reactor units for central manufacture and transportable installation. This approach draws parallels with established practices in the shipbuilding industry, such as modular engine building. This methodology has the potential to result in reduced capital expenditure, enhanced safety through standardisation, and increased flexibility. The high thermal efficiency (approximately 40-50%) achieved through high-temperature operation makes the implementation of advanced thermodynamic cycles, such as the Brayton cycle, possible. Also, these cycles are deemed suitable for both propulsion and the provision of emission-free power to onshore facilities during port stays. This enhances their operational flexibility and economic viability [1]. Achieving these cost and efficiency targets in practice remains a significant challenge, as historical and recent projects have struggled with substantial cost escalation and delays, underlining that the economic case is not yet proven [20].

Despite historical challenges, the recent successful deployment and operation of the HTR-PM pebble-bed reactor in China [25] has demonstrated the technical viability of the pebble-bed concept at a commercial scale. This achievement, however, has required significant state investment and a conservative engineering approach that includes a traditional containment structure. The economic competitiveness and export potential of the technology outside of state-driven models remain to be proven.

2.1.2. Operational Characteristics

For a nuclear-powered vessel, the reactor must not only provide steady propulsion power, but also possess the flexibility to adjust its output efficiently and safely in response to changing operational demands, such as varying ship speed or auxiliary power needs. The High-Temperature Gas-cooled Reactor (HTGR) is a promising candidate due to its inherent safety characteristics and thermodynamic efficiency. The reactor's operational behaviour, especially with respect to power manoeuvrability, is determined by a set of overlapping mechanisms that regulate power output, namely control rods, coolant flow adjustment, burnable poisons, and pebble management.

- Control rods constitute the most established method for adjusting reactor output. They contain neutron-absorbing materials, such as boron carbide (B_4C), which are inserted into the core to take up neutrons and thereby suppress reactivity and reduce power. In the case of a pebble bed reactor, the control rods can be inserted into the graphite reflectors surrounding the core [26]. While their effectiveness is evident, the implementation of these measures leads to the generation of highly localised alterations in neutron flux, this results in substantial axial and radial power distortions, as well as the occurrence of temperature gradients within the core. This may induce significant thermal stresses within fuel elements and graphite structures and makes them unsuitable for fine or continuous manoeuvring. Control rods are therefore typically reserved for shutdowns and large adjustments rather than continuous load-following [27, 6].

- Coolant mass flow regulation is relied on as the primary method for rapid load-following. A higher helium flow rate removes heat more efficiently, lowering the average core temperature. It is important to note that HTGRs have a strong negative temperature coefficient of reactivity, which is one of their most important safety features. A cooler core increases reactivity, leading to a rise in neutron population and thermal power. Conversely, a reduction in flow enables the core to increase its temperature, thereby decreasing reactivity and lowering power. This method facilitates power changes without the necessity of moving control rods, thereby circumventing substantial axial power distortions. Research has demonstrated that load-following between 65% and 100% of rated power can be achieved safely when employing this method alone [6]. The same research of Balestra shows that when operating a HTGR with a nominal temperature of 900 K, the average temperature difference of the fuel and moderator are approximately 50 K apart between 65 and 100% of nominal power.

- Fixed Burnable Poisons (FBPs), which can be a boride coating on fuel particles in case of a HTGR, are used for long-term reactivity control over the fuel cycle. In a fresh core, FBPs absorb excess neutrons, gradually burning out as fissile material depletes. This results in a flattening of the power distribution over time. A trade-off exists, as FBPs reduce the neutron economy, potentially shortening the core lifetime. This can be mitigated by design strategies such as spectrum hardening, which involves modifying the reflectors of the core to reduce the probability of fission [27].

- Non-fixed burnable poisons are primarily employed in LWRs through the addition of boron to the water that is used to cool the core. In the context of gas-cooled reactors, this approach is not feasible due to

the incompatibility of heavy elements with the use of light cooling gases. However, a viable alternative would be the injection of nitrogen into specific channels within the core of a carbon dioxide-cooled reactor, as previously outlined by Gosset et al. [26]. It has been established that, in comparison with boron, this gas does not exhibit a high degree of neutron absorption; however, it does demonstrate a significantly higher level of neutron absorption in comparison with the coolant.

- Whereas burnable poisons address long-term reactivity in a relatively static manner, pebble-bed HTGRs employ a dynamic fuel-cycling strategy to manage reactivity over the fuel lifetime. Fresh pebbles are added to the core, while burned-up pebbles are discharged. This facilitates online refuelling and constant reactivity maintenance; however, it does not permit rapid power changes due to the slow circulation time of pebbles through the core.

These mechanisms act on fundamentally different time scales and are therefore treated differently in dynamic reactor models. Reactivity-based control introduces direct but potentially disruptive core transients, whereas flow-based and indirect approaches modify thermal conditions more gradually. From a modelling perspective, the load-following behaviour of HTGR-based systems is commonly represented using low-order, lumped-parameter dynamic models. Although the underlying neutronic and thermal-hydraulic phenomena are complex, the dominant load-following response is often governed by a limited number of characteristic time constants associated with reactor thermal inertia, coolant transport, and balance-of-plant dynamics. This makes first-order or low-order representations suitable for analysing power manoeuvrability, control strategies, and the interaction with external loads [28].

The capacity to rapidly adjust power output is of paramount importance for marine applications. Research indicates that HTGRs have the capacity to achieve significant load-following ramp rates. As Balestra et al. [6] demonstrated, a prismatic HTGR can reliably follow a daily land applicable load profile using coolant flow control. Simulations showed that coolant flow could change by ±35 % points in 100 seconds with minimal overshoot and rapid stabilisation.

Yan et al. [7] conducted a study on a co-generating HTGR (GTHTR300C) with a direct-cycle gas turbine. They stated that this system was designed to handle power changes at a rate of ±5% of rated power per minute for electricity generation. It was also noted that faster, more extreme transients, such as a 1-second ramp, could cause power to exceed 100%, thus highlighting the necessity for controlled manoeuvring.

While these studies demonstrate promising manoeuvrability, the practical limit is ultimately set by fuel integrity under thermal cycling conditions. Studies on LWR fuel show that excessive thermal cycling can induce failures such as strain-ratcheting fatigue. HTGR TRISO fuel has been demonstrated to be robust; nevertheless, it is imperative to acknowledge the potential impact of excessive and frequent thermal cycles resulting from aggressive load-following on the long-term performance of the fuel [7]

For the purpose of comparison, it is important to note that studies undertaken by the OECD/NEA demonstrate that modern LWRs are generally designed to achieve ramp rates of 3–5%/min between 50–100% power [8]. In the domain of frequency regulation, the execution of rapid manoeuvres is facilitated, with the capability to achieve 5%/s within a narrow ±10% power band or 20%/min for downward ramps. However, such transients have been shown to accelerate fuel pellet cracking, fission gas release, and cladding corrosion. In comparison with LWRs, HTGRs employ a flow-control approach that circumvents mechanical pellet-cladding interaction. Nevertheless, thermal cycling stresses on graphite and TRISO fuel remain a limiting factor.

Beyond solid-fuel reactors such as HTGRs and LWRs, Molten Salt Reactors (MSRs) present a contrasting case, with inherently different load-following dynamics. The results of simulations of generic MSRs demonstrate that ramp rates of 10% per minute can be achieved by modulating heat removal in the steam generator [29]. This affords MSRs a theoretical advantage in terms of flexibility over HTGRs and LWRs, however their maturity level is considerably lower.

In addition to control strategies and ramp rates, fission product behaviour is a limiting factor to load-following capabilities. A key example is the build-up of xenon-135. This fission product strongly absorbs neutrons, and its concentration rises as power decreases. This can result in operational complexities when an attempt is made to increase the power level again. However, the elevated operating temperatures and the core design of HTGRs have been shown to mitigate the severity of xenon oscillations in comparison to LWRs, thereby enhancing their stability during transients [6, 7]. In contrast, MSRs have the capability to actively remove xenon due to their molten core, a property that LWRs and HTGRs lack.

While the implementation is technically feasible, frequent load-following has been demonstrated to increase the thermo-mechanical cycling of components. This can result in increased maintenance costs and a

potential reduction in the overall plant capacity factor and, consequently, revenue, as the primary cost savings of nuclear power are realised during base-load operation [7].

Although economic and operational challenges remain, the intrinsic safety characteristics of HTGRs, particularly the strong negative temperature coefficient, underpin their suitability for marine applications. The simulations conducted by Balestra et al. [6] corroborated the hypothesis that fuel and moderator temperatures remained well within safety limits during all of the tested transients.

In conclusion, coolant flow modulation should serve as the primary method of load-following in marine HTGRs, achieving ramp rates of around 5%/min while maintaining safety through the negative temperature coefficient. Control rods remain essential for startup, shutdown, and major adjustments, while burnable poisons primarily contribute to lifetime reactivity management rather than dynamic operation. From a control-modelling perspective, low-order reactor dynamics are particularly useful for studying the interaction between nuclear systems and external buffering elements such as thermal or electrical energy storage [28]. These operational characteristics underscore the need for complementary energy storage solutions, which are examined in section 2.2.

2.2. Energy Storage Systems

This section explores different options for energy storage that could be applicable to the nuclear propulsion system onboard ships with the objective to manage the variable load of a ship. From this report hydrogen production, compressed air storage and flywheels were left out since these storage systems were too large, complicated, or not developed far enough to be useable. The idea behind storage types are still mentioned in Table 2.1, however an estimation of energy density or costs could not be given.

2.2.1. Electrical Storage

Direct electrical energy storage (EES) in land application is convenient for peak shaving and managing the daily charge/discharge cycles [30]. This comes from the characteristic of fast charge/discharge possibilities that an EES provides. There are different ways to store electrical energy directly, super capacitors and super magnetic energy storage will be discussed in this section.

Super capacitors store energy in an electric field that is created between two high surface area electrodes. These are separated by an ion-permeable membrane (electrolyte ionic conductor). During charging the charges are separated and create a current when discharging. The amount of stored energy is mainly influenced by the voltage (V), Equation 2.1 gives the calculation. Capacitance (C), the ability to store charge, is dependant on the area of each plate (A), distance between the plates (d) and the permittivity of the free space and medium between plates ($\varepsilon_0, \varepsilon_r$) as shown in Equation 2.2, which holds for an ideal parallel-plate capacitor [31].

A super capacitor can be used for up to 12 years with a cycle efficiency of 85-98%. Minimal degradation is reported in deep discharge or overcharge and up to 500,000 cycles with full discharge can be reached. However, there is an approximate 5% per day self-discharge, so the energy is better used quickly [32, 33]. Research is being done on decreasing this loss by modifying the electrode, electrolyte and ion exchange membrane [34]. A super capacitor can have a power density of up to 10,000 W/kg, however its energy density is rather low at 5 Wh/kg. So high power, but for short time. This characteristic renders supercapacitors suitable for mitigating large, rapid fluctuations, and can be useful in power-quality applications such as frequency regulation, and voltage stabilisation [35].

$$E = \frac{1}{2} C V^2 \tag{2.1}$$

$$C = \frac{\varepsilon_r \varepsilon_0 A}{d} \tag{2.2}$$

Superconducting magnetic energy storage (SMES) systems store energy in a magnetic field generated by a current flowing through a superconducting coil. Their stored energy, Equation 2.3, depends on the inductance of the coil (L) and the current (I) [36].

Since superconducting materials exhibit negligible electrical resistance when cooled below their critical temperature, SMES systems can achieve exceptionally high cycle efficiencies [37]. Despite this advantage, the technology remains relatively immature, with limited large-scale demonstrations. Currently, commercially available devices are primarily so called micro-SMES units which can deliver power in the range of 1–10 MW, alongside a few U.S.-based installations of approximately 50 MW for power quality enhancement [38].

Widespread deployment is hindered by low energy density, but mainly high costs, estimated between 1,000 and 10,000 USD per kW, largely due to the expense of cryogenic systems required to maintain superconducting conditions [39]. Also, there are some safety concerns, which may pose health risks due to exposure to strong magnetic fields [30].

$$E = \frac{1}{2} L I^2 \tag{2.3}$$

In summary, these two EES technologies exhibit similar characteristics and thus similar use cases. Due to the cooling needed for the SMES, this technology will be more expensive per unit of power and also super capacitors are used more and thus more developed.

2.2.2. Electrochemical Storage

Electrochemical energy storage (EES) systems convert electrical energy into chemical energy through reversible electrochemical reactions, allowing reconversion to electricity when required. These systems exhibit a broad range of power and energy densities [40]. Figure 2.2 illustrates the position of electrochemical storage relative to other electrical storage technologies in terms of specific power and specific energy per unit mass. In most applications, electrochemical storage systems are referred to as batteries.

Unlike capacitive storage, the energy capacity of electrochemical batteries is governed by the amount of charge that can be transferred through reversible redox reactions in the active materials. From Faraday's law, the total battery energy capacity can be expressed as Equation 2.4.

$$E = \frac{m_{\text{act}}}{M} z F V_{\text{cell}} \tag{2.4}$$

In this formula m_{act} is the mass of electrochemically active material, M its molar mass, z the number of electrons transferred per reaction, F Faraday's constant, and V_{cell} the average cell voltage. This relation shows that battery capacity scales fundamentally with the quantity of active material and the achievable cell voltage. This section includes Li-ion type batteries, flow batteries and solid state batteries.

Among available battery technologies, lithium-ion (Li-ion) batteries dominate the market owing to their high energy density, near-100% efficiency, and relatively low weight. Alternative chemistries, such NiCd, Ni-MH, Pb-acid, and NaS, exhibit notable drawbacks, including toxicity, high self-discharge, bulkiness, or the need for high-temperature operation. Despite their advantages, Li-ion batteries still face challenges related to high cost and limited lifetime under deep discharge conditions [38].

Currently, Li-ion battery systems are widely deployed for frequency regulation and grid stabilisation. Reported performance varies considerably, with power densities ranging from 60 to 10,000 kW/m^3 and energy densities from 90 to 750 kWh/m^3, providing flexibility across different operational contexts [41]. A key advantage is their low self-discharge rate, typically around 8% per month depending on system configuration [40].

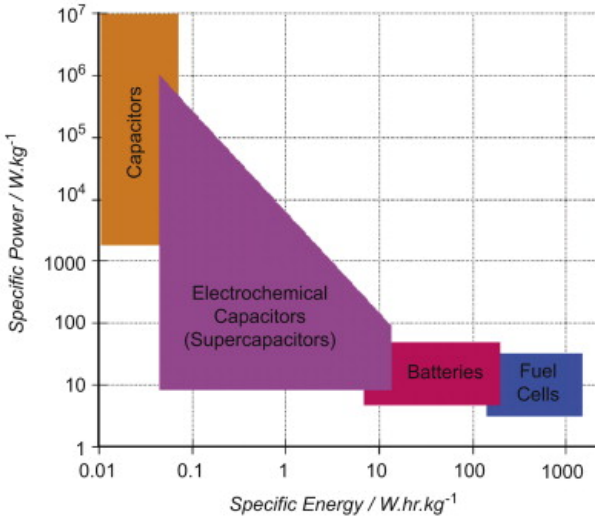

Figure 2.2: Specific energy vs specific power of electrical and electrochemical storage [38]

For maritime applications, Nickel Manganese Cobalt (NMC) Li-ion batteries are particularly promising due to their favourable balance between specific energy and power capability [42]. NMC cells achieve energy densities of 150–260 Wh/kg and approximately 950 Wh/L [43, 44], with power densities ranging from 500 to 2500 W/kg depending on the energy–power trade-off [45]. On the other hand lithium iron phosphate (LFP) batteries offer improved safety and lower cost, and are therefore coming into the picture for maritime use. There are even more different Li-ion battery types, like the LTO version which is capable of more (dis)charge cycles, so which version to use is dependant on the specific loads that the ship endures [46].

Another important category of electrochemical energy storage is the flow battery. These systems store energy in liquid electrolytes circulated through an electrochemical cell composed of a cathode, an anode, and an ion-selective membrane. The energy density is primarily determined by the electrolyte's volume and concentration, while power density depends on the kinetics of the redox reactions. Compared with Li-ion systems, flow batteries typically provide lower energy density but offer advantages such as longer lifetime, full-depth discharge capability without degradation, lower fire risk, and immunity to overcharging. However, the inclusion of pumps and associated piping increases system complexity and cost, making them more suitable for large-scale stationary applications [47]. While several pilot and commercial-scale demonstrations exist, deployment remains limited due to high costs and lower energy density relative to Li-ion batteries. Overall system efficiency typically ranges between 75% and 85%, lower than that of Li-ion systems owing to additional mechanical and auxiliary losses [38].
Finally, solid-state batteries represent a next-generation technology that replaces liquid electrolytes with solid materials, enabling potentially higher energy and power densities while improving safety. Reported energy densities reach up to 402 Wh/kg, although large-scale commercial deployment has not yet been demonstrated [48].

2.2.3. Thermal Storage

There are two main groups of thermal storage types, latent and sensible heat storage. Latent storage relies on phase change, while sensible storage relies on sensible temperature difference. With an HTGR, thermal storage requires no energy conversion, as reactor heat is stored directly before electricity generation. Furthermore, this configuration decouples the reactor operation from power demand [9]. Which allows the reactor to run at a constant, optimal power level for efficiency and longevity, while the stored energy enables the power block to deliver variable output for propulsion and pulsed systems.

Heat storage energy can be calculated with Equation 2.5, total thermal energy (Q) is dependant on mass (m), specific heat capacity of the storage medium (c) and the temperature difference (ΔT), this part of the equation is for the sensible heat stored. In latent heat storage the phase change also needs to be taken into account, this is done by adding the last part of the equation where Δq is the energy of phase change per unit mass [49].

$$Q = m \cdot c \cdot \Delta T + m \cdot \Delta q \tag{2.5}$$

One of the possibilities to efficiently store sensible thermal energy is a two tank system. Though configurations vary, the principle is simple: reactor heat is transferred to a Heat Transfer Fluid (HTF) and this is stored in the 'hot' tank, the fluid can be drawn from the tank if the power cycle required more heat for scaling up. After the heat is used for the power cycle, it returns to the 'cold' tank. It is then reheated in the reactor or a heat exchanger and returned to the hot tank. Figure 2.5 and 2.3 show two potential configurations for a two tank system. A common example of this system uses molten nitrate salts as the HTF, for example Solar Salt which is a 60-40 mix of sodium nitrate and potassium nitrate. These salts are excellent for their high thermal capacity (113 kWh/m^3 over ΔT=125 K), providing power in the range of hours, and stability at the target temperatures [50].

In the first configuration the heat exchanger which is connected to the storage system is placed in parallel to the power cycle. The second configuration has its heat exchanger placed in series with the power cycle, this means all the thermal energy goes through the hot tank before reaching the power cycle. The hot tank, in both cases, transfers over 99% of heat energy above 550 °C to the power cycle, making series integration a simplification of the system rather than a loss [50]. Placing the tank between the nuclear and power cycles also has the advantage that it prevents radioactive transfer, adding an extra safety barrier. Two-tank systems are highly efficient but costly and bulky, since they require both full size hot and cold tanks, which essentially doubles tank volume installed.

A solution to the sizing problem is using one tank, called a thermocline system. This tank contains both the hot and the cold HTF, this reduces the total size significantly since the total capacity of hot or cold fluid does not need its own tank. A basic example of this system can be seen in Figure 2.4. The thermocline system can only deliver 65% of the heat above a temperature of 550 °C, making it less efficient then the two tank system. This efficiency loss stems from diffusion and mixing in the thermocline layer, which degrades delivered temperature and thus thermal energy. This can be mitigated by tall, slender geometry or using conductive fillers like granite or quartzite, to minimise the amount of HTF needed and thus reduce cost. This thermocline configuration presents a trade-off possibility among thermal efficiency, economic feasibility, and volumetric capacity [51].

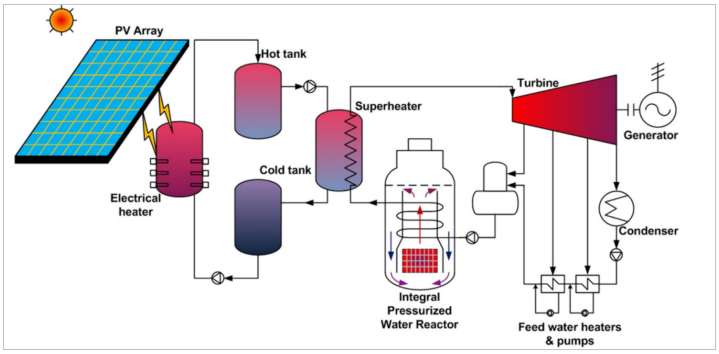

Figure 2.3: Two tank thermal storage configuration 2 [52]

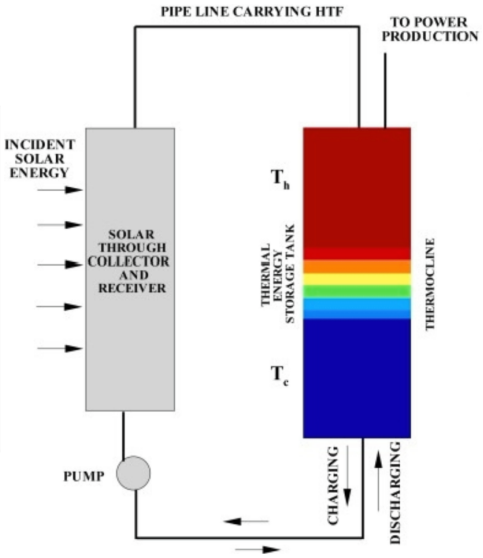

Figure 2.4: Thermocline system [50]

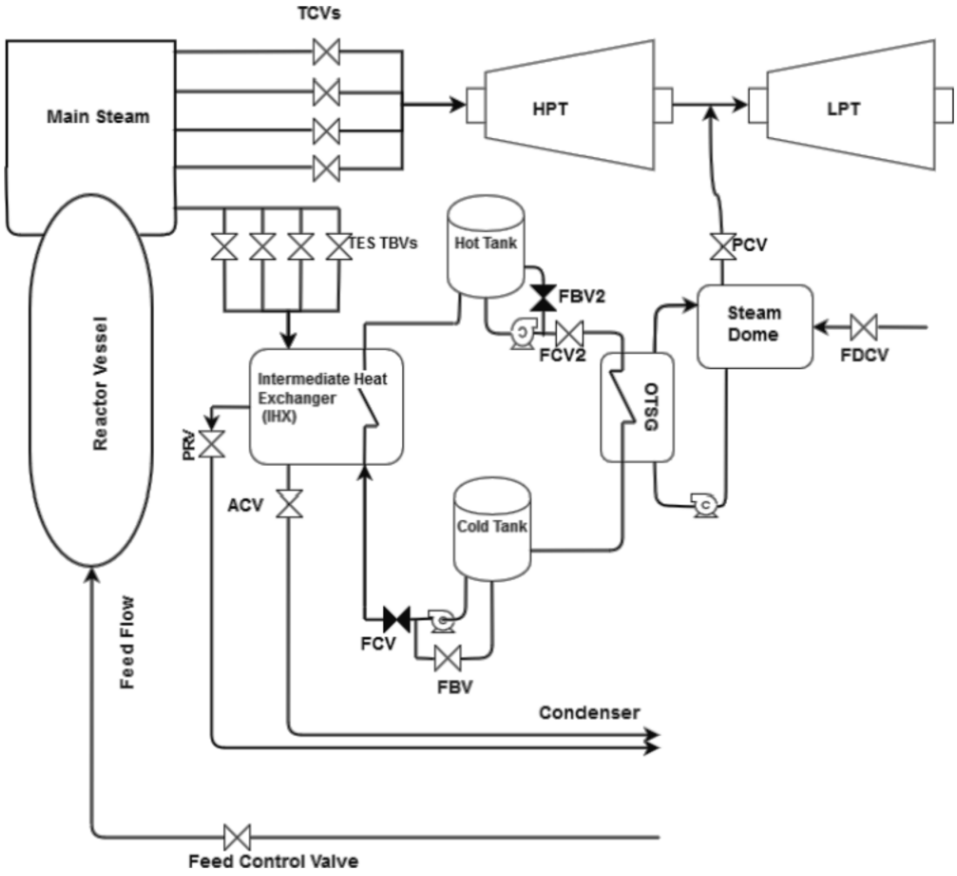

Figure 2.5: Two tank thermal storage configuration 1 [53]

The two tank and thermocline system both use liquids to store thermal energy. However, liquid storage on a ship could impose additional problems like tank sloshing. Two-tank systems could potentially slosh heavily since tanks are always partly filled when in use, creating dynamic stability issues. Thermocline tanks are fuller but rely on gravity to stabilise and limit the thermocline region. Movement of the ship will mix the HTF in the tank, reducing the efficiency even further.

The last option to store sensible thermal energy is solid storage. Solid blocks, like firebrick or concrete can be heated with reactor heat and supply this heat to the power cycle when needed. Solid sensible storage

normally operates between 600 and 1000 °C and for example firebrick can hold 88 kWh/m^3 over a temperature change of 125 °C with a round trip efficiency of about 75%.

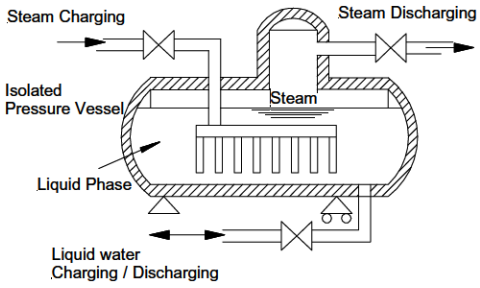

Figure 2.6: Sliding pressure steam accumulator [54]

For marine applications, solid-state storage offers a critical advantage: it is inherently immune to sloshing. This makes it well-suited to marine use, offering a stable thermal battery that decouples the reactor without sloshing risks [9]. The primary trade-off is the significant weight addition and a slow ramp time. However, solid storage does provide power on hour scale. A faster way to provide thermal energy is the steam accumulator. This is a well-established latent thermal storage technology that employs the phase change energy of water. Operating principles are based on the control of a vessel containing pressurised saturated water between 200 and 300 °C. On demand, pressure reduction triggers flash evaporation, instantly supplying steam to the power cycle. This mechanism provides an exceptionally fast ramp rate for a thermal system, making the technology suitable for grid-balancing services such as frequency regulation or the faster ramps in power demand [54].

The system's compact footprint, which is comparable to that of a large heat exchanger, facilitates integration. However, it can only operate for 5–10 minutes at full power with an energy density of 20–30 kWh per cubic metre [54].

The round-trip efficiency for this process is moderate, ranging from 60% to 80% [50]. Despite limited capacity, its proven reliability, rapid response, and high readiness make it a pragmatic option for short-term transients.

In summary, while liquid-based sensible TES systems offer efficiency advantages, their vulnerability to sloshing, mixing and space requirements make them challenging for marine use. Solid storage and steam accumulators, despite their respective drawbacks of mass and limited duration, provide inherently stable and compact solutions that may be better aligned with the operational realities of ships.

2.2.4. Combined Storage Systems

This subsection evaluates combinations of energy storage systems that are operationally compatible with a HTGR power plant installed on a ship. The aim is to identify complementary combinations that could meet typical marine requirements, make use of HTGR-specific advantages, and respect safety and classification constraints. Table 2.1 gives an overview of the broad characteristics of the storage technologies including why they should be combined with an HTGR. Tables 2.2 and 2.3 state the ranges of power and energy densities together with specific costs of the most promising energy storage technologies.

1. Thermal storage (solid or sensible molten salt) + electrical battery + supercapacitor. An HTGR can deliver steady high-grade heat that charges a thermal storage, one of the molten salt or solid sensible storage systems. The thermal store is well suited to supply the power cycle for multi-hour operation. Batteries supply minutes-to-hours electrical buffering with high energy density and good round-trip electrical efficiency. Supercapacitors can handle millisecond-to-seconds transients and peak-power spikes and with that can control frequency regulation and rapid thruster demands. The reasons to combine batteries and super capacitors on the electrical storage side are that capacitors can endure more frequent and faster charging and discharging, which results in more reliability of the system.

This three-layer architecture aligns each device to its strength: supercapacitors for instantaneous power, battery for medium-duration electrical buffering, and thermal storage for sustained energy while letting the HTGR run at steady conditions. For ships with operations that do not have a large change in energy demand over time, the thermal storage can be replaced with more batteries to eliminate the extra system.

Several recent reviews and marine-specific studies support the battery + supercapacitor hybrid as the preferred electrical hybrid for ships, and HTGR–thermal storage coupling for multi-hour decoupling has been modelled in HTGR studies. [9, 55, 56].

Molten salts require slosh mitigation and non-trivial tank geometry for ships, for example thermocline or solid-particle approaches can reduce paired-tank volume and sloshing, while solid-block thermal storage eliminates slosh but increases mass and volume. Supercapacitors and Li-ion batteries are proven for shipboard applications but Li-ion fire risk and classification-society requirements must be addressed [57].

2: Steam accumulator + longer-term thermal energy storage. A combined thermal solution pairs a steam accumulator for immediate, second-to-minute turbine support with a longer-term thermal energy storage like solid sensible TES or a thermocline molten-salt system to cover hour-scale demands. The accumulator delivers high-power steam instantly for turbine ride-through and short peak shaving, thereby enabling the reactor to keep steady-state operation.

The longer-term TES supplies the power block for multi-hour load shifts or mission segments while the HTGR remains at optimal output. Solid sensible media are recommended for shipboard use because they avoid sloshing, are mechanically simple, and provide reliable storage at high temperatures compatible with HTGR secondary loops. Thermocline molten-salt tanks are an alternative when higher volumetric capacity is required, but they demand anti-slosh measures and careful tank geometry to retain thermal stratification at sea [50, 51, 54]. Integration on the non-radioactive secondary loop preserves containment and simplifies maintenance. Operationally, the accumulator handles seconds–minutes at full power while the TES covers the minutes–hours regime. This method minimises the need for large electrical storage volumes [9]. However, it does induce large and frequent load variations on the turbine.

3. Steam accumulator + electrical battery. A hybrid concept combining steam accumulators with electrochemical batteries offers a robust and efficient short-to-medium duration storage solution for an HTGR-driven ship. Steam accumulators provide instantaneous to minute-scale response releasing steam directly to the turbine during transients, effectively decoupling the reactor from rapid load fluctuations on the thermal side.

Complementing this, batteries cover the minute-to-hour range, supplying or absorbing electrical power within the ship's grid for propulsion and auxiliary systems. The combination thus delivers a smooth response spectrum—from sub-second electrical events managed by the battery to minute-scale thermal support from the steam accumulator—allowing the HTGR to operate at steady output without frequent power swings. This enables the thermal and electrical system to operate parallel on the power train, resulting in less storage efficiency losses.

This configuration exhibits high overall efficiency, compactness, and operational flexibility. It is particularly suited for vessels with moderate to fast load variations, where maintaining reactor stability and rapid power quality control are both critical. Optionally, a small super capacitor bank may be added upstream to handle millisecond spikes in the electrical grid.

Technology	Response	Duration	Marine-fit	HTGR combination
Supercapacitor	ms–s	seconds	Excellent	Electrical only (no direct heat)
Li-ion (NMC)	s–min	minutes–hours	Good (fire mitigation req.)	Electrical buffer
Flow battery	s–min	hours	Moderate (complex BOP)	Electrical buffer, scalable energy
Molten salt TES	slow–min	hours	Challenging (slosh)	Direct thermal coupling, temperature match
Solid sensible TES	slow	hours	Excellent (no slosh)	Direct thermal coupling, heavier
Steam accumulator	ms–s	minutes	Excellent	Direct steam-cycle integration
CAES (adiabatic)	minutes	hours	Moderate (tank design)	Reheat with HTGR heat improves efficiency
Hydrogen	minutes–hours	hours–days	Challenging (storage/safety)	Thermochemical cycles can use HTGR heat
Flywheel	ms–s	seconds–minutes	Good	Electrical only
SMES	ms	seconds	Poor (cryogenics, magnetic safety)	Electrical only, cryogenic penalties

Table 2.1: Qualitative comparison of storage options for HTGR ship integration.

For the TES in Table 2.2, the specific power and power density was not stated explicitly. For this a calculation is made from the sources given where the total amount of stored energy per volume is divided by the amount of hours that the system could deliver energy. These numbers give an indication on what kind of power density could be expected or at least what has already been accomplished on system level.

Category - Technology	Spec P (W/kg)	Spec E (Wh/kg)	Vol P (kW/m3)	Vol E (kWh/m3)	Cycle efficiency
Electrical - Supercapacitor [30, 33]	<10,000	5-15	10,000-30,000	10-30	85-98%
Electrochemical - Li-ion (NMC) [37, 58, 59]	300–1000	150-250	800-2000	500-700	95+%
Electrochemical - Solid-state [60]	150-400	300-500	400-1000	350-500	95+%
Thermal - Molten salt TES (two tank) [61]	100-300	60 (th)	30	100-150 (th)	90%
Thermal - Thermocline TES [62]	50-150	40-75 (th)	25	80-150 (th)[a]	60-75%
Thermal - Solid sensible TES (Firebrick) [63]	50-200	40-50 (th)	55	80-100 (th)[b]	75%
Thermal (latent) - Steam accumulator [54]	200-500	20-30 (th)	100	20–30 (th)	60-80%
Mechanical - Flywheel	2,000–10,000	10–150	500-1500	40-70	90-95%

Table 2.2: Ranges of specific power and energy for possible types of ESS

[a] ΔT≈ 200-400°C
[b] Δ T≈ 125°C

Category - Technology	Cost ($/kW)	Cost ($/kWh)
Electrical - Supercapacitor [30]	100-300	300-2000
Electrochemical - Li-ion (NMC) [64]	1200-1500	400-500
Electrochemical - Solid-state [65]	-	400-600
Thermal - Molten salt TES (two tank) [30]	-	30-60
Thermal - Thermocline TES [66]	-	15-25
Thermal - Solid sensible TES (Firebrick) [67]	~90	1-10
Thermal (latent) - Steam accumulator [68]	~15	~15
Mechanical - Flywheel [30]	250-350	1000-5000

Table 2.3: Approximate cost per unit of power or energy for possible types of ESS

2.3. Integration of ESS in Nuclear-Powered Vessels

Next to the possibilities for storages, the integration also needs to be evaluated. This section will look at the physical integration as well as the safety and regulations involved.

2.3.1. Physical integration

ESS integration in HTGR-powered ships varies by storage medium and dynamic response. Electrical storage devices, such as lithium-ion batteries or supercapacitors, are interfaced with the ship's electrical bus via bidirectional DC/DC converters or inverters. In this arrangement, the ESS buffers rapid load changes between the turbine-generator set and the propulsion or hotel loads, allowing the reactor and power conversion unit to operate steadily. The American Bureau of Shipping [69] specifies that such systems must maintain voltage and frequency stability and meet the International Electrotechnical Commission (IEC) 60092 harmonic limits. To limit ageing from deep cycling, battery management systems maintain a 20–80% state-of-charge window. [69, 70]. When the ESS operates in parallel with other generation sources, its charge and discharge are coordinated by the ship's power-management system to prevent reverse power flow or overloading.

TES connects upstream of electrical conversion, using the high outlet temperature helium from the HTGR to charge molten-salt or similar media through an intermediate, non-radioactive loop. This configuration ensures physical separation between the radioactive primary coolant and the power cycle, improving safety and permitting the reactor to operate at constant power [71]. During charging, part of the reactor heat is routed through the TES, while the remainder drives the turbine directly. Additional heat-exchange stages introduce measurable but modest thermal losses due to extra temperature-approach limits and pressure drops, though the coupling maintains the steam-generator inlet design point and overall turbine efficiency [71].

A hybrid architecture, combining fast electrical ESS and long-duration TES, establishes two layers of decoupling between reactor and demand. This improves flexibility and redundancy but requires hierarchical control that separates non-safety energy-management functions from reactor safety systems [10]. Considering the typical 30–45% efficiency of nuclear power cycles, storing thermal energy before conversion means storing a larger portion of total energy output than post-conversion electrical storage [71]. As all energy must eventually be converted to electricity at some point, storing it as electrical energy would mean needing less

storage capacity. Beyond the physical integration of ESS, its operational role in managing variable loads is equally critical.

2.3.2. Safety and Regulatory Considerations

The IAEA Safety Guide for Auxiliary and Supporting Systems defines these systems as those which provide electricity or other services that are essential for the operation and safety of nuclear power plants [72]. The reliability of these systems is dependent on their importance within the overall system. The primary regulatory concern is that ESS operation must not compromise nuclear safety.

The IAEA identifies three principal safety functions: control of reactivity, removal of heat from the reactor and fuel store, and confinement of radioactive material. Any system that contributes to these functions must be assessed for its role in maintaining plant safety. The utilisation of an ESS as an emergency power source or to facilitate cooling during a station blackout results in its incorporation into the safety architecture [73].

SSG-30 [73] further elaborates on this by emphasising the necessity of considering the consequences of failure, the frequency of the initiating event, and the significance of the function in achieving a controlled or safe state.

It is noteworthy that, according to the aforementioned methodology, an ESS may be classified into one of several distinct safety classes, depending on its designated function. In the event that the ESS provides emergency power for cooling or instrumentation during severe accidents, or functions as a heat sink in the event of excessive core temperature, it could be classified as Class 2, requiring higher reliability and qualification. Conversely, if the ESS supports only non-critical loads or efficiency improvements, it would likely be classified as Class 3, with less stringent requirements.

The classification determines the design basis for ESS, including environmental and seismic qualification, quality assurance, and defence-in-depth provisions.

In addition to SSG-30, SSG-34 [74] addresses electrical power systems and emphasises the need for reliable emergency power sources under all conditions, which must also be considered for an ESS. Together, these guides form the regulatory foundation for integrating ESS into nuclear power plants, thereby ensuring that such systems are designed, qualified, and maintained to support nuclear safety functions without introducing additional risks.

Beyond the classification and design basis, provisions for accident management are critical when integrating ESS with nuclear power plants. The Fukushima Daiichi incident has provided a valuable lesson regarding the vulnerability of auxiliary systems during extended loss of power events [75].

In the context of ESS, the critical considerations include ensuring physical protection against external hazards such as flooding, fire, and seismic events, as well as implementing redundancy and diversity in power supply pathways. In the context of maritime operations, the significance of these hazards is further accentuated. Together, these provisions ensure that ESS integration enhances overall plant resilience without compromising nuclear or maritime safety.

2.3.3. Classification Society Regulations

The international regulatory framework for civilian nuclear-propelled ships is defined by SOLAS Chapter VIII *Nuclear ships* and the 1981 *Code of Safety for Nuclear Merchant Ships* (IMO Assembly Resolution A.491(XII)) [76]. This regime, based on pressurised water reactors with direct steam-cycle propulsion, is widely considered outdated. In June 2025, the IMO Maritime Safety Committee agreed to comprehensively revise the Nuclear Code and related SOLAS provisions. The revision aims to incorporate modern reactor concepts and all-electric ship architectures while coordinating with the IAEA to streamline regulations [77, 78].

Both electrical and thermal energy storage technologies are increasingly relevant to hybrid propulsion and decarbonisation strategies. However, their regulatory treatment differs markedly.

The IMO has not yet issued prescriptive global rules for electrical energy storage systems. Instead, safety requirements are defined mainly by classification societies and, in Europe, by the European Maritime Safety Agency (EMSA). These frameworks aim to mitigate hazards such as thermal runaway, fire, and explosion. Classification society rules, such as DNV Part 6, Chapter 2, ABS's *Requirements for Lithium-ion Batteries and Hybrid Power Systems*, and Lloyd's Register's functional requirements for large battery installations, specify measures including fire-rated battery rooms, ventilation, and off-gas handling systems. These measures are further complemented by the use of certified Battery Management Systems (BMS) with fault detection and emergency shutdown capabilities [79, 80, 81]. EMSA's 2023 guidance reinforces these principles, requiring risk assessments and safety measures equivalent to those for conventional machinery.

In contrast, no dedicated IMO or class society rules exist for thermal energy storage. TES installations are assessed under general provisions for machinery, pressure vessels, and fire safety, supplemented by risk-based approval for novel systems. DNV applies regulations for thermal oil and heat transfer systems, while ABS uses thermal analysis methods for tanks and structural components [79, 82]. TES approval requires demonstrating structural integrity, overpressure protection, and fire safety comparable to thermal oil systems, along with hazard analyses for leaks, solidification, and other failures. For nuclear-powered ships, both electrical and thermal storage must be addressed in the Safety Assessment required by SOLAS Chapter VIII to ensure that their integration does not compromise nuclear safety.

2.4. Current use and Improvements

This section will explore what advantages including an ESS would bring to a ship. Hazards and mitigation strategies will be discussed as well as how current nuclear-powered vessels are operated and land-based nuclear power plants will be evaluated shortly.

2.4.1. Hazards and Mitigation Strategies

The integration of ESS on ships presents distinct safety challenges, arising from the confined nature of maritime environments and the complexity of emergency response. The primary hazards associated with electrical and thermal energy storage systems, and the strategies for mitigating these risks will be discussed.

Battery Energy Storage Systems (BESS) pose significant onboard hazards, necessitating robust risk mitigation strategies. The primary hazard identified by classification societies is thermal runaway, a phenomenon associated with lithium-ion batteries. Thermal runaway, an uncontrolled heat generation process triggered by internal faults or external stresses, leads to cell decomposition and flammable gas release. This process releases flammable gases, such as hydrogen and carbon monoxide, which can propagate to adjacent cells and cause fires or explosions within confined ship compartments [83, 84]. In maritime environments, limited space and complex evacuation procedures amplify these risks, making early detection and containment essential [42, 85].

In order to mitigate these hazards, classification societies have implemented stringent design and operational measures. Dedicated battery spaces with continuous mechanical ventilation prevent gas accumulation. Furthermore, fire detection and suppression systems, such as water mist or inert gas, cool affected cells and prevent escalation. The requirements for venting are guided by standards developed by the National Fire Protection Association (NFPA), which serve as global references for fire risk mitigation. In particular, NFPA 68 [86] specifies deflagration venting to safely release pressure and reduce explosion hazards [85]. Propagation control is achieved by isolating cells or limiting module capacity to less than 11 kWh, ensuring failures remain localized [42]. Battery Management Systems (BMS) provide real-time monitoring of temperature, voltage, and state of charge, thereby facilitating early intervention before conditions deteriorate [83]. These measures address the unique challenges posed by shipboard environments, where confined spaces and limited emergency response capabilities demand rapid detection and mitigation.

Thermal Energy Storage (TES) systems—particularly those using phase, change materials (PCMs) or molten salts, present different safety concerns. High operating temperatures can result in thermal leakage, material degradation, and localised overheating, posing fire hazards and compromising structural integrity [87, 88, 89]. Coraddu [42] acknowledges that TES systems require significant weight and volume, which can influence ship design and operational considerations, even if stability risks are not explicitly stated. The ingress of seawater further increases risks by causing corrosion and contamination, particularly in PCM-based units exposed to humid marine conditions [90].

Mitigation measures for TES focus on effective insulation and containment to prevent heat loss, combined with corrosion-resistant materials to counter seawater ingress. Real-time thermal monitoring facilitates early detection of abnormal temperature gradients, while modular TES configurations integrated with stability analysis tools minimise structural risks and support safe operation under dynamic conditions [90, 89]. Collectively, these measures collectively address the unique thermal and structural challenges posed by TES systems in confined marine environments.

The integration of BESS and TES systems offers operational advantages but introduces hazards requiring careful management. Lithium-ion systems demand thermal runaway prevention and gas venting, whereas TES systems necessitate high-temperature containment and structural resilience. The combination of robust design standards, real-time monitoring, and compliance with international guidelines such as those established by the NFPA, has been shown to mitigate these risks significantly and ensure the safe and reliable

storage of energy in maritime applications.

2.4.2. Nuclear-Powered Vessels

As discussed in chapter 1, most nuclear-powered vessels in operation are naval ships and submarines, with only a limited number of icebreakers. These vessels typically employ one of two propulsion configurations: mechanical or electric drive. In both cases, heat generated by the reactor is used to convert water into steam, which then drives a turbine.

In a mechanical power train, the turbine is connected to the propeller shaft via a reduction gearbox. In contrast, an electric drive uses the turbine to power a turbo-generator, which produces electricity to drive an electric motor that propels the ship. In the former system, a turbo-generator would still be needed for auxiliary power [91].

Currently, neither configuration incorporates an energy storage system to balance reactor output with the vessel's power demand. Reactor output is generally maintained at a near-constant level, and consequently, the steam production rate remains steady. Power regulation is achieved by throttling the amount of steam admitted to the turbine, which adjusts the turbine's output. This arrangement is simple and allows rapid power upscaling by reducing steam bypass, but turbine efficiency varies significantly under different load conditions [92].

Although this design minimizes complexity and ensures direct power availability, it leaves unused potential for optimization. Modern designs, such as the French Barracuda-class submarines, employ hybrid systems with electric propulsion for cruising speeds and mechanical drive for higher speeds. For redundancy and emergency power, nuclear-powered vessels are equipped with auxiliary diesel generators or small battery systems to ensure the ship can reach a safe state in the event of an incident [91]. However, the electrical coupling in electric-drive systems makes them technically suitable for ESS integration, which could enable load-following and improve overall efficiency [93]. Despite these benefits, ESS adoption is hindered by added complexity, weight, and cost.

2.4.3. Diesel-Electric Ships

In contrast, conventional diesel-electric ships have successfully integrated ESS to improve efficiency and reduce emissions. For example, on the e-shuttle tanker *Aurora Spirit*, the installation of a hybrid system combining batteries and diesel engines resulted in a 14% reduction in installed mechanical power. This allowed the diesel engines to operate at more efficient speeds, reducing fuel consumption and harmful emissions [94, 95].

Another example is the E-Kotug tugboat, where a 117 kWh battery system was installed to provide power during low-load conditions. This integration reduced engine running hours and improved overall efficiency [94]. These cases demonstrate that ESS enables peak shaving, load levelling, and optimized engine operation, making diesel-electric platforms more adaptable and environmentally friendly compared to nuclear-powered vessels, where ESS remains largely absent.

There are small TES like applications in shipping. For example in waste heat recovery from the engine to supply the warm water needs of the ship, leading to a reduction of fuel consumption of the boiler [96]. However, large scale thermal energy storage has not been applied. This is mainly due to the use of engines, which produce mechanical energy, not thermal [97].

2.4.4. Land-Based Nuclear Plants

On land-based nuclear sites, ESS are already coupled with nuclear reactors. The primary factors driving this integration are the volatility of energy production and market prices. In an ideal scenario, a nuclear reactor would supply a consistent baseload. However, with an ESS, it is possible to modify the baseload while maintaining a steady load for the reactor [17, 16]. Placing a reactor with an ESS on land connected to the grid offers a more predictable form of load-following, where lessons could be learned for implementation aboard a ship.

Beyond electricity markets, the role of energy storage is increasingly recognised as a key enabler for industrial applications through the integration of energy systems. Coupling nuclear reactors with TES facilitates combined heat and power configurations, thereby enabling simultaneous delivery of electricity and process heat for sectors such as chemical manufacturing, district heating, and hydrogen production [98, 99].

The utilisation of these ESS in combination with a reactor enhance thermodynamic efficiency and reduce greenhouse gas emissions by replacing fossil-based heat sources with nuclear-derived thermal energy. Recent studies highlight TES's potential in supporting hydrogen production through high-temperature electrolysis,

leveraging the steady thermal output of advanced reactors such as HTGRs to stabilize industrial energy supply chains [100].

Another emerging application involves grid-scale pumped thermal energy storage (PTES), which was previously introduced as a two-tank system. This has been integrated with nuclear plants in order to manage variability in renewable generation. PTES systems store surplus nuclear heat in molten salts or solid media, and later convert it into electricity during periods of peak demand. This approach has been validated through real-time simulations, demonstrating enhanced operational flexibility during transient conditions such as start-up and shut-down phases, which traditionally challenge nuclear systems [101]. Furthermore, TES integration enhances resilience against extreme weather events and improves the economic viability of nuclear plants in competitive energy markets, positioning nuclear-plus-storage systems as a cornerstone of future low-carbon grids [102, 103].

Whilst thermal energy storage remains the most efficient option for coupling with nuclear power plants on land, electrical energy storage technologies — such as batteries and hybrid systems - play a critical role in enhancing grid stability and providing fast-response services. Electrochemical storage, in particular lithium-ion batteries, offer rapid response for frequency regulation, black start capability, and short-duration load balancing, thereby complementing the slower dynamics of nuclear generation [16, 98]. Despite their reduced cost-effectiveness in large-scale energy shifting when compared with TES, the ability of batteries to deliver auxiliary services renders them valuable in markets characterised by high levels of renewable energy penetration and stringent reliability requirements [104].

Although TES systems dominate large-scale and high-temperature applications, EES technologies demonstrate particular excellence in the domain of rapid-response and short-duration support. This highlights the complementary nature of thermal and electrical storage for nuclear systems. In addition to their role in the provision of grid services, batteries are imperative for the safety of nuclear power plants, as they facilitate the supply of emergency power to cooling and lubrication systems during periods of outage, thereby ensuring the maintenance of reactor integrity. Large-scale battery installations are also being deployed at decommissioned nuclear sites, demonstrating the potential for nuclear infrastructure to support renewable integration and grid decarbonisation [103]. Despite these advancements, challenges remain regarding cost, lifecycle management, and scalability, thus positioning EES as a complementary rather than primary storage solution for nuclear systems on land.

2.5. Literature Review Conclusions

This literature review has examined the operational characteristics of High-Temperature Gas-Cooled Reactors (HTGRs), the suitability of different energy storage technologies, and the constraints associated with integrating energy storage systems (ESS) into nuclear-powered vessels. The HTGR was selected prior to this study as the reactor concept for maritime application; the purpose of this review was therefore not to justify this choice, but to assess its operational implications and identify how ESS can support its use under variable shipboard load conditions.

The reviewed literature shows that HTGRs are well suited to providing stable, efficient baseload power, but are inherently limited in their ability to follow rapid load variations. Thermal inertia, negative temperature feedback, xenon dynamics, and permissible ramp rates restrict power manoeuvrability to a few percent of nominal power per minute, making direct tracking of maritime load profiles infeasible [6, 7, 8]. As a result, HTGRs can contribute to load following only on slower time scales and require external buffering to accommodate faster transients.

Energy storage therefore emerges as an enabling component rather than an auxiliary addition. The literature consistently distinguishes storage technologies by their response time and functional role. Electrical energy storage is most effective for managing fast transients and short-duration power mismatches, while thermal energy storage enables decoupling of the reactor from the power cycle and supports slower load variations [9, 50]. This naturally leads to a hybrid storage concept in which thermal storage assists the HTGR in medium-timescale load following, while electrical storage handles rapid fluctuations and residual mismatches.

Based on the reviewed studies, a hybrid ESS combining thermal and electrical storage is identified as the most appropriate architecture for HTGR-powered vessels. This configuration aligns storage functionality with reactor physics, operational demands, and maritime constraints, while maintaining separation between reactor safety systems and non-safety energy management functions [9, 10]. These conclusions directly inform the subsequent chapters, where load profiles are analysed, dynamic models are developed, and hybrid

ESS configurations are sized and evaluated for maritime nuclear propulsion.

3

Load profile analyses and ESS Requirement Definition

This chapter analyses the load profile (LP) of the case study vessel *Hidden Gem* and evaluates how well the proposed nuclear-electric power plant can meet its operational power demand. Understanding the temporal behaviour of the load profile is essential for determining whether the High Temperature Gas-cooled Reactor (HTGR) can supply the required power during all mission phases. It also enables identification of periods in which power deficits occur and quantification of the Energy Storage System (ESS) needed to support peak loads or rapid transients that the reactor cannot follow.

The chapter therefore forms the basis for defining the ESS requirements, operational philosophy, and constraints of the hybrid nuclear–diesel power system.

3.1. Case Study Vessel and Load Profile

Allseas is a major offshore engineering contractor pioneering new technologies for the offshore energy and seabed minerals industries. Alongside its established expertise in pipe lay and heavy-lift operations, the company is developing a seabed poly-metallic nodule collection system, designed to recover nodules from the ocean floor for critical metals needed in the energy transition. Currently it is being investigated what negative effects this type of mining brings with it and how this can be minimised.

The deep-sea mining vessel Hidden Gem, operated by Allseas, has been selected as the reference platform for this study. Its suitability for nuclear conversion stems from the combination of long-duration offshore operations, steady power demand, and the need for extended autonomy. The load profile of the ship will give more insight in what the ship needs.

The 14-day load profile shown in Figure 3.1 (adapted from [18]) gives the load of the *Hidden Gem* in megawatt electric every minute, giving a good level of detail for the purpose of this project without enormous amounts of data points. The load profile is representative of a typical operational cycle, which comprises three distinct phases:

Day 1-3: Transit On the first three days the ship sails to the mining location. For this the ship consumes between 16 and 18 MW of power on thrusters and hotel load. The load is relatively stable, due to the constant speed of 4 meters per second, with small fluctuations due to changing weather conditions and waves.

Day 4-8: Riser assembly When arrived at the mining location, the riser will be deployed. This operation takes five days with a small peak period at the beginning of day 5 when the collector is deployed. During the riser assembly the demanded load is around 10 MW, with a short peak period up to 14 MW and at the beginning and end of operations a dip in power demand is observed due to the switching of operations.

Day 9-14: Mining During mining the power demand of the ship is highest. Here loads from 30 to 32 MW are requested with peaks of up to almost 35 MW. The ship collects nodules with a speed of 0.5 m/s and turns every 3.5 days resulting in small peaks. Between these turns the ship encounters head wind and the power demands goes up to around 33 MW.

These variations originate from mission-driven equipment loads (collector and riser systems), dynamic positioning, thruster usage, and hotel/auxiliary loads. A summary of the operational phases is given in Table 3.1 to clarify typical power levels and durations.

Table 3.1: Summary of load characteristics during the mission profile

Phase	Duration (days)	Typical Load (MW)	Observed Peaks / Dips (MW)
Transit	1–3	16–18	Small fluctuations (weather-driven)
Riser assembly	4–8	~10	Peak to 14; dips to ~6 (start/end of operation)
Mining	9–14	30–32	Peaks to ~35; mid-cycle rises to ~33

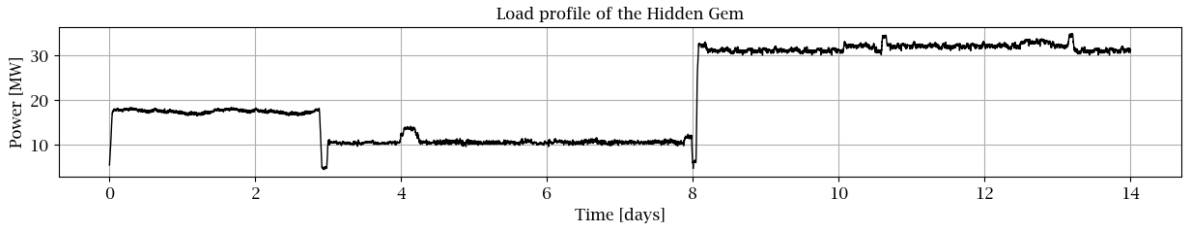

Figure 3.1: Load profile of the Hidden Gem [18]

In the present configuration, the vessel uses six diesel generator sets rated at approximately 7 MW each, resulting in 42 MW total installed electric capacity. This exceeds the peak operational demand of approximately 35 MW, providing redundancy and operational flexibility.

Table 3.2: Measures from the load profile of the Hidden Gem Figure 3.1.

Measure	Value	Unit
$P_{\max}$	34.9	MW
$P_{\max \text{ramp,up}}$	1.55	MW/min
$P_{\min}$	4.32	MW
$P_{\max \text{ramp,down}}$	1.50	MW/min

The standardised HTGR that Allseas is developing will be delivering 25 MW of electrical power output and will be installed on the *Hidden Gem* as the primary power source. Two of the original diesel generators are retained to cover periods of high demand or transient loads that the reactor cannot follow. These generators will only be used when the reactor cannot sustain the load demand of the vessel on its own for a longer period of time, to minimise emissions. In this particular load profile that is only during mining operation.

The fundamental configuration of the power train is illustrated in Figure 3.2. In this power train, the reactor produces heat, which in turn heats the intermediate molten salt (MS) loop, and subsequently the steam in the power cycle (PC). This cycle is then pushed through a turbine generator to produce electricity. The molten salt loop is positioned between the reactor and the power cycle as a design choice by Allseas. This configuration is intended to prevent the transmission of radiation from the reactor to the turbine. It functions as a decoupling mechanism, effectively isolating the reactor from the power cycle and preventing the accumulation of water from the steam cycle within the reactor. The diesel generators are positioned in a separate location to deliver supplementary power to the electrical circuit if required.

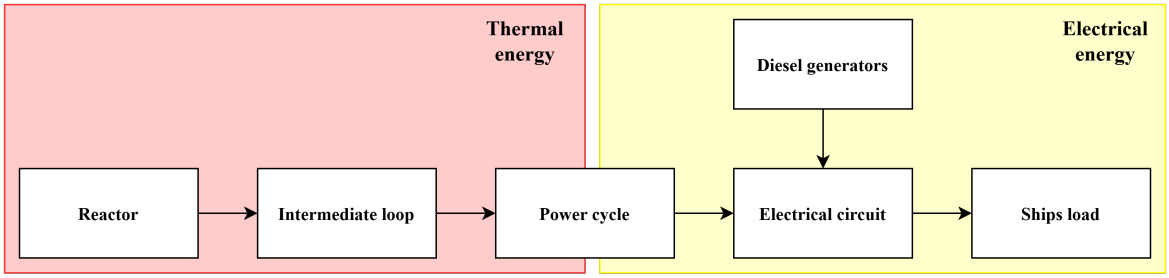

Figure 3.2: Power delivery in the ship

3.2. Power Plant Operational Constraints

The components shown in Figure 3.2 must be modelled with their operational constraints and intended roles within the power-train. This section describes how each component is represented in the simulation environment, the physical and operational limitations imposed on its behaviour, and the inputs and outputs that its model receives and produces. For clarity, each component is accompanied by a flowchart that broadly outlines the computational sequence and provides a concise conceptual overview. These flowcharts are complemented by detailed textual explanations, and each subsection contains tables summarising the model's inputs, outputs, parameters, and constraints. How these components are coupled and work together will be explained in subsection 3.3.1.

The models described in this section and the rest of the report are implemented in Python to allow flexible and transparent representation of component behaviour and control logic. Python enables straightforward implementation of operational constraints, while keeping the model structure modular and easy to modify. In addition, it supports efficient post-processing and visualisation, which are required for the analyses presented in later chapters.

3.2.1. HTGR logic

The High-Temperature Gas-cooled Reactor (HTGR) serves as the primary thermal power source within the hybrid propulsion system. Its dynamic behaviour is fundamentally constrained by reactor physics. As summarised in chapter 2, the response speed of an HTGR is limited by:

- the large thermal inertia of the graphite moderator,
- negative fuel-temperature reactivity feedback,
- limits on control rod insertion and withdrawal rates, and
- allowable axial and radial temperature gradients in fuel and core structures to prevent thermal fatigue.

Detailed transient studies of prismatic and pebble-bed HTGRs report manoeuvrability limits of approximately ±5% of rated power per minute when coolant-flow control is used [6, 7, 28]. These characteristics make it neither physically advisable nor operationally meaningful for the reactor to follow high-frequency fluctuations in the vessel's load demand. While the reactor may be technically capable of responding to a subset of the faster load variations, doing so is undesirable, as it would lead to excessive thermal cycling of the moderator and fuel. Instead, the reactor should track only the slower-varying component of the load profile to preserve long-term operational integrity.

Figure 3.3 shows a broad overview of the code and the inputs and outputs of the code will be summarised in Table 3.3. The rest of this subsection will explain the code and its inputs and outputs in more detail.

Table 3.3: Inputs and outputs of the HTGR reactor model.

Inputs	Symbol	Unit
Thermal or electrical power setpoint	P_{set} / Q_{set}	$\text{kW}_{\text{e/th}}$
Filter strategy (none / MA / EMA)	–	–
Time step	Δt	s
Conversion efficiency	η_{thermo}	–
Outputs	Symbol	Unit
Reactor thermal power	Q_{out}	kW_{th}
Filtered setpoint	Q_{filt}	kW_{th}
Applied ramp rate	ΔQ	$\text{kW}_{\text{th}}/\text{min}$
Saturation flag (min/max limit)	True/False	–

Overview modelling approach

To incorporate these physical constraints in the Python model, the HTGR dynamics and limits are represented through three coupled mechanisms: (i) minimum and maximum thermal power constraints, (ii) ramp-rate limiting and (iii) setpoint filtering. Together, these mechanisms reproduce the manoeuvrability behaviour expected from HTGR literature and operational guidelines [105].

i **Minimum and maximum power constraints** reflect limits due to helium fan limitations, fuel temperature margins, and the power cycle's maximum electrical capacity. When either bound is reached, a saturation flag is recorded.

ii **Ramp-rate limits** impose a hard bound on the maximum permitted change in reactor thermal power per second, consistent with the ±5%/min manoeuvrability range. Which comes from Xenon build up during the ramp-down. When ramping down too fast, the reactor cannot 'burn' the Xenon by ramping up again. The reactor may even shut down due to too much neutrons being absorbed, breaking the chain reaction. This ramp-rate limit is included as an extra safeguard to ensure the reactor never goes over this limit, even though the dynamics of the reactor will keep the ramp-rate lower than this limit.

iii **Setpoint filtering** smooths the requested reactor power and models the thermal inertia of the HTGR core and primary system using a first-order dynamic response between requested and effective reactor thermal power [28]. This smooths high-frequency power requests, enforces physical ramp behaviour, and approximates the thermal response of the reactor without resolving detailed neutronic or spatial thermal dynamics. This approach is usable for control-oriented and grid-coupled studies where system-level flexibility and energy balance are of primary interest [106].

Figure 3.3: Working principle HTGR python model

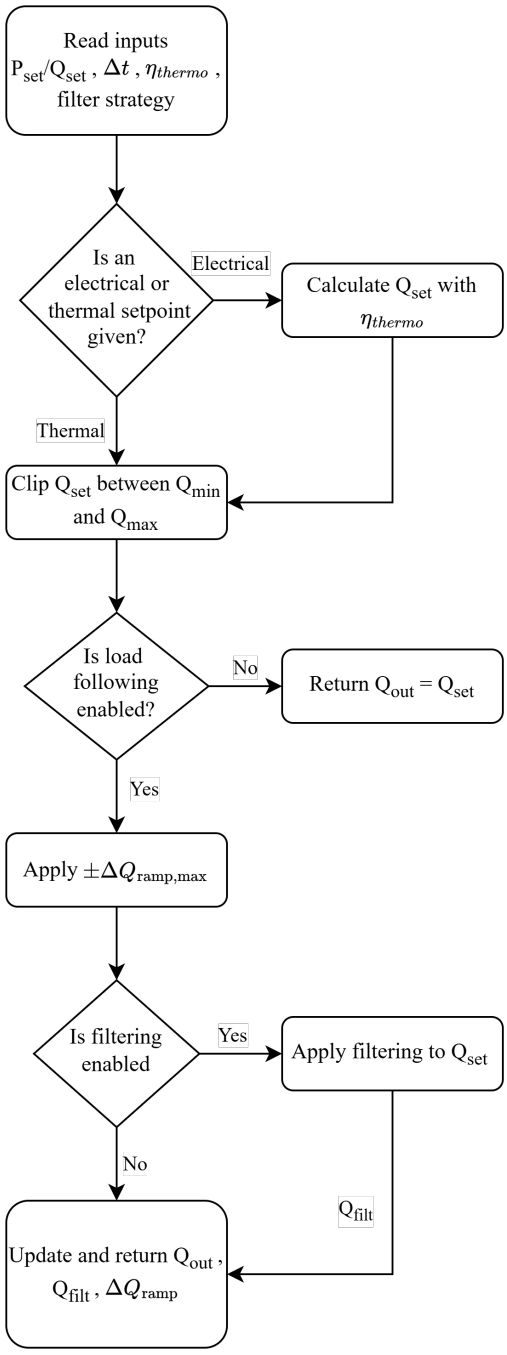

Electrical set point

Since the load profile is expressed in electric power demand while the reactor produces thermal power, an electric setpoint must first be converted into an equivalent thermal request. If a thermal setpoint is not provided directly for testing purposes, the model converts the electric demand using the thermodynamic efficiency η_{thermo}, calculated in subsection 3.2.3, in Equation 3.1 as follows.

$$Q_{\text{set}} = \frac{P_{\text{set}}}{\eta_{\text{thermo}}} \tag{3.1}$$

At each simulation step the reactor receives this thermal setpoint, and the system dynamics are then evaluated. After the power cycle has been solved, the updated efficiency η_{thermo} is stored and used in the next time step for a consistent electric-to-thermal conversion. This approach ensures that the reactor setpoint reflects the instantaneous thermodynamic conditions of the overall plant rather than a fixed nominal efficiency. The resulting thermal power is then constrained within the admissible operating window $[Q_{\text{min}}, Q_{\text{max}}]$, and whenever either boundary is reached the model records a saturation flag which can be used to determine if the diesels should be started. Equation 3.2 shows how the setpoint is clipped. The setpoint will be updated multiple times until it reaches the reactor itself.

$$Q_{\text{set}} = \begin{cases} Q_{\text{min}}, & Q_{\text{set}} < Q_{\text{min}} \\ Q_{\text{set}}, & Q_{\text{min}} \leq Q_{\text{set}} \leq Q_{\text{max}} \\ Q_{\text{max}}, & Q_{\text{set}} > Q_{\text{max}} \end{cases} \tag{3.2}$$

The initial reactor power output will be Q_{min}. It is assumed that at the start of the reviewed load profile the ship is made ready to set sail. However that the reactor will only be operating at its minimum power output to have warmed up the systems and is not yet prepared for any possible load.

Base-load mode

For selected analyses, the model allows a base-load operating mode in which the reactor output is kept constant at the requested setpoint directly, bypassing both ramp-rate limits and setpoint filtering, since the reactor does not change output. This mode can be used for diagnostic and comparison purposes and can be used if different HTGR operation is preferred.

Ramp limit

The requested reactor power is subjected to a ramp-rate constraint that limits how quickly the thermal power output may change. This constraint represents the safety limitations of HTGR load-following behaviour and prevents unsafe power gradients.

At each time step, the requested change in reactor power is computed as the difference between the filtered setpoint and the actual reactor output of the previous time step, as shown in Equation 3.3.

$$\Delta Q_{\text{req}}[k] = Q_{\text{set}}[k] - Q_{\text{out}}[k-1] \tag{3.3}$$

The magnitude of this change is limited by the maximum allowable ramp per time step. This limit is derived from the admissible manoeuvrability γ, expressed as a fraction of nominal power per minute, and the simulation time step Δt. The formula and calculation for the case study vessel are shown in Equation 3.4.

$$\Delta Q_{\max} = \frac{\gamma\, Q_{\text{nom}}}{60}\,\Delta t = \frac{0.05 \cdot 72.5}{60} \cdot 60 = 3.625\,\text{MW}_{\text{th}}/\text{min} \tag{3.4}$$

The applied ramp is obtained by clipping the requested change to the maximum ramp limit:

$$\Delta Q[k] = \begin{cases} -\Delta Q_{\max}, & \Delta Q_{\text{req}}[k] < -\Delta Q_{\max} \\ \Delta Q_{\text{req}}[k], & -\Delta Q_{\max} \le \Delta Q_{\text{req}}[k] \le +\Delta Q_{\max} \\ +\Delta Q_{\max}, & \Delta Q_{\text{req}}[k] > +\Delta Q_{\max} \end{cases} \tag{3.5}$$

Finally, the setpoint for the reactor thermal power output is updated by applying the ramp-limited change, Equation 3.6, and enforcing the operating window bounds, the same way as shown in Equation 3.2.

$$Q_{\text{set}}[k] = Q_{\text{out}}[k-1] + \Delta Q[k] \tag{3.6}$$

If the power bounds prevent the reactor from reaching the setpoint, a saturation flag is raised for that time step.

Setpoint filtering

Two filtering approaches were considered: a simple moving average (SMA) and an exponential moving average (EMA). Although the SMA offers a straightforward finite-window smoothing approach, its abrupt window boundary leads to artificial discontinuities in the filtered setpoint and does not reflect the gradual, inertia-dominated response characteristic of HTGR load-following. The EMA more naturally reflects HTGR behaviour, as HTGR load-follow transients are dominated by strong thermal inertia and long characteristic lag times in the moderator. For this reason, only the EMA is adopted. Rigby et al. [107] and Balestra et al. [6] show that these inertia-driven dynamics govern the transient response of HTGR systems, resulting in gradual, smoothed changes in thermal output, which an EMA captures effectively. The EMA updates the filtered setpoint according to Equation 3.7. In this formula the setpoint ($y[k]$) is determined based on the previous setpoint ($y[k-1]$) and the current requested setpoint ($x[k]$).

$$y[k] = y[k-1] + \alpha\,(x[k] - y[k-1]) \tag{3.7}$$

α determines the sensitivity to new load requests (see Equation 3.8). Unlike the SMA, the EMA implicitly retains information from the signal history and naturally produces the smooth, progressive changes that align with the thermal inertia and moderator-driven dynamics of HTGR systems. Since this smoothing filter makes sure the dynamics of the reactor are simulated more realistic, disabling the filter should only be used as a tool to see what the strict limits of the reactor are.

Time constant selection

To link the setpoint filtering directly to reactor physics, the smoothing factor α is expressed in terms of a time constant τ:

$$\alpha = 1 - e^{-\Delta t/\tau}, \tag{3.8}$$

$$\tau = -\frac{\Delta t}{\ln(1-\alpha)}. \tag{3.9}$$

The characteristic response time of a high-temperature gas-cooled reactor is on the order of several minutes and is dominated by the large thermal inertia of the graphite moderator and primary system, rather than by fast neutronic effects. System-level transient studies of pebble-bed and prismatic HTGR designs show smooth power and temperature evolution during load-following operation, with practical manoeuvrability typically limited to approximately ±5% of nominal power per minute [105, 6, 28, 106].

Based on this behaviour, a time constant of $\tau = 10$ minutes is adopted for the reactor setpoint filter. This corresponds to a 10–90% rise time of $t_{10\text{–}90} \approx 22$ minutes, which is consistent with reported HTGR load-following dynamics and ensures that only the slow-varying component of the ship load is tracked by the reactor. Faster fluctuations are intentionally attenuated to avoid excessive thermal cycling and operation near ramp-rate limits.

The resulting exponential moving-average filter produces smooth, physically realistic setpoint trajectories while limiting unnecessary reliance on auxiliary generation during moderate load changes. A complete history of raw and filtered setpoints, ramp-limited transients, and saturation events is retained for analysis. The reactor parameters and constraints discussed, which are applied in the model are summarised in Table 3.4.

Table 3.4: Parameters, and constraints for the HTGR reactor model.

Reactor parameters	Symbol	Value	Unit
Nominal thermal power	Q_{nom}	72.5	MW_{th}
Initial thermal power	Q_{init}	29	MW_{th}
Default conversion efficiency	η_{default}	0.35	–
Filtering time constant	τ	600	s
Constraints	Symbol	Constraint value	Unit
Minimum reactor power	Q_{min}	$0.40\,Q_{\text{nom}} = 29$	MW_{th}
Maximum reactor power	Q_{max}	$1.00\,Q_{\text{nom}} = 72.5$	MW_{th}
Maximum ramp %/minute	γ	5	%/min
Maximum ramp per minute	ΔQ_{max}	3.625	MW_{th}/min

3.2.2. Intermediate Molten-Salt Loop

The intermediate molten-salt (MS) loop forms a fixed and essential part of the Allseas system architecture. Its purpose is threefold. First, it provides a radiological barrier between the primary helium coolant of the HTGR and the water–steam power cycle. Because the molten salt is non-volatile and chemically stable at high temperature, it prevents transfer of radioactive material to the secondary side and also reduces radiation towards the power cycle by increasing the distance. Second, the salt's high heat capacity and thermal stability introduce beneficial thermal inertia. Short-term fluctuations originating at the reactor or in the power cycle are naturally smoothed as heat is transported through the salt. Third, the intermediate loop creates a physical barrier between the water in the steam cycle and the helium in the primary loop, ensuring no water will enter the primary cycle where it could work as a moderator. The overall configuration of the HTGR, MS loop, and power cycle is shown in Figure 3.4, and Table 3.5 shows the values of the parameters and constraints used in the model.

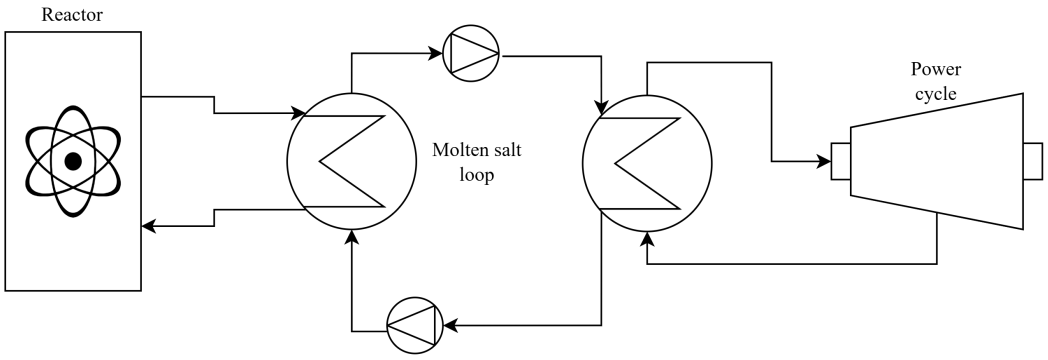

Figure 3.4: Heat-transfer section of the power system, illustrating the placement of the intermediate molten-salt loop.

Table 3.5: Parameters, and constraints of the intermediate molten-salt loop model.

Parameters	Symbol	Value	Unit
Source HX UA	UA_{ch}	0.5	MW/K
Load HX UA	UA_{dis}	0.5	MW/K
Transport delay	t_{delay}	0	s
Salt cold temperature	$T_{\mathrm{c,salt}}$	290	°C
Salt hot temperature	$T_{\mathrm{h,salt}}$	565	°C
Salt density	$\rho(T)$	see Tab. 3.6	kg/m^3
Heat capacity of salt	$c_p(T)$	see Tab. 3.6	kJ/kgK
Constraints	Symbol	Value	Unit
Salt allowable temperature range	T_{min} / T_{max}	260/620	°C
Minimum pinch temperature	ΔT_{min}	5	°C
Maximum mass flow salt	$\dot{m}_{\mathrm{max}}$	180	kg/s

The dynamics of the molten-salt loop are restricted by several physical limits:

- allowable operating temperatures of the salt,
- a minimum pinch temperature in the heat exchangers,
- a maximum permissible molten-salt mass-flow rate,
- and the finite heat-transfer capacity of the heat exchangers.

These restrictions ensure that the system remains within safe and realistic thermodynamic bounds. The Python model incorporates these limits explicitly through a set of thermal constraints applied at each simulation time step. Figure 3.5 shows a broad overview of how the molten salt loop is modelled consisting of heat-exchanger evaluation, limiting constraints, and delayed energy release. Each step will be explained more thoroughly in the rest of this subsection and the inputs and outputs of the model will be summarised in Table 3.7 after the model overview.

Molten-salt properties

The intermediate loop uses standard solar salt, a 60/40 wt% mixture of $NaNO_3$ and KNO_3 [108]. Representative thermophysical properties are listed in Table 3.6. Although the MS loop is not intended to function as a long-duration thermal store, its intrinsic thermal inertia helps buffer short-term disturbances in the power system.

Table 3.6: Thermophysical properties of solar salt (60% $NaNO_3$, 40% KNO_3) used in the molten-salt loop [108].

Property	Representative value range
Operating temperature range	290–565°C
Density	1700–1900 kg/m^3
Specific heat capacity	1.48–1.54 kJ/kgK
Thermal conductivity	0.49–0.55 W/mK
Allowable temperature range	~260–620°C
Freezing point	~220°C

Figure 3.5: Flow chart of the molten-salt loop model.

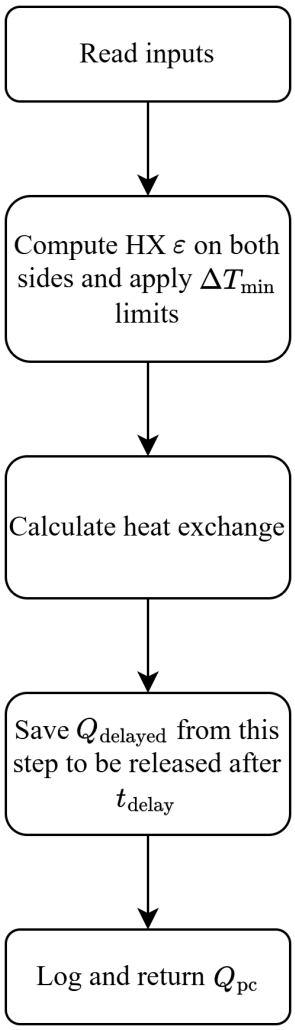

Overview modelling approach

The MS loop is represented as a lumped-parameter thermal system connecting the reactor-side inlet temperature to the power-cycle inlet temperature. At each time step, the model computes the physically allowable heat transfer using standard effectiveness–NTU relations, combined with mass-flow limits, pinch constraints, and operating-temperature bounds. The resulting heat transfer is then passed through a transport-delay buffer, if applied, representing the finite salt transit time between the two heat exchangers (HX).

Consistent with the approach used for the HTGR, this representation aims to capture the main system-level thermal behaviour relevant for long-duration hybrid operation, without modelling detailed thermal-hydraulic processes like pressure drop and fluid mixing. The temperatures at the entrance and exit of the heat exchangers will be assumed constant, meaning change in power throughput will come from adjusted mass flow in the loop. In doing so, the model preserves the essential thermodynamic constraints while remaining computationally efficient for integrated system studies. The reactor-side inlet temperature $T_{\text{hot,in}}$, power-cycle inlet temperature $T_{\text{cold,in}}$, and the molten-salt hot and cold setpoint temperatures $T_{\text{h,salt}}$ and $T_{\text{c,salt}}$ fully define the thermal boundary conditions of the intermediate loop.

The molten-salt loop is modelled using a lumped-parameter approach with fixed exchanger characteristics and simplified transport dynamics. Detailed thermal-hydraulic effects such as axial temperature gradients, pressure losses, and pump dynamics are neglected. The main modelling assumptions are summarised at the end of this subsection.

In this model, all intermediate heat-transfer quantities are denoted by q. The symbol Q_{pc} is reserved for the thermal power delivered to the power cycle after all physical constraints have been applied.

The molten-salt loop model is based on a number of simplifying assumptions that define its intended level of fidelity and applicability:

- The loop is represented as a lumped-parameter thermal system with spatially uniform temperatures during a time step;
- Heat-exchanger outlet temperatures are prescribed design values, and variations in heat transfer are realised through changes in mass flow rate rather than temperature rise;
- Heat-exchanger performance is modelled using fixed overall heat-transfer coefficients (UA) and a constant minimum approach temperature;
- Pressure-drop effects, pump dynamics, and flow-dependent transport delays are neglected;
- The molten-salt loop contains no internal energy storage when thermal energy storage is not enabled.

These assumptions are revisited and discussed in detail at the end of this subsection.

Table 3.7: Inputs and outputs of the intermediate molten-salt loop model.

Inputs	Symbol	Unit
Reactor-side inlet temperature	$T_{\text{hot,in}}$	°C
Power-cycle inlet temperature	$T_{\text{cold,in}}$	°C
Requested discharge power	$Q_{\text{d,req}}$	kW
Time step	Δt	s
Outputs	Symbol	Unit
Delivered heat (current step)	Q_{pc}	kW
Delayed delivered heat	Q_{delayed}	kW
Heat-exchanger effectiveness	ε	–

Input handling

The model receives the requested discharge power $Q_{\text{d,req}}$, inlet temperatures ($T_{\text{hot,in}}$, $T_{\text{cold,in}}$) of the heat exchangers from the reactor and power-cycle sides, and the time step Δt. In the present model configuration, the molten-salt inlet and outlet temperatures ($T_{\text{c,salt}}$ and $T_{\text{h,salt}}$) of both heat exchangers are prescribed and assumed constant over a simulation time step. This represents an idealised operating condition in which temperature control is maintained by upstream reactor and power-cycle systems. Changes in heat transfer are therefore realised exclusively through variations in mass flow rate.

Heat Exchanger Physics

The heat exchangers are modelled using the same counterflow ε–NTU framework commonly applied in high-temperature systems [109, 110, 111]. The basis of heat transfer can be found in Equation 3.10. The amount of heat (Q) is calculated with the mass flow ($\dot{m}$), the heat capacity (c_p) of the fluid and the difference in temperature (ΔT) between in- and outlet. Since this paragraph explains the modelling principles of two heat exchangers the variables may contain subscripts 'hot' and 'cold', which refers to the hotter and colder fluid that passes the heat exchanger. The same equations are applied to both exchangers with different boundary conditions. For the first heat exchanger the hot fluid is the helium from the reactor, for the second it is the salt from the intermediate loop. And for the second heat exchanger the salt from the intermediate loop is the hot fluid and the steam from the power cycle is the cold medium.

$$Q = \dot{m} \cdot c_p \cdot \Delta T \tag{3.10}$$

However, not all the heat present in the inlet stream of a heat exchanger is effectively transferred to the other fluid, for the amount of heat transferred there are some limiting factors which are explained in this paragraph. At each time step, the physically achievable heat-transfer rate is constructed by calculating heat-exchanger effectiveness, pinch-point constraints, and mass flow capacity limits separately to see which is the limiting factor of heat transfer and thus how much heat is transferred between the mediums by taking the heat transfer from the limiting factor.

First the heat exchanger counterflow effectiveness, for this the heat-capacity rate of each stream can be calculated with Equation 3.11. After this calculation of both streams that go into the heat exchanger, the lowest heat-capacity rate determines the heat exchange and is denoted C_{min}.

$$C = \dot{m}\, c_p, \tag{3.11}$$

Jiang et al. [112] report an implied overall heat transfer capacity (UA) of approximately 0.15 MW/K for a 10 MW molten-salt heat exchanger operating at a log-mean temperature difference of 68 K. In this study, a maximum heat rate of 72.5 MW is considered with a temperature difference of approximately 275 K, resulting in a minimum required heat transfer capacity of 0.26 MW/K. A larger value of 0.5 MW/K is adopted to ensure heat-transfer resistance does not dominate system dynamics. The exact value for the overall heat transfer capacity can be implemented when the heat exchangers are designed for the system.

With the heat transfer capacity (UA), the counterflow effectiveness can be calculated using Equation 3.12.

$$\varepsilon = \frac{1 - \exp[-\text{NTU}(1 - C_r)]}{1 - C_r \exp[-\text{NTU}(1 - C_r)]}, \quad \text{with} \quad \text{NTU} = \frac{UA}{C_{\text{min}}}, \quad \text{and} \quad C_r = \frac{C_{\text{min}}}{C_{\text{max}}}. \tag{3.12}$$

The resulting effectiveness-limited heat-transfer rate (q_ε) between streams, Equation 3.13, is determined with the effectiveness (ε), lowest heat-capacity rate (C_{min}) of the streams and the difference between inlet temperatures.

$$q_\varepsilon = \varepsilon\, C_{\min}(T_{\text{hot,in}} - T_{\text{cold,in}}) \tag{3.13}$$

A second, independent limiting mechanism is the pinch-point constraint, which prevents temperature crossover between streams by enforcing a minimum approach temperature, this is shown in Equation 3.14. The temperature $T_{\text{cold,set}}$ denotes the prescribed outlet temperature of the cold-side fluid. In the present lumped-parameter model, heat-exchanger outlet temperatures are not solved dynamically, the molten-salt hot and cold temperatures are fixed design values, and variations in heat transfer are accommodated through changes in mass flow rate. The pinch constraint therefore limits the transferred heat such that the assumed cold-side outlet temperature does not violate the minimum approach temperature $\Delta T_{\min}$.

$$q_{\text{pinch}} = C_{\text{cold}}\left[(T_{\text{hot,in}} - \Delta T_{\min}) - T_{\text{cold,set}}\right]^+ \tag{3.14}$$

Here, $[\cdot]^+$ denotes the positive-part operator, such that $[x]^+ = \max(x,0)$, ensuring that no heat transfer is permitted when the minimum approach temperature would be violated. This expression limits the transferred heat such that the cold-side outlet temperature never exceeds the hot-side inlet temperature minus the minimum allowed approach difference $\Delta T_{\min}$, called pinch temperature, thereby preventing temperature crossover within the heat exchanger. The design temperatures $T_{\text{hot,in}}$ and $T_{\text{cold,set}}$ are inputs every time step and the minimum pinch can be found in Table 3.5. In the pinch constraint, the heat-capacity rate of the colder stream (C_{cold}) is used, corresponding to the limiting side of the heat exchanger at the point of minimum temperature difference.

A third limit arises from the maximum salt circulation rate, calculated as the heat transfer limit in Equation 3.15. Where the maximum mass flow ($\dot{m}_{max}$) is put in to calculate the constraint of maximum heat that can be in the fluid. The simplified formula is added to make an estimate of this maximum salt mass flow.

$$q_{\text{mass}} = \dot{m}_{\max} \int_{T_{\text{c,salt}}}^{T_{\text{h,salt}}} c_p(T)\,\mathrm{d}T \approx \dot{m}_{\max}\,\overline{c_p}\,(T_{\text{h,salt}} - T_{\text{c,salt}}) \tag{3.15}$$

Since the purpose of this research is to model the total power system on a nuclear ship, the limit on mass flow is set just above the mass flow that the salt needs to have to transfer the maximum amount of heat coming from the reactor, since the pumps are the determining factor for this and these can be chosen accordingly. Equation 3.16 shows an estimate of the salts mass flow to accommodate the transfer of the maximum heat output of the reactor, the average specific heat capacity between the MS loop hot and cold temperature is denoted $\overline{c_p}$ and the maximum mass flow is rounded up to be used as a limit, the value can be found in Table 3.5

$$\dot{m}_{\max} \approx \frac{Q}{\overline{c_p}\cdot\Delta T} = \frac{72.5\cdot 10^6}{1516.4\cdot(565-290)} = 173.86\,\text{kg/s} \tag{3.16}$$

The last factor is the amount of heat output requested, $q_{\text{request}} = Q_{\text{d,req}}$. The final heat-transfer rate is obtained by taking the minimum over all heat transferring limits and the requested heat transfer, Equation 3.17. At each time step, the active limiting mechanism is identified by comparing the individual bounds, allowing post-processing diagnostics of whether heat transfer is limited by exchanger effectiveness, minimum pinch, mass-flow capacity, or external demand.

$$q = \min(q_\varepsilon,\, q_{\text{pinch}},\, q_{\text{mass}},\, q_{\text{request}}) \tag{3.17}$$

The resulting heat-transfer rate, the heat-transfer from the limiting factor, represents the thermal power made available to the power cycle during the current time step:

$$Q_{\text{pc}}[k] = q[k] \tag{3.18}$$

Transport delay

Because the molten salt must physically travel between the reactor-side heat exchanger and the steam-side heat exchanger, heat absorbed at one end becomes available only after a certain transport time [113, 114]. However, compared to the thermal inertia of the reactor this transport delay will be much smaller and also smaller than the time step in this model [112]. To keep the option open to add a delay in the delivered heat

due to salt travel time when designing the full system in detail, there is a possibility to add a fixed delay t_{delay}. The delayed heat release further decouples the HTGR from high-frequency changes in steam demand and is especially important in short transients.

When enabled, the transport delay is implemented as a discrete time shift, such that the delivered power becomes:

$$Q_{\text{pc}}[k] = Q_{\text{delayed}}[k - n_{\text{delay}}], \quad \text{with} \quad n_{\text{delay}} = \frac{t_{\text{delay}}}{\Delta t} \tag{3.19}$$

Detailed discussion of modelling assumptions

The following paragraphs provide a detailed justification of the modelling assumptions summarised earlier, explaining their physical motivation and implications for model accuracy. The molten-salt loop model relies on several simplifying assumptions that reduce computational complexity while preserving the essential system-level behaviour of the MS loop. These assumptions define which physical processes are captured explicitly and which are treated in a simplified manner:

- **Lumped-parameter representation:** The molten-salt temperature and flow are treated as spatially uniform values during a time step. Axial temperature gradients, mixing zones, and local difference in density are not resolved, as the model aims to capture net heat transport rather than detailed thermal-hydraulics.

- **Constant minimum approach temperature ΔT_{min}:** The pinch-point limit in both heat exchangers is implemented using a fixed approach temperature. Although real heat exchangers may exhibit varying pinch behaviour under different flow or fouling conditions, a constant ΔT_{min} provides a simplified, stable and transparent constraint.

- **No fouling or degradation:** Time-dependent reductions in heat-transfer performance due to fouling, corrosion, or salt impurities are neglected. These effects evolve slowly relative to the dynamic time scales studied here and would not meaningfully influence the short-term thermal behaviour.

- **Fixed UA values:** Both heat exchangers use constant overall heat-transfer coefficients (UA). Variations of UA with flow rate, temperature, or material ageing are ignored, lowering the accuracy of the model while allowing the NTU–ε formulation to remain analytically tractable. The UA values of 0.5 MW/K are intentionally chosen high enough that the heat exchanger is rarely the limiting factor under normal operation and can be changed when the full system is designed in detail.

- **Constant transport delay:** The time required for the molten salt to travel between the primary and secondary heat exchangers is not used, since it is negligible with the time steps used. If this transport delay would be used in following system, the delay is modelled as a fixed time. Although real transport delay depends on flow rate, a constant value provides numerical stability and captures the essential decoupling between the reactor and the power cycle, but misses the coupling with mass flow rate.

- **No pressure-drop or pumping-power constraints:** The model assumes that the required salt mass flow can always be achieved without exceeding pump limits or incurring significant pressure losses. Because the full system is not designed yet, this model simulates an ideal working molten salt loop to give an insight into the whole system.

This set of assumptions enables the model to capture the primary heat-transfer behaviour and dynamic interaction between the reactor and the power cycle, while maintaining computational efficiency suitable for full-voyage, long-duration simulations even though missing accuracy on complex points of the system.

3.2.3. Power Cycle

After heat is transferred from the molten-salt loop to the steam circuit, the working fluid is expanded through a turbine to generate electricity. The power cycle is modelled using a load-dependent thermodynamic efficiency map which is shown in Figure 3.7. Figure 3.6 shows the broad computational structure of the model and Table 3.8 summarises the inputs and outputs of the model.

Overview modelling approach

The power cycle is modelled as a static thermal-to-electric conversion unit with load-dependent efficiency and explicit operational constraints. At each simulation time step, the model converts the incoming thermal power into electrical power using an interpolated efficiency curve, applies capacity limits and auxiliary consumption, and enforces a maximum ramp rate on the net electrical output.

The conversion efficiency is expressed as a function of the thermal power entering the steam cycle. The fitted efficiency curve used for interpolation will be discussed further in the next paragraph.

Table 3.8: Inputs and outputs of the power-cycle model.

Inputs	Symbol	Unit
Thermal heat input	$Q_{\text{pc,in}}$	kW_{th}
Efficiency curve	$Q_{\text{pts}}, \eta_{\text{pts}}$	–
System power consumption	P_{sys}	kW_{e}
Time step	Δt	s
Outputs	Symbol	Unit
Gross electric power	P_{gross}	kW_{e}
Net electric power	$P_{\text{pc,out}}$	kW_{e}
Instantaneous efficiency	η_{thermo}	–

Efficiency modelling

At every simulation step, the thermal-to-electric efficiency η_{thermo} is obtained by linearly interpolating the static efficiency curve as a function of the thermal input $Q_{\text{th,in}}$. The efficiency curve used in this work is based on representative performance of marine-scale Rankine-cycle turbines, which reach approximately 38% efficiency at full load [115, 116, 117, 118]. The efficiency curve is only valid for normal turbine operation above a minimum thermal input. At very low load, steam turbines experience severe off-design effects such as flow separation, windage losses, and vanishing work output in the low-pressure stages. Experimental and numerical studies report that continuous operation below approximately 30–40% of rated load is not representative of steady-state turbine performance [115, 116, 117]. Below a minimum thermal input of 30%, $Q_{\text{th,min}}$, the turbine is therefore assumed to be offline and produces no electrical power. This gives the gross electrical output as shown in Equation 3.20.

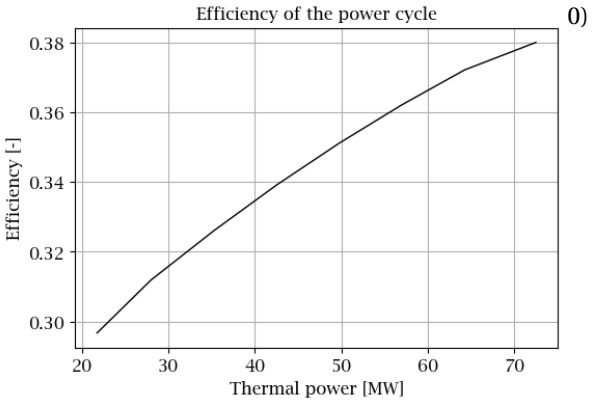

Figure 3.7: Load-dependent efficiency of the power cycle.

0)

Figure 3.6: Working principle of the power-cycle model.

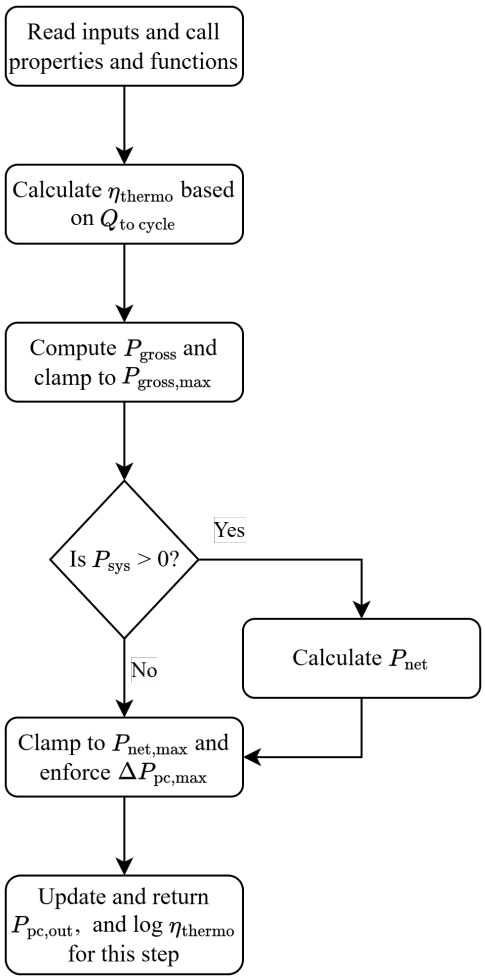

This electrical output is then capped at the maximum generator rating of 27.5 MW_e ($P_{gross,max}$), a design choice specified by Allseas. A constant auxiliary consumption of 2.5 MW_e represents loads such as pumps, control systems, and cooling fans. In the present model, auxiliary power consumption is treated as a constant, although the formulation allows it to be extended to a load-dependent value in future system studies. For this first estimate of the system it is kept constant at $P_{sys} = 2.5\ MW_e$. The resulting net electrical output is capped at $P_{net,max}$.

$$P_{net} = P_{gross} - P_{sys} \tag{3.21}$$

Ramp-rate limitation

The turbine is assumed to operate at constant rotational speed, as required for synchronous operation with the ship's electrical grid. Under constant-speed operation, electrical frequency is fixed, and changes in power output are achieved by adjusting the steam mass flow rather than shaft speed.

As a result, the power cycle itself can become a limiting component on the thermal side of the system. Although the reactor is constrained to a maximum ramp rate of 5% per minute, the turbine is subject to a similar limitation of 5% per minute of its rated power output based on nuclear reactor standards [119]. When a thermal energy storage system is installed, reactor ramp-rate limits alone are insufficient to guarantee safe turbine operation, as stored thermal energy can bypass reactor inertia and impose faster transients on the power cycle. An explicit ramp-rate constraint is therefore imposed within the power-cycle model to protect turbine integrity and ensure stable grid operation.

To represent this operational constraint, the rate of change of the net electrical output is limited. The maximum allowable ramp rate of the power cycle is defined as a fraction γ_{pc} of the rated net power per minute. The maximum permissible change in net electrical power per time step is:

$$\Delta P_{pc,max} = \frac{\gamma_{pc} P_{net,max}}{60} \Delta t = \frac{0.05 \cdot 25.0}{60} \cdot 60 = 1.25\,MW_e/min \tag{3.22}$$

The requested change in net electrical power is given by:

$$\Delta P_{req}[k] = P_{net}[k] - P_{pc,out}[k-1] \tag{3.23}$$

P_{net} denotes the unconstrained net electrical output at the current time step prior to ramp-rate limitation. The applied change is then obtained by clipping the requested change to the admissible ramp range:

$$\Delta P_{pc}[k] = \begin{cases} -\Delta P_{pc,max}, & \Delta P_{req}[k] < -\Delta P_{pc,max} \\ \Delta P_{req}[k], & -\Delta P_{pc,max} \le \Delta P_{req}[k] \le +\Delta P_{pc,max} \\ +\Delta P_{pc,max}, & \Delta P_{req}[k] > +\Delta P_{pc,max} \end{cases} \tag{3.24}$$

Finally, the net electrical output of the power cycle is updated as:

$$P_{pc,out}[k] = P_{pc,out}[k-1] + \Delta P_{pc}[k] \tag{3.25}$$

For this subsystem the heat losses through piping are not taken into account since the intermediate loop has all the calculations for the heat in this part of the system, including the thermal losses due to isolation. Table 3.9 shows the parameters, and constraints of the power-cycle model.

Table 3.9: Parameters, and constraints of the power-cycle model.

Parameters and Constraints	Symbol	Value	Unit
Maximum gross electric output	$P_{gross,max}$	27.5	MW_e
Maximum net electric output	$P_{net,max}$	25.0	MW_e
Maximum ramp %/min	γ_{pc}	5	%/min
Maximum ramp rate per minute	$\Delta P_{pc,max}$	1.25	MW_e/min

3.2.4. Diesel generator logic

The diesel generator system provides auxiliary electrical power when the reactor and power cycle are unable to meet the vessel's instantaneous load demand. It consists of two hierarchical components: (i) the behaviour of an individual diesel generator unit, and (ii) the overall diesel-plant dispatch logic that determines how multiple units are started, stopped, and load-shared. The operating principles of a single diesel unit are shown in Figure 3.9, and the complete diesel plant control logic is illustrated in Figure 3.10.

The diesel generators are not intended to follow rapid fluctuations. Instead, they compensate for medium- to long-duration deficits when the reactor approaches its ramp-rate or maximum-power limits, or when the power cycle saturates. In the hybrid power system the diesel plant therefore acts as a reliability mechanism rather than a primary load-following asset. This choice reflects the diesel fuel consumption and thus emissions, mechanical wear associated with frequent diesel load changes, as well as the slower start-up and ramping behaviour of diesel generators compared to an electrically driven subsystem.

A key component of the diesel-plant logic is the headroom criterion that determines when diesel generators are permitted to start. The controller compares the current power-cycle output with the maximum attainable electrical output of the reactor–steam-cycle combination. Only when the power cycle approaches its upper production limit, leaving less than 500 kW of reactor headroom ($\Delta P_{\text{headroom}}$), are diesel units allowed to start. This prevents unnecessary diesel operation in situations where the reactor could still carry the load, even if more slowly, and ensures that nuclear power is prioritised over fossil-fuel generation. This operating principle aligns with the overarching objective of minimising emissions from the propulsion system, by deploying diesel generation only when the nuclear plant is genuinely at its operational limit.

Overview modelling approach

The diesel generator system is modelled using a discrete-time, control-oriented approach. Individual diesel units are represented as finite-state machines with explicit start-up, ramp-rate, and load constraints, while the diesel plant layer coordinates unit commitment and load allocation based on system-level power deficits. The model is intended to capture operational behaviour and fuel consumption trends rather than detailed combustion or engine dynamics.

Diesel generator unit model

Each diesel generator (DG) unit is described by a small set of internal state variables and external inputs. The primary state variables are the operational state (*OFF, STARTING, RUNNING*), the delivered electrical power, and the elapsed time within the current state. The only external input to an individual unit is the requested electrical power setpoint.

Each diesel generator unit is modelled as a finite-state machine with three possible operational states:

- **OFF** — engine shut down, no fuel consumption;
- **STARTING** — engine igniting and accelerating towards minimum load;
- **RUNNING** — engine delivering electrical power.

State transitions are governed by the applied power setpoint of the unit $P_{\text{set,i}}$ and the elapsed start-up time, as shown in Table 3.10.

Table 3.10: State transitions of a diesel generator unit

Current state	Next state	Condition
OFF	STARTING	$P_{\text{set,i}} > 0$
STARTING	RUNNING	$t_{\text{state}} \geq t_{\text{start}}$
RUNNING	OFF	$P_{\text{set,i}} \to 0$

When a positive power setpoint is issued to a diesel generator that is currently off, the unit transitions to the *STARTING* state. During start-up the engine ramps towards its minimum operating power over a fixed start-up time, and a one-time fuel penalty is applied to represent enrichment, inefficient combustion, and auxiliary loads during engine ignition and acceleration. No electrical power is delivered in this state, but some fuel is consumed as the engine accelerates towards idle.

The magnitude of the start-up fuel penalty is chosen as a conservative, order-of-magnitude estimate consistent with short-duration idling and start-up fuel usage reported for medium-speed marine diesel generators, and its influence on long-duration energy balances is negligible.

Fuel consumption is state-dependent. In the *OFF* state no fuel is used. During the *STARTING* state, the engine consumes fuel until it reaches its minimum stable load. Once in the *RUNNING* state, fuel use follows a load-dependent simplified specific fuel consumption (SFC) curve, shown in Figure 3.8a where efficiency increases as the load fraction approaches roughly 80% of nominal power and decreases again at near-maximum loads. This behaviour is embedded directly in the model to give estimates of fuel usage across the entire operating envelope and can be updated with a detailed SFC function if available. The total amount of fuel use per hour for steady operation is shown in Figure 3.8b.

Fuel consumption during steady operation is calculated using the load-dependent specific fuel consumption (SFC) function which is expressed in units of g/kWh and converted internally to kg/h for consistency with the time step. The power input for this formula ($P_{\mathrm{DG},i}$ is expressed in kW.

$$\dot{m}_{\mathrm{fuel},i} = \frac{\mathrm{SFC}}{1000} P_{\mathrm{DG},i} \tag{3.26}$$

The fuel consumed during one simulation step is then:

$$\Delta m_{\mathrm{fuel},i} = \dot{m}_{\mathrm{fuel},i} \frac{\Delta t}{3600} \tag{3.27}$$

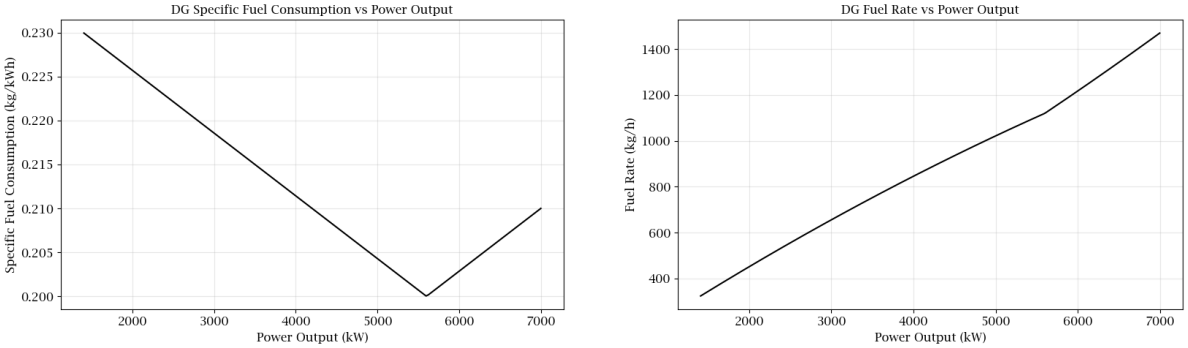

(a) Diesel specific fuel consumption against power output

(b) Diesel fuel rate as a function of power output

Figure 3.8: Diesel fuel consumption measures per engine dependent on power output

Once the start-up time has elapsed, the generator transitions to the *RUNNING* state. In this state the delivered electrical power is subject to:

- minimum and maximum permissible load ($P_{\mathrm{DG,min}}$ and $P_{\mathrm{DG,max}}$) per unit,
- ramp-rate limitations expressed as a fraction of nominal power per minute, and
- the load-dependent specific fuel consumption characteristics.

Table 3.11: Inputs and outputs of an individual diesel generator unit.

Inputs (diesel unit)	Symbol	Unit
Generator power setpoint	$P_{\mathrm{set,i}}$	kW
Outputs (diesel unit)	Symbol	Unit
Electrical power output	$P_{\mathrm{DG,i}}$	kW
Fuel mass this step	$\Delta m_{\mathrm{fuel,i}}$	kg
Cumulative fuel consumption	$m_{\mathrm{fuel,tot,i}}$	kg

The electrical output of a running diesel generator is limited by a maximum permissible ramp rate. The maximum permissible ramp rate, expressed as an equivalent change per simulation time step, is given by Equation 3.28, where also the maximum permissible ramp rate is calculated for Table 3.12.

$$\Delta P_{\mathrm{DG,max},i} = \frac{\gamma_{\mathrm{DG}} P_{\mathrm{nom}}}{60} \Delta t = \frac{0.5 \cdot 7}{60} \cdot 60 = 3.5\,\mathrm{MW_e/min} \tag{3.28}$$

Figure 3.9: Operating principle of one diesel generator unit.

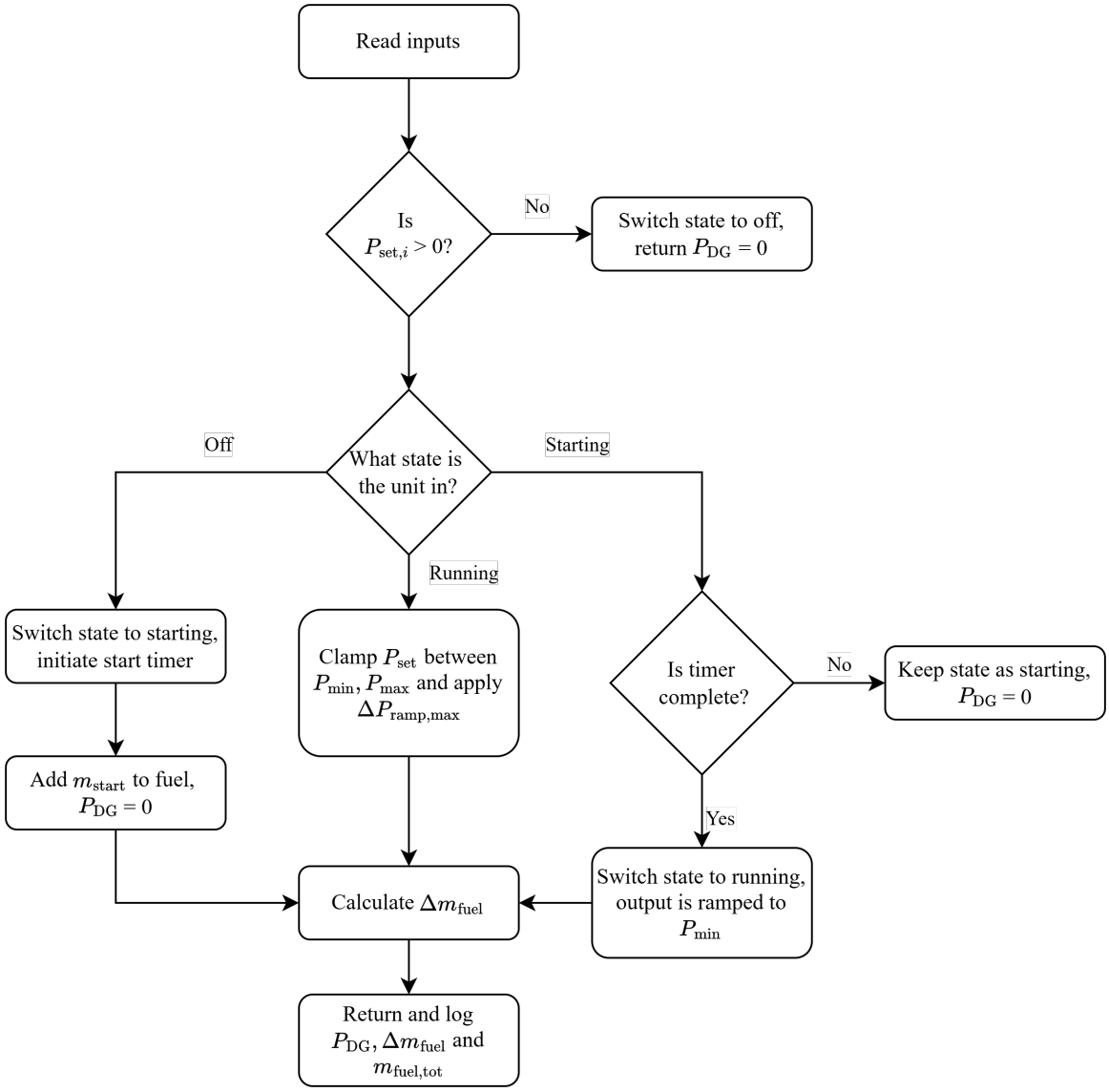

The applied power change is obtained by clipping the requested change:

$$\Delta P_{\mathrm{DG,req},i}[k] = P_{\mathrm{set,i}}[k] - P_{\mathrm{DG,i}}[k-1] \tag{3.29}$$

$$\Delta P_{\mathrm{DG},i}[k] = \begin{cases} -\Delta P_{\mathrm{DG,max},i}, & \Delta P_{\mathrm{DG,req},i}[k] < -\Delta P_{\mathrm{DG,max},i} \\ \Delta P_{\mathrm{DG,req},i}[k], & -\Delta P_{\mathrm{DG,max},i} \le \Delta P_{\mathrm{DG,req},i}[k] \le +\Delta P_{\mathrm{DG,max},i} \\ +\Delta P_{\mathrm{DG,max},i}, & \Delta P_{\mathrm{DG,req},i}[k] > +\Delta P_{\mathrm{DG,max},i} \end{cases} \tag{3.30}$$

The ramp-limited power change is then applied to the electrical output of the previous time step to obtain the tentative generator output, Equation 3.31. This ensures that the diesel generator output evolves continuously in time and never exceeds the permissible ramp-rate constraint. Equation 3.32 shows the minimum allowable power output.

$$P_{\mathrm{DG},i}[k] = P_{\mathrm{DG,i}}[k-1] + \Delta P_{\mathrm{DG},i}[k] \tag{3.31}$$

$$P_{\mathrm{DG,min}} = P_{\mathrm{min,frac}} P_{\mathrm{nom}} = 0.2 \cdot 7 = 1.4\,\mathrm{MW_e} \tag{3.32}$$

Minimum and maximum load fractions are imposed through the clipping operation in Equation 3.33 to reflect stable diesel engine operation. Operation below approximately 20%, $P_{\text{min,frac}}$, of nominal power is avoided due to incomplete combustion, wet stacking, and accelerated engine degradation, while sustained operation above nominal rating is not permitted to prevent thermal and mechanical overloading.

$$P_{\text{DG},i}[k] = \begin{cases} P_{\text{DG,min}}, & P_{\text{DG,i}}[k] < P_{\text{DG,min}} \\ P_{\text{DG,i}}[k], & P_{\text{DG,min}} \leq P_{\text{DG,i}}[k] \leq P_{\text{DG,max}} \\ P_{\text{DG,max}}, & P_{\text{DG,i}}[k] > P_{\text{DG,max}} \end{cases} \tag{3.33}$$

Fuel consumption for each time step is logged, together with cumulative fuel usage and instantaneous electrical output which is subjected to the minimum and maximum power and ramp rate.

When the diesel setpoint falls to zero, the unit ramps down at its permitted rate. If the power reduces to near zero, the model transitions the unit back to the *OFF* state. If a shutdown occurs while the unit is still in the *STARTING* phase, the start-up process is aborted and the engine immediately returns to *OFF*. This behaviour prevents unnecessary fuel expenditure and reflects the operational response of marine diesel generators when load demand disappears.

Table 3.11 and 3.12 summarises the principal parameters, limitations, inputs and outputs of a single diesel generator unit. Next to this the state of the individual units is needed to determine the power output and fuel consumption.

Table 3.12: Parameters and constraints of an individual diesel generator unit.

Parameters and constraints (diesel unit)	Symbol	Value	Unit
Nominal generator rating	P_{nom}	7	MW
Minimum load	$P_{\text{DG,min}}$	1.4	MW
Maximum load	$P_{\text{DG,max}}$	7	MW
Maximum ramp %/min	γ_{DG}	50	%/min
Maximum ramp rate per minute	$\Delta P_{\text{DG,max},i}$	3.5	MW/min
Start-up time	t_{start}	60	s
Start-up fuel penalty	m_{start}	5	kg

Diesel plant control logic

While individual units enforce their own operating constraints, the diesel plant determines how many generators are active and how load is shared among them. The plant monitors:

- the vessel load demand, and
- the electrical power delivered by the reactor and power cycle.

If the power cycle can still meet the load within the available reactor headroom, all diesel units remain off. Once the reactor approaches its maximum output by $\Delta P_{\text{headroom}}$, or the residual load increases, the plant begins its dispatch procedure. The overall structure is shown in Figure 3.10.

To avoid rapid on/off cycling of diesel units, the residual load is passed through an exponential smoothing filter with a time constant of $\tau_{\text{trend}} = 180$ s. This filtering suppresses short-duration load transients that can be absorbed by the ESS, while still allowing the diesel plant to respond to sustained power deficits.

The requested aggregated diesel power, $P_{\text{DG,req}}[k]$, is defined as the total diesel power required to cover the residual electrical load after application of the reactor headroom criterion and residual-load filtering, but prior to enforcement of the plant-level ramp-rate limit.

Although each diesel generator enforces its own ramp-rate limit, the simultaneous start-up or load increase of multiple units would otherwise allow the aggregated diesel output to change faster than is realistic for a coordinated plant-level controller. A plant-level ramp-rate constraint is therefore imposed to represent supervisory control actions that stagger unit loading and limit total power transients. The plant ramp limit is simply calculated by adding the ramp limits of the individual generator units.

The maximum allowable change in aggregated diesel output is:

$$\Delta P_{\text{DG,max}} = \sum_{i=1}^{k} \Delta P_{\text{DG,max},i} \tag{3.34}$$

The aggregated diesel power request is subjected to a plant-level ramp-rate constraint to prevent unrealistically steep power changes when multiple units ramp simultaneously. The requested change in total diesel output is defined as:

$$\Delta P_{\mathrm{DG,req}}[k] = P_{\mathrm{DG,req}}[k] - P_{\mathrm{DG}}[k-1] \tag{3.35}$$

$$\Delta P_{\mathrm{DG}}[k] = \begin{cases} -\Delta P_{\mathrm{DG,max}}, & \Delta P_{\mathrm{DG,req}}[k] < -\Delta P_{\mathrm{DG,max}} \\ \Delta P_{\mathrm{DG,req}}[k], & -\Delta P_{\mathrm{DG,max}} \le \Delta P_{\mathrm{DG,req}}[k] \le \Delta P_{\mathrm{DG,max}} \\ +\Delta P_{\mathrm{DG,max}}, & \Delta P_{\mathrm{DG,req}}[k] > \Delta P_{\mathrm{DG,max}} \end{cases} \tag{3.36}$$

$$P_{\mathrm{DG}}[k] = P_{\mathrm{DG}}[k-1] + \Delta P_{\mathrm{DG}}[k] \tag{3.37}$$

The desired diesel power is then allocated to individual units using a fuel-optimal dispatch strategy inspired by Barone's method [120]. For a given number of active generators, all but the last unit are assigned a fixed operating point near 80% of nominal power, corresponding to the region of lowest specific fuel consumption. The final unit supplies the remaining load, bounded by its minimum and maximum permitted output. The controller evaluates all feasible combinations of one to i active generators and selects the one with the lowest estimated total fuel consumption.

$$\Delta m_{\mathrm{fuel,tot}} = \sum_i \Delta m_{\mathrm{fuel},i} \tag{3.38}$$

Each unit is then advanced one time step according to its individual state, and both per-unit and total fuel usage are recorded by adding the individual fuel usage like Equation 3.38. Table 3.13 summarises the inputs and outputs the diesel plant, and Table 3.14 shows the values of the diesel parameters and constraints.

Figure 3.10: Flow chart of the diesel plant model logic.

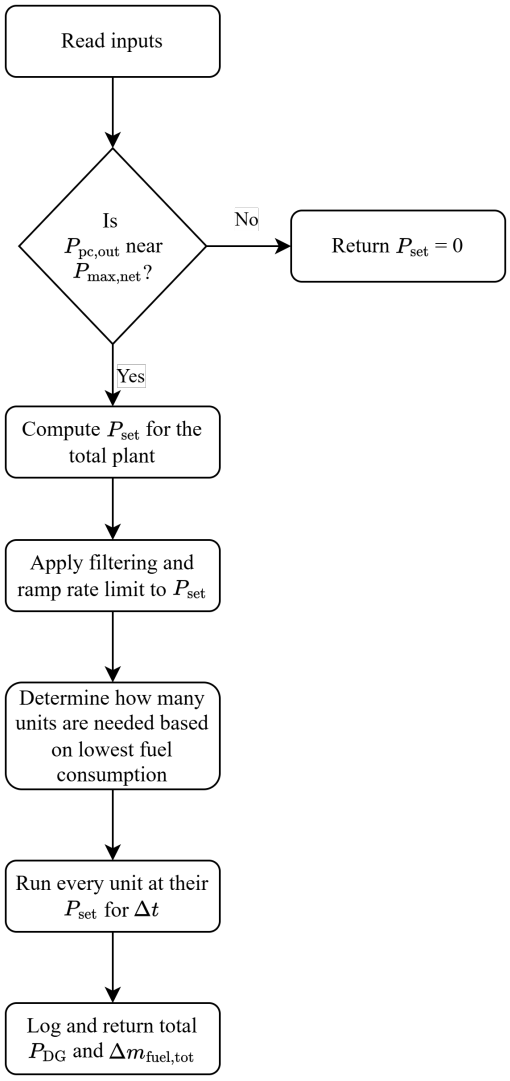

Table 3.13: Inputs and outputs of the diesel plant model.

Inputs (diesel plant)	Symbol	Unit
Requested load to cover	P_{req}	kW
Power-cycle electric output	$P_{\mathrm{pc,out}}$	kW
Reactor electric equivalent	P_{reactor}	kW
Outputs (diesel plant)	Symbol	Unit
Total diesel output power	P_{DG}	kW
Per-unit delivered power	$P_{\mathrm{DG},i}$	kW
Fuel consumption this step	$\Delta m_{\mathrm{fuel,tot}}$	kg
Cumulative fuel consumption	$m_{\mathrm{fuel,tot}}$	kg

Table 3.14: Parameters and constraints of the diesel plant dispatch model.

Parameters and constraints	Symbol	Value	Unit
Trend filter time constant	τ_{trend}	180	s
Plant ramp limit	$\Delta P_{\text{plant,max}}$	120	kW/s
Total number of diesel units	k	2	–
Reactor headroom for diesel start	$\Delta P_{\text{headroom}}$	500	kW
Individual unit bounds	$P_{\min} \leq P_i \leq P_{\max}$	–	kW
Start-up requirement	t_{start}	60	s

3.3. Power Mismatch Analysis and ESS requirements

To see what characteristics and power distribution is required from the ESS, the current possibilities and failures of the system need to be checked. First the energy management system will be explained where the components described above will be put together to an energy system. With this energy management tool the system will be tried to determine the mismatch between the power system and the load profile.

3.3.1. Component Coupling and Power Balance

This subsection describes how the reactor, molten-salt loop, power cycle, and diesel generators, depicted in Figure 3.2, are coupled and coordinated during each simulation time step in the absence of active energy storage. This model part is called the basic Ship Energy Management (SEM). The objective is to maintain power balance while respecting the operational constraints of each subsystem. This model will step by step execute the models of the individual components and ensure input and output between systems are aligned. A flow chart with broad computational steps can be found in Figure 3.11 and will be supported by text and equations.

At each discrete simulation time step k, the basic Ship Energy Management executes all subsystems, parameters and efficiency maps are treated as constant within a single simulation time step, and no iterative convergence is performed within a step.

The ship electrical load request $P_{\text{load}}[k]$ is read from the load profile. The reactor is treated as the primary power source and receives an electric-equivalent power setpoint equal to the ship load plus auxiliary consumption, Equation 3.39. Which is limited to the maximum electrical output of the system, $P_{\text{gross,max}}$. This setpoint represents a desired electrical output and may not be fully achieved due to reactor ramp-rate and power limits enforced within the HTGR model, subsection 3.2.1, or the power cycle subsection 3.2.3.

Figure 3.11: Flow chart of the basic Ship Energy Management model logic.

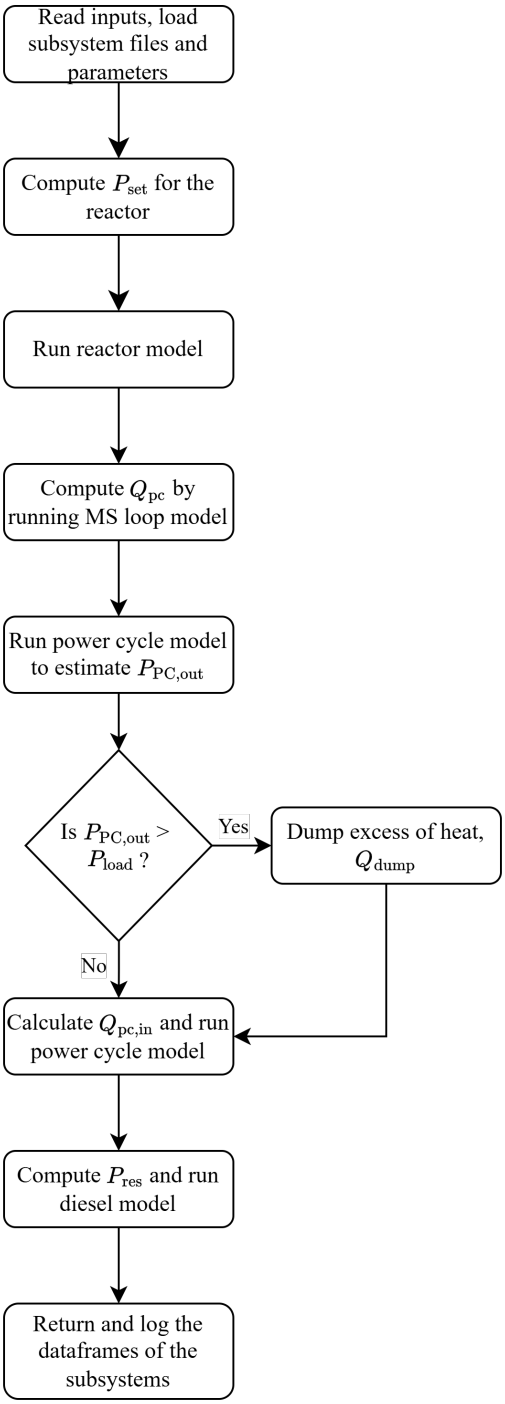

$$P_{\text{set}}[k] = \min\big(P_{\text{load}}[k] + P_{\text{sys}}[k],\, P_{\text{gross,max}}\big) \tag{3.39}$$

This electric setpoint is converted internally by the reactor model to a thermal power request, with Equation 3.40, using the power-cycle efficiency of the previous time step.

$$Q_{\text{set}}[k] = \frac{P_{\text{set}}[k]}{\eta_{\text{thermo}}[k-1]} \tag{3.40}$$

The reactor model is used to apply internal ramp-rate limits and minimum and maximum thermal power constraints, producing an actual reactor thermal output $Q_{\text{out}}[k]$ that may differ from the requested setpoint.

The reactor thermal output is transferred to the power cycle through the intermediate molten-salt loop. In the present configuration the molten-salt loop acts only as a thermal transport and buffering element. Heat loss will be because of ineffective heat transfer and will be calculated in the MS loop model. The heat left will be transferred to the power cycle.

To estimate the electrical power output, the power cycle model is executed with the total heat coming from the MS loop, Q_{pc}, and converts this thermal power to electricity using a load-dependent efficiency map as explained in subsection 3.2.3, a simplification can be found in Equation 3.41.

$$P_{\text{pc,gross}}[k] = \eta_{\text{thermo}}[k]\, Q_{\text{pc}}[k] \tag{3.41}$$

The net electrical output supplied to the ship is obtained by subtracting auxiliary consumption and enforcing the generator capacity limit:

$$P_{\text{pc,out}}[k] = \min\big(P_{\text{pc,gross}}[k],\, P_{\text{pc,max}}\big) - P_{\text{sys}} \tag{3.42}$$

If the predicted net electrical output exceeds the ship load, excess thermal energy is removed through controlled dumping, which prevents electrical overproduction and ensures power balance at the ship bus.

$$Q_{\text{dump}}[k] = \frac{P_{\text{pc,out}}[k] - P_{\text{load}}[k]}{\eta_{\text{thermo}}[k]}, \quad \text{if} \quad P_{\text{pc,out}}[k] > P_{\text{load}}[k] \tag{3.43}$$

$$Q_{\text{pc,in}}[k] = Q_{\text{pc}}[k] - Q_{\text{dump}}[k] \tag{3.44}$$

The amount of dumped energy is subtracted from the full heat input and $Q_{\text{pc,in}}$ is the actual heat expanded through the turbine.

After thermal dumping, the power cycle is evaluated again and enforces efficiency limits, maximum electrical capacity, and ramp-rate constraints, resulting in an actual net output $P_{\text{pc,out}}[k]$. The remaining power deficit is computed as shown in Equation 3.45. A positive residual indicates a power deficit, while a negative residual indicates a surplus.

$$P_{\text{res}}[k] = P_{\text{load}}[k] - P_{\text{pc,out}}[k] \tag{3.45}$$

The diesel plant is only permitted to operate when the reactor–power-cycle combination approaches its maximum capability, as determined by the reactor headroom criterion described in subsection 3.2.4. If this condition is not satisfied, the diesel plant enforces $P_{\text{DG}}[k] = 0$ and all generators remain offline. When diesel operation is allowed, the residual demand is passed to the diesel plant dispatch model, which determines unit commitment, load sharing, and ramp-limited power output by enforcing unit-level and plant-level ramp limits, load constraints and fuel-optimal dispatch which returns actual diesel power output P_{DG}. From which the total electrical power delivered to the ship is calculated with:

$$P_{\text{bus}}[k] = P_{\text{pc,out}}[k] + P_{\text{DG}}[k] \tag{3.46}$$

Any remaining power deficit is logged as unmet demand:

$$P_{\text{gap}}[k] = P_{\text{load}}[k] - P_{\text{bus}}[k] \tag{3.47}$$

In the present configuration, electrical or thermal energy storage systems are not present, and any remaining mismatch is recorded for later analysis rather than actively compensated. In subsection 3.3.2 the results will be analysed.

3.3.2. Basic Power System Results

Figure 3.12 shows the load profile and the power systems trying to match this load with its restrictions that are described per component in the previous section.

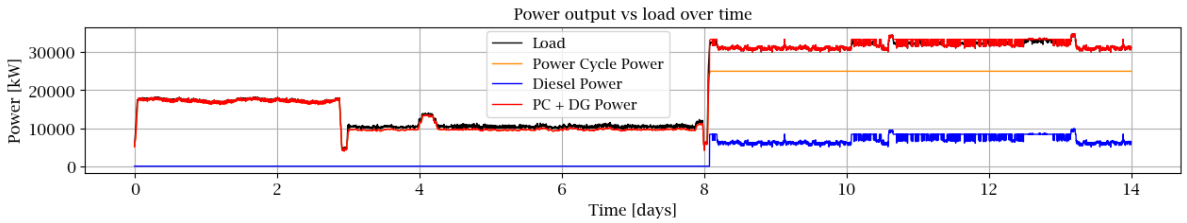

Figure 3.12: Electrical power outputs and load profile

This results in a power mismatch between the load and the power systems which is shown in Figure 3.13. Due to the dynamics of the reactor and the restricted use of the diesels the unmet request sums up to 108.6 MWh_e over the load profile of 14 days. The main mismatches are when transitioning from one operation into another as can be seen around day 3 and day 8. During relatively stable operation well within the power range of the reactor the load can be met relatively well, like when sailing on the first 3 days. However, when the operation of the ship requests power around the lower limits of the reactor the mismatch increases and become more fluctuating, like during the build up of the riser between days 4 and 8. Important measures to see what energy storage systems (ESS) could be useful can be found in Table 3.15.

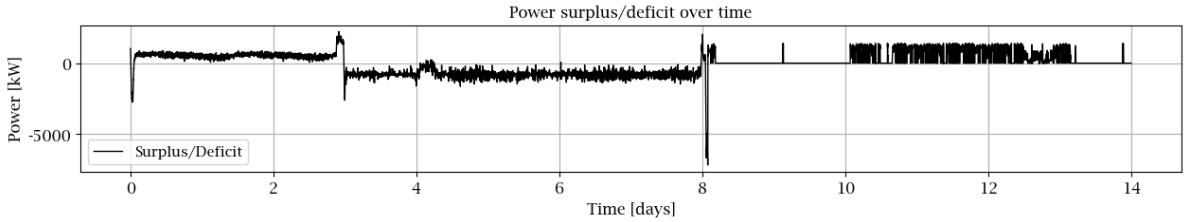

Figure 3.13: Power surplus or deficit over time, positive means surplus, negative means deficit.

These power mismatches could be stored by an ESS. The 108.6 MWh of unmet energy could be supplied with the potentially stored surplus energy, which is a total of 112.9 MWh in this specific case. The potentially stored energy can be seen in Figure 3.14. Here the missed energy is depicted as a potential state of charge (SOC) of an ideal battery without any losses or power constraints. If all the energy needs to be stored this would lead to a battery sizing of 94.3 MWh.

Table 3.15: Measures from power surplus/deficit Figure 3.13

Metric	Value	Unit
$P_{max,out}$	7154	kW
$P_{maxramp,up}$	1399	kW/min
$P_{max,in}$	2201	kW
$P_{maxramp,down}$	6234	kW/min

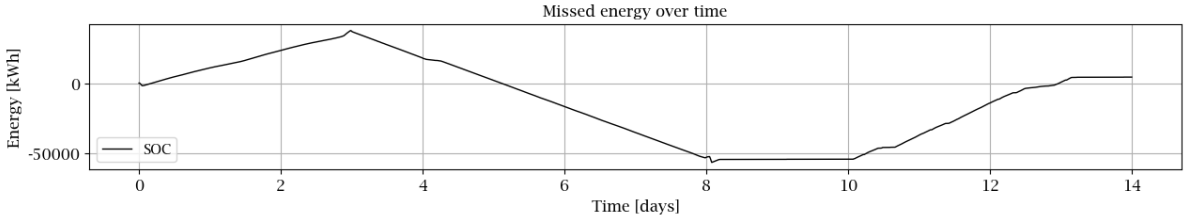

Figure 3.14: Electrical energy potential to be stored

This first estimate of this battery sizing is taken as the biggest possible battery to cover all power surplus and deficit on the ship. However, this estimate is made with a reactor that operates without having energy storage as an option. By adjusting the use of the power systems described in this chapter 3 and adding the potential to store energy, the operation of the power systems can be adjusted so that there is less storage needed to

fulfil the power requirements of the ship. How this can be done and how the storage systems are operated can be found in chapter 4.

An important note is that in order to fully phase out the diesel generators a total energy storage capacity of almost 1 GWh_e is needed for this specific load profile of only 14 days. This is due to the system mismatch during mining operation, which is the most desirable but also most demanding operation of the ship to make a profit and would be maximised in real operation of the ship. This means that this operational profile cannot be met without auxiliary diesel generation, given the current sizing of the reactor.

4

Modelling and Integration of ESS

This chapter describes the modelling of the electrical and thermal energy storage subsystems (ESS), the physical limits applied, and the way energy flows are coordinated with the reactor, intermediate molten-salt (MS) loop, diesel plant, and power cycle. The thermal storage is used primarily to cover ramp deficits that the HTGR cannot follow without violating manoeuvrability constraints, whereas the electrical storage provides fast peak-shaving for residual, short-duration transients that persist after the power cycle and (if started) the diesel plant.

4.1. ESS Component Models

A thermal and electrical storage system is incorporated to assist the HTGR in meeting the load demand. This section explains how these systems are modelled and how their desired operation is defined. The capacity of the ESS will be determined in chapter 5, so in this chapter the capacities of the storages will not specifically be named.

4.1.1. Thermal Energy Storage Model

The thermal storage is a two-tank molten-salt TES, integrated into the intermediate MS loop between the HTGR and the power cycle by adding two tanks to store molten salt as shown in Figure 4.1. This means that part of this subsection and also the parameters and constraints, Table 4.1, are the same as in the MS loop described in subsection 3.2.2.

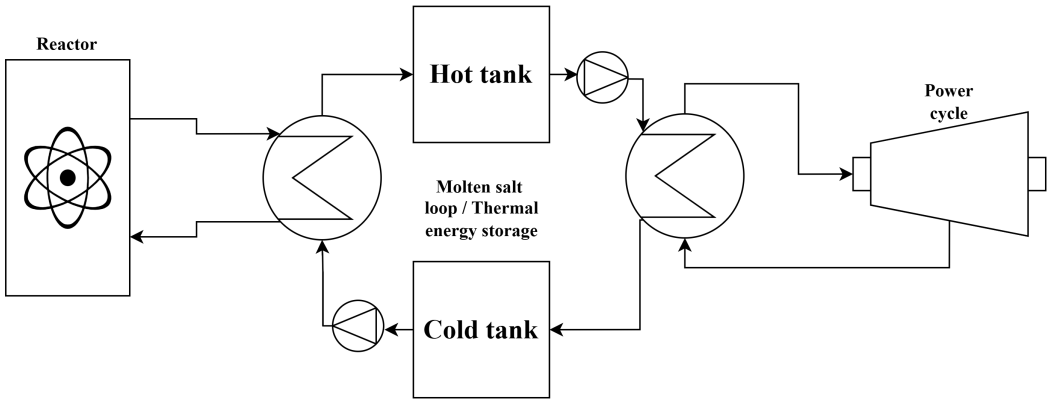

Figure 4.1: Thermal energy storage tanks integrated into the molten salt loop.

The TES provides medium-timescale flexibility [9, 71]: it charges by storing salt heated by the reactor through the MS charge heat exchanger and discharges by supplying the hot salt to the power cycle through the MS discharge heat exchanger. The storage uses solar salt (60% $NaNO_3$ / 40% KNO_3), with temperature-dependent properties drawn from industry data and literature [108, 121] which have been specified in subsection 3.2.2 and are also displayed in Table 4.2. The parameters of the thermal storage can be found in Table 4.1 together with the constraints that are applicable. From this the total energy capacity of the storage $E_{\text{cap,th}}$ is left out, since this will be a variable to change to make sure the energy system can follow the load profile of the ship.

The TES is modelled at a system level, focusing on energy storage capacity, heat-transfer limitations, and inventory dynamics rather than detailed tank stratification or transient thermal gradients. The formulation therefore prioritises physically consistent energy balances and operational constraints over high-fidelity local thermal effects. A detailed discussion of the modelling assumptions and their implications is provided at the end of this subsection.

Table 4.1: Parameters, and constraints of the TES integrated with the intermediate molten-salt loop.

Parameters	Symbol	Value	Unit
Maximum heat transfer	$Q_{\text{max,ch/dis}}$	75	MW_{th}
Overall heat-transfer conductance (both HX)	UA_{ch}, UA_{dis}	0.5 / 0.5	MW/K
MS transport delay	t_{delay}	0	s
Salt temperature setpoints	T_{hot}, T_{cold}	565 / 290	°C
Salt density	$\rho(T)$	see Tab. 4.2	kg/m^3
Heat capacity of salt	$c_p(T)$	see Tab. 4.2	kJ/kgK
Constraints	Symbol	Value	Unit
Salt allowable temperature range	$T_{\text{min}}/T_{\text{max}}$	260/620	°C
Minimum pinch temperature	ΔT_{min}	5	°C
Maximum salt mass flow	$\dot{m}_{\text{max}}$	180	kg/s

Modelling approach and state definition

Figure 4.2 shows the working principle and flow of the TES model for which the in- and outputs can be found in Table 4.3. The thermal storage system is placed within the intermediate MS loop that is described in subsection 3.2.2.

The required heat that is asked by the power cycle is first clamped between maximum charge/discharge ($Q_{\text{max,ch/dis}}$) like shown in Equation 4.1. If thermal storage is not enabled, the molten salt loop will operate like described in subsection 3.2.2.

$$Q_{\text{req}} = \begin{cases} -Q_{\text{max,ch}}, & Q_{\text{req}} < -Q_{\text{max,ch}} \\ Q_{\text{req}}, & -Q_{\text{max,ch}} \leq Q_{\text{req}} \leq Q_{\text{max,dis}} \\ Q_{\text{max,dis}}, & Q_{\text{req}} > Q_{\text{max,dis}} \end{cases} \tag{4.1}$$

When thermal storage is disabled or the storage capacity is zero, the TES model operates in bypass mode. In this mode, no internal energy is stored and heat is transferred directly from the reactor-side molten-salt loop to the power cycle subject only to heat-exchanger effectiveness and pinch constraints. The TES state of charge is fixed at zero.

The charge HX couples the reactor to the salt loop; the discharge HX couples the salt loop to the steam cycle. The working principle and calculations of the heat exchangers are the same as in subsection 3.2.2. A short summary of the limiting mechanisms can be found in Equation 4.4 where Q_{req} is the requested heat transfer and q will be the transferred heat between mediums. The heat exchangers apply limits on heat transfer efficiency, pinch constraint and maximum mass flow. The different heat exchangers will be denoted ch for charge and dis for discharge. Charge and discharge are treated as independent, non-negative heat requests, $Q_{\text{req,ch}} \geq 0$ and $Q_{\text{req,dis}} \geq 0$, which are evaluated separately within the TES model.

For the TES, the heat-capacity rate of the salt stream is given by:

$$C_{\text{TES}} = \dot{m}_{\text{TES}}\, c_p(T_{\text{TES}}) \tag{4.2}$$

Where $\dot{m}_{\text{TES}}$ is the actual salt mass-flow rate after mass-flow and inventory constraints, and c_p is evaluated at the corresponding tank temperature (T_{cold} for charging and T_{hot} for discharging).

Because the TES operates between fixed hot and cold tank temperatures, the maximum heat that can be transferred by the TES for a given mass flow is limited by the available temperature lift:

$$q_{\text{TES}} = C_{\text{TES}}\,(T_{\text{hot}} - T_{\text{cold}}) \tag{4.3}$$

The q_{TES} term enforces the intrinsic storage limitation associated with the fixed TES temperature band. Even if the heat exchangers and salt mass-flow would permit higher heat transfer, the TES cannot exchange more

heat than allowed by the temperature difference between the hot and cold tanks. This limiter is specific to the TES model and is not present in the intermediate molten-salt loop when operated without storage.

$$q = \min\left(q_\varepsilon, q_{\text{pinch}}, q_{\text{mass}}, q_{\text{TES}}, Q_{\text{req}}\right) \tag{4.4}$$

When the TES is present in the system, the model computes the needed values for the amount of energy per kilogram of salt and the mass transfer needed to transport a certain amount of energy. The TES receives independent charge and discharge heat requests $Q_{\text{req,ch}}$ and $Q_{\text{req,dis}}$ from the energy Management system. A positive charge request corresponds to storing reactor heat, while a positive discharge request corresponds to supplying heat to the power cycle. For this the temperatures around the loop are needed.

T_{hot} and T_{cold} denote the design outlet temperatures of the hot and cold TES tanks, respectively. With temperature-dependent heat capacity $c_p(T)$, available from Table 4.2, the specific storable energy per kg of salt across the band can be calculated with Equation 4.5.

$$E_{\Delta T} = \int_{T_{\text{cold}}}^{T_{\text{hot}}} c_p(T)\,\mathrm{d}T \tag{4.5}$$

Given the total salt mass m, the nominal storage capacity is $E_{\text{cap,th}} = m\,E_{\Delta T}$. The dynamic state is the split between hot and cold inventories, m_{hot} and m_{cold}, which tells the state of charge of the TES.

$$SOC_{\text{th}} = \frac{E_{\text{del}}}{E_{\text{cap,th}}} = \frac{m_{\text{hot}}}{m_{\text{hot}} + m_{\text{cold}}} \tag{4.6}$$

In this way the deliverable energy is $E_{\text{del}} = m_{\text{hot}}\,E_{\Delta T}$. Charge and discharge exchange hot/cold mass at a rate like calculated in Equation 4.7 in kilograms per second.

$$\Delta m = \frac{Q_{\text{req}}\,\Delta t}{E_{\Delta T}} \tag{4.7}$$

In the discrete-time formulation used here, the corresponding mass-flow rate is given by $\dot{m} = \Delta m/\Delta t$, which is the quantity subject to mass-flow and heat-exchanger constraints. The required heat transfer Q_{req} tells the amount of salt that needs to be transported in the TES per time step. This is calculated with Equation 4.7 where the amount of energy required is divided by the energy per kilogram salt, resulting in the amount of salt that needs to be transferred that time step.

For charging, mass is transferred from the cold tank to the hot tank:

$$\Delta m_{\text{ch}} = \frac{Q_{\text{ch,req}}\,\Delta t}{E_{\Delta T}} \tag{4.8}$$

For discharging, mass is transferred from the hot tank to the cold tank:

$$\Delta m_{\text{dis}} = \frac{Q_{\text{dis,req}}\,\Delta t}{E_{\Delta T}} \tag{4.9}$$

This mass flow of salt ($\dot{m}$) is restricted by the maximum salt flow in the system $\dot{m}_{\text{max}}$ and the available mass in the tank where the salt needs to come from, m_{cold} for charge

Figure 4.2: TES model working principle

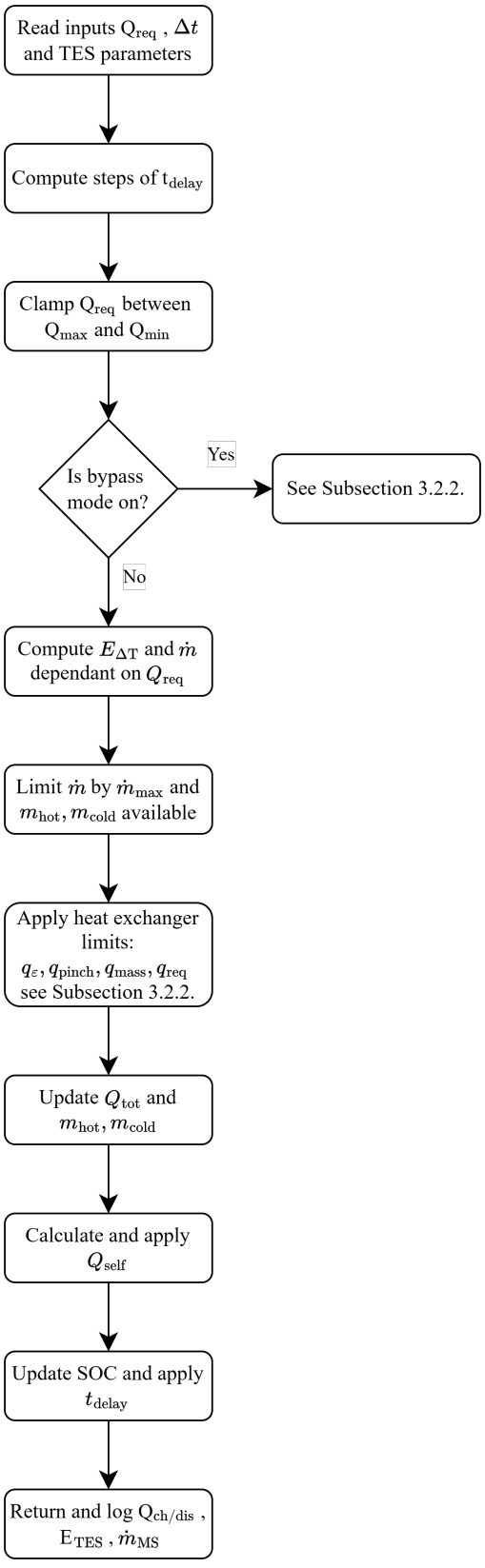

and m_{hot} for discharge. With this mass flow of salt determined, the heat exchanger limitations are implemented like described in subsection 3.2.2. After the actual heat throughput is calculated the masses of both tanks are updated as well as the total energy transfer Q_{tot} which is split into Q_{ch} and Q_{dis}.

Similar to the intermediate molten-salt loop, a transport delay can be applied to the externally delivered charge and discharge heat flows. This delay affects only the heat exchanged with the rest of the system and does not influence the internal TES energy balance. For the time step and design level used in this study, the transport delay is set to zero, as discussed in subsection 3.2.2, because its effect is negligible compared to the reactor thermal inertia.

Thermal losses (Q_{loss}) from the TES are modelled via a heat-transfer coefficient to the ambient environment. These losses represent self-discharge and are implemented by transferring a small amount of hot-tank energy to the cold tank. The instantaneous thermal loss rate is given by:

$$Q_{\text{loss}} = UA_{\text{hot}}\left(T_{\text{hot}} - T_{\text{amb}}\right) \tag{4.10}$$

The TES internal energy state is updated using the net balance of charging, discharging, and losses. The deliverable thermal energy evolves according to:

$$E_{\text{del}}[k] = E_{\text{del}}[k-1] + \left(Q_{\text{ch,real}} - Q_{\text{dis,real}} - Q_{\text{loss}}\right)\Delta t \tag{4.11}$$

The corresponding thermal state of charge is obtained directly from Equation 4.6. The net thermal contribution of the TES to the heat flow between the reactor and the power cycle is defined as:

$$Q_{\text{TES,net}} = Q_{\text{dis,real}} - Q_{\text{ch,real}} \tag{4.12}$$

The net thermal contribution of the TES modifies the thermal power flowing through the intermediate molten-salt loop. The resulting thermal power requested at the inlet of the molten-salt loop is:

$$Q_{\text{MS,req}} = Q_{\text{reactor}} + Q_{\text{TES,net}} \tag{4.13}$$

The requested heat flow $Q_{\text{MS,req}}$ is subsequently subjected to the heat-transfer limits and transport dynamics of the intermediate molten-salt loop described in subsection 3.2.2. The physically achievable thermal power delivered to the power cycle is therefore:

$$Q_{\text{pc,in}} = \min\left(Q_{\varepsilon,\text{MS}}, Q_{\text{pinch,MS}}, Q_{\text{mass,MS}}, Q_{\text{MS,req}}\right) \tag{4.14}$$

The individual molten-salt loop limits are defined in subsection 3.2.2. This formulation ensures that the thermal power delivered to the power cycle is constrained by both the TES operating limits and the intermediate molten-salt loop heat-transfer limits.

$Q_{\text{TES,net}}$ represents the net thermal output of the TES, positive when discharging to the power cycle and negative when charging from the reactor. The thermal power delivered to the power cycle is constrained by both the TES operating limits and the intermediate molten-salt loop heat-transfer limits as explained in this subsection. The quantity $Q_{\text{pc,in}}$ therefore represents the final thermal power delivered to the inlet of the power cycle and is the sole thermal input used by the power-cycle model.

Table 4.2: Thermophysical properties of solar salt (60% $NaNO_3$, 40% KNO_3) used in the molten-salt loop [108].

Property	**Representative value range**
Operating temperature range	290–565°C
Density	1700–1900 kg/m^3
Specific heat capacity	1.48–1.54 kJ/kgK
Thermal conductivity	0.49–0.55 W/mK
Allowable temperature range	~260–620°C
Freezing point	~220°C

Table 4.3: Inputs and outputs of the TES model.

Inputs	Symbol	Unit
Charge/discharge request	$Q_{\text{req,ch}}$, $Q_{\text{req,dis}}$	kW
Reactor hot-side inlet (MS charge HX)	$T_{\text{hot,in}}$	°C
Power-cycle cold-side inlet (MS discharge HX)	$T_{\text{cold,in}}$	°C
Ambient temperature	T_{amb}	°C
External heat-capacity rates (optional)	C_{src}, C_{ld}	W/K
Time step	Δt	s
Outputs	Symbol	Unit
Charge/discharge heat (delayed external)	Q_{ch}, Q_{dis}	kW
Effectiveness (charge/discharge)	ε_{ch}, ε_{dis}	–
Salt mass-flow (actual)	$\dot{m}_{\text{MS}}$	kg/s
TES state of charge (deliverable)	E_{del}	kWh

Sizing context and empirical trends

Reported molten-salt TES deployments alongside concentrated solar power plants show a broad but correlated distribution of power rating versus energy capacity, reflecting constraints from tank volumes, HX sizing, and allowable ramping [122] to be within the set boundaries of this system representation.

Assumptions (TES/MS)

The TES is modelled as a simplified two-tank system with fixed hot- and cold-tank temperatures, using ε–NTU heat-exchanger formulations with constant overall conductance UA and a fixed minimum pinch temperature difference ΔT_{min}. These simplifications remove the need to resolve detailed transient tank stratification or dynamic $U(T)$ behaviour, which keeps the model lightweight and applicable for system-level integration. A fixed transport delay represents molten-salt loop transit and is not dependent on the actual mass flow. Thermophysical properties are taken from nitrate-salt correlations [121, 108], providing realistic temperature-dependent behaviour where it matters most: in the calculation of stored energy and HX capacity rates.

No limits are imposed on how quickly tank temperatures or heat flows can change, although simple rate effects could be approximated by restricting the allowable mass-flow or heat transfer per time step. More detailed features such as thermal stratification within the tanks, temperature-dependent UA, multidimensional loss modelling, or explicit hydraulics of the molten salt loop would increase realism, especially during fast transients or part-load behaviour, but would also add complexity and computational cost.

Overall, the chosen assumptions offer a balance between physical realism and computational efficiency suitable for long-horizon, system-level simulations.

4.1.2. Electrical Energy Storage Model

The electrical energy storage (EES) is modelled as a generalised battery pack with state-of-charge (SOC) dynamics, voltage-dependent round-trip efficiencies, and a first-order thermal model. The battery responds on the fastest time scales in the propulsion plant and is therefore well-suited to cover high-frequency load spikes that remain after the reactor, the TES, and the diesel dispatch responses have been accounted for [10]. It is important to note that the simulation is conducted with a one-minute time step.

The EES is modelled using a deliberately simplified, quasi-static representation that is appropriate for the one-minute simulation time step employed in this study. The model captures the dominant system-level effects of electrical storage—namely power limits, energy availability, and efficiency losses—without resolving detailed electrochemical or fast internal battery dynamics. The underlying assumptions and their justification are discussed in detail at the end of this subsection.

Operating policy

The EES covers the remaining short spikes after the reactor setpoint filtering/ramp limits, TES/Molten-salt buffering, and diesel dispatch. Ramp limits for EES are not imposed in the baseline (the battery is the fastest actuator). Minimum and maximum SOC are enforced at 10% and 95% respectively to limit degradation and

preserve usable capacity; at the bounds, charge/discharge requests that would violate the limits are curtailed and logged as unmet charge/discharge.

The values of the parameters and constraints of the EES model are summarised in Table 4.4 and will be explained in the rest of this subsection.

Table 4.4: Parameters and constraints of the battery EES model.

Parameters	Symbol	Value	Unit
Base / slope efficiency	$\eta_{\text{base}}, \eta_{\text{diff}}$	0.85 / 0.12	–
Voltage range	$V_{\min}, V_{\max}$	3.0 / 4.2	V
Constraints	Symbol	Value	Unit
SOC window	$E_{\min} \le E \le E_{\max}$	10–95%	–
(dis)charge limits	$0 \le P_{\text{ch/dis}} \le P_{\max}$	6/10	MW

Figure 4.3: EES model working principle

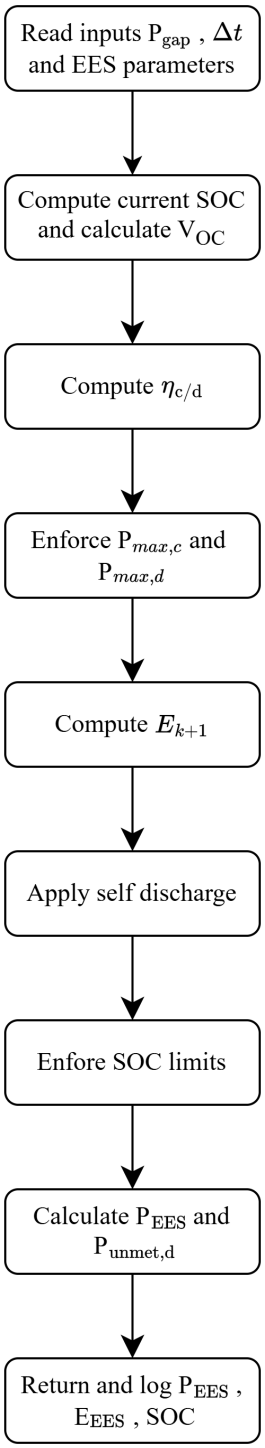

Modelling approach

The operating principle of the EES model can be found in Figure 4.3. At each time step, the battery detects the net electric gap (P_{gap}), which is calculated by subtracting the power produced and delivered by the power systems from the total load demand. The EES needs to supply or take up any unmet energy that is left. First the current state of charge (SOC) is updated by dividing the current energy in the EES (E_k) by the total energy ($E_{\text{cap,e}}$) the battery could potentially store. From this the voltage and efficiency can be calculated.

Power request and limiting

At each time step, the electrical energy storage receives the net electrical power gap P_{gap}, defined as the remaining difference between the ship load demand and the electrical power supplied by the reactor–power-cycle combination and, if enabled, the diesel generators. A positive P_{gap} corresponds to a power deficit requiring battery discharge, while a negative P_{gap} corresponds to surplus power requiring battery charging.

$$P_{\text{dis,req}} = \max(P_{\text{gap}}, 0), \qquad P_{\text{ch,req}} = \max(-P_{\text{gap}}, 0) \tag{4.15}$$

Because the electrical energy storage represents the fastest actuator in the system, no explicit ramp-rate limitation is imposed on battery charge or discharge; all upstream ramp-rate constraints are enforced at the reactor, power-cycle, TES, and diesel-plant levels.

$$P_{\text{dis}} = \begin{cases} 0, & P_{\text{dis,req}} < 0 \\ P_{\text{dis,req}}, & 0 \le P_{\text{dis,req}} \le P_{\text{dis,max}} \\ P_{\text{dis,max}}, & P_{\text{dis,req}} > P_{\text{dis,max}} \end{cases} \tag{4.16}$$

$$P_{\text{ch}} = \begin{cases} 0, & P_{\text{ch,req}} < 0 \\ P_{\text{ch,req}}, & 0 \le P_{\text{ch,req}} \le P_{\text{ch,max}} \\ P_{\text{ch,max}}, & P_{\text{ch,req}} > P_{\text{ch,max}} \end{cases} \tag{4.17}$$

Voltage and efficiency model

The simplified linear function for open-circuit voltage depending on SOC can be found in Equation 4.18. It is calculated with the minimum and maximum voltage of a cell. General Li-ion battery voltage ranges are between 3 and 4.2 Volt [123].

$$V_{\text{OC}} = V_{\min} + (V_{\max} - V_{\min})\,\text{SOC} \tag{4.18}$$

The charge and discharge efficiency are dependent on the voltage of the EES. This model uses a simple efficiency that increases at high voltage and decreases with lowering voltage. Equation 4.19 shows how the efficiency is calculated depending on the voltage. This efficiency will be between 85 and 97% depending on the voltage.

$$\eta = \eta_{\text{base}} + \eta_{\text{diff}} \frac{V_{\text{OC}} - V_{\text{min}}}{V_{\text{max}} - V_{\text{min}}} \tag{4.19}$$

This captures that the pack is slightly more efficient at higher SOC/voltage, while remaining computationally light. The maximum charge and discharge rate of the battery are enforced, the inverter efficiency is assumed constant and disabled for this case since more information about the exact battery pack is needed.

The potential electrical energy (E_{k+1}) of the battery updates as shown in Equation 4.20. Where the total energy for the next time-step ($E_{\text{k+1}}$) is calculated from the previous total energy and in which voltage-dependent efficiencies $\eta_{c,d} = \eta$ and (dis)charge limits $0 \leq P_{\text{ch}} \leq P_{\text{ch,max}}$, $0 \leq P_{\text{dis}} \leq P_{\text{dis,max}}$ are applied.

$$E_{k+1} = E_k + \eta_c P_{\text{ch}} \Delta t - \frac{P_{\text{dis}}}{\eta_d} \Delta t \tag{4.20}$$

Table 4.5: Inputs and outputs of the EES model.

Inputs (EES)	Symbol	Unit
Net power gap (charge < 0, discharge > 0)	P_{gap}	kW
Time step	Δt	s
Outputs (EES)	Symbol	Unit
Net battery power (to bus)	$P_{\text{batt,net}}$	kW
Unmet power after EES	P_{unmet}	kW
State of charge	SOC	–

On this potential energy a self-discharge rate is applied, this may be enabled but is set to zero in the baseline case. SOC limits are enforced by clipping the total calculated energy between the minimum and maximum energy allowed in the EES: $E_{k+1} \in [E_{\text{min}}, E_{\text{max}}]$. These limits come from the minimum and maximum SOC percentages which are set to 10 and 95% to ensure longer battery life [123].

SOC bounds and curtailment

The battery state of charge is constrained within predefined lower and upper limits to prevent deep discharge and overcharge. When a requested charge or discharge would violate these bounds, the corresponding power is curtailed such that the SOC remains within the allowable window.

$$E_{\text{min}} = \text{SOC}_{\text{min}} E_{\text{cap,e}}, \qquad E_{\text{max}} = \text{SOC}_{\text{max}} E_{\text{cap,e}} \tag{4.21}$$

$$E_{k+1} = \begin{cases} E_{\text{min}}, & E_{k+1} < E_{\text{min}} \\ E_{k+1}, & E_{\text{min}} \leq E_{k+1} \leq E_{\text{max}} \\ E_{\text{max}}, & E_{k+1} > E_{\text{max}} \end{cases} \tag{4.22}$$

If the unconstrained update of Equation 4.20 exceeds these limits, the applied charge or discharge power is reduced such that the SOC constraint is satisfied. Any remaining unmet power is passed back to the system as residual demand.

$$P_{\text{batt,net}} = P_{\text{dis}} - P_{\text{ch}} \tag{4.23}$$

$$P_{\text{unmet}} = P_{\text{gap}} - P_{\text{batt,net}} \tag{4.24}$$

The quantity $P_{\text{batt,net}}$ represents the actual electrical power exchanged between the battery and the ship grid, while P_{unmet} is the remaining power deficit or surplus after EES action.

Assumptions

The electrical energy storage model applies deliberately simplified assumptions that are appropriate for system-level control and high-level energy simulations. It uses a simplified state-of-charge representation together with a linear relationship between SOC and open-circuit voltage, allowing voltage to be computed directly without resolving detailed electrochemical behaviour. Charge and discharge efficiencies are expressed as simple functions of this voltage rather than being derived from full cell-level kinetics. No explicit ageing, cycle-life

degradation, or internal dynamic behaviour is modelled, and the battery does not impose any current- or C-rate-dependent limits beyond the maximum charge and discharge power allowed.

These simplifications are justified because, in this study, the electrical energy storage functions as a fast system-level power buffer rather than as a component whose internal electrochemical behaviour is of primary interest. The dominant quantities governing system behaviour are the available charge and discharge power, the usable energy capacity, and the associated efficiency losses, all of which are represented explicitly. Battery internal dynamics occur on time scales that are much shorter than the thermal and mechanical dynamics of the reactor, molten-salt loop, power cycle, and diesel generators, making a quasi-static battery representation appropriate at the simulation time resolution used.

Model realism is ensured by verifying that battery operation remains within physically reasonable power and SOC limits throughout all simulations, and that the battery is used only to absorb short-duration residual mismatches rather than to supply sustained energy deficits. Because the EES primarily influences high-frequency transients, moderate variations in assumed efficiency or voltage–SOC characteristics would not materially affect system-level outcomes such as power balance, diesel usage, or ESS sizing. The model therefore provides a computationally efficient yet sufficiently realistic representation for assessing energy flows, subsystem interaction, and power-management behaviour at the ship level.

4.2. Hybrid ESS Architecture

This section describes the physical and functional integration of the hybrid energy-storage system (ESS), consisting of the high-temperature gas-cooled reactor (HTGR), the thermal energy storage (TES), the battery-based electrical energy storage (EES), and the diesel generator (DG) backup plant. The objective of the architecture is to combine the favourable long-term, high-power thermal dynamics of the HTGR and TES with the fast electrical response of the battery, while maintaining the capability to supply the ship grid under all operational conditions. The role and key features of the systems are described in Table 4.6 and further explained in section 4.3.

Figure 4.4 shows the high-level architecture of the system. The HTGR delivers thermal power to the molten salt loop with the integrated TES which is then transferred to the power cycle. The power cycle converts thermal input to electric power, which together with the battery and diesel generators supplies the ship grid. All subsystems exchange power through the so-called Ship Energy Management system, which implements architecture as well as the operational logic of the system.

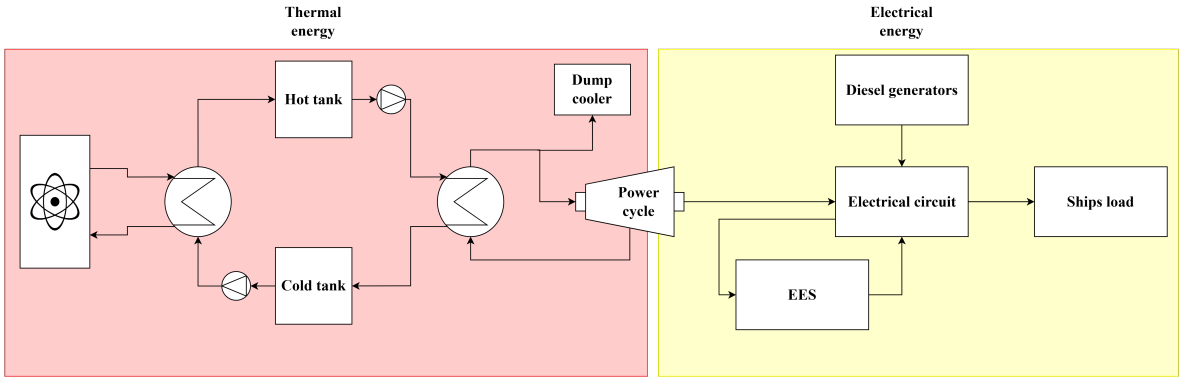

Figure 4.4: Total system overview

As the reactor produces heat the molten salt loop with integrated TES accepts charge power Q_c through the primary heat exchanger and provides discharge power Q_d to the power cycle at the secondary heat exchanger. Internal physics limit Q_c and Q_d as explained in subsection 4.1.1.

The power cycle converts the heat from the intermediate loop to electricity. It enforces a fixed thermal-to-electric efficiency map η dependent on the incoming heat and a strict $\pm 5\%$/min ramp-rate limit on net electric power. This ramp limit is central to the coordination logic, since this is a limiting factor of the system.

Once the power is converted to electrical power, the diesel generators supply additional electrical power during large deficits, when the reactor and TES cannot meet the power demand due to capacity limitations. They are used in a most fuel efficient favourable way so that their emissions are kept to a minimum.

The battery is the last line of defence for power supply. It provides fast bidirectional electrical power for high-frequency load fluctuations and for bridging transient deficits before the reactor and TES respond. The battery model enforces physical SOC bounds, power limits, and charge/discharge efficiencies.

Table 4.6: Subsystem functions and key interfaces.

Subsystem	Role and Key Interfaces
HTGR	Provides thermal power; has limited ramp; supports TES SOC control; interacts with TES, EES and power cycle.
TES	Buffers reactor ramp-rate limitations; supplies/absorbs thermal power; subject to HX, $\Delta T_{\min}$, mass-flow and inventory constraints; delayed thermal power delivery.
Power Cycle	Converts thermal power to electric power output; enforces ±5%/min ramp limit; provides conversion efficiency η_{thermo} for the system.
Diesel Plant	Provides electric power when reactor saturates; supports EES SOC control.
EES	Fast-response electrical buffer; constrained by SOC, power limits, and efficiencies; controlled SOC.
Management system	Determines all power flows; applies SOC control; dispatches TES, EES, reactor, and diesel units.

4.3. Operational Coordination Strategies

This section describes how the different subsystems work together controlled by the Ship Energy Management during each time step. The goal is to maintain power balance, respect subsystem constraints, and minimise diesel usage.

The Ship Energy Management sits between all subsystems and:

- executes all component models,
- computes reactor power setpoints,
- computes charge/discharge requests for TES and EES,
- applies SOC-control logic,
- enforces operational constraints (ramp rate, overdrive, relax modes),
- resolves residual mismatch using diesel generators or battery,
- logs all states for analysis.

Explanation of terms and how this is done is described in this section. The order of the operation can also be found in Figure 4.5. An advantage of this Management system is that in adjusting the way the ESS are used their size is also determined. Section 3.3 states a total energy storage of 94.3 MWh_e would be needed. However with this management logic, mainly the way that the systems are used compared to each other, this amount of stored energy can potentially be decreased.

The SEM described here, with integrated energy storage systems, follows the same logic as the power mismatch analyses of section 3.3, with the exception of storage availability.

During each simulation time step k, the Ship Energy Management evaluates the ship load, subsystem states, efficiency maps, and operational constraints to coordinate the hybrid nuclear–thermal–electrical power system. The objective is to maintain electrical power balance, respect subsystem limitations, minimise diesel use, and ensure stable behaviour. All control decisions are evaluated sequentially within a single time step, ensuring that slower thermal subsystems act first, while the electrical energy storage compensates only the final residual mismatch.

Reactor setpoint composition, SOC centring, and overdrive

Within each time step, the management tool first forms an electrical reactor setpoint by combining the baseline load-following demand with additive correction terms arising from energy-storage control objectives.

These corrections are computed before any thermal or electrical subsystem is stepped, ensuring that all downstream components respond to a single, consistent reactor command.

$$P_{\text{set}} = P_{\text{load}} + P_{\text{sys}} + P_{\text{overdrive}} + P_{\text{boost}} - P_{\text{relax}} + P_{\text{gain}} \tag{4.25}$$

Here, P_{gain} is a small proportional SOC-centring correction, $P_{\text{overdrive}}$ is a temporary positive increase used to accelerate TES charging when sufficient power-cycle headroom exists, P_{boost} represents low-SOC charging requests that may be supplied by the reactor or diesel generators, and P_{relax} represents high-SOC reductions in generation that encourage discharge of stored energy. While both boost and overdrive increase generation, boost is driven by battery SOC requirements, whereas overdrive is driven specifically by low TES SOC and available power-cycle headroom.

The power of the systems P_{sys} involved in the delivery of power to the ship is taken constant and added to the load profile. In the first time step an estimated cycle efficiency is used to calculate the required thermal input like in Equation 4.26.

$$Q_{\text{set}} = \frac{P_{\text{set}}}{\eta_{\text{thermo}}}. \tag{4.26}$$

The management tool next evaluates the state of charge (SOC) of both energy-storage systems, SOC_{th} and SOC_{e}.

$$SOC_{\text{e}} = E_{\text{Batt}} / E_{\text{cap,e}} \tag{4.27}$$

$$SOC_{\text{th}} = E_{\text{del}} / E_{\text{cap,th}} \tag{4.28}$$

Battery SOC triggers two layers of behaviour which can request more or less power from the reactor or the diesel generators than is required to support the load.

- **SOC centring:** A soft correction drives SOC_{e} towards the target value of $SOC_{\text{e,des}} = 50\%$ using a gain proportional to the error:

  $$P_{\text{gain}} = C_{\text{gain}}\left(SOC_{\text{e,des}} - SOC_{\text{e}}\right) \tag{4.29}$$

  This can be positive for charge or negative for discharge. C_{gain} is a changeable constant for how heavy the centring is. The desired SOC is chosen so that the battery is always able to support power surplus or deficit, since the system is automated in such a way that it does not know what the next operation might require.

- **Outer-limit control:** If SOC drops below the boost threshold or exceeds the relax threshold, more aggressive corrections are taken to ensure the battery does not run into its fixed SOC boundaries of 10 and 95% SOC. The thresholds for these requests are set at 20 and 80% with a 10% hysteresis to ensure the battery does not fall back to this threshold immediately after the boost or relax addition stops. The use of hysteresis prevents rapid switching between boost and relax modes when the SOC fluctuates near the threshold, thereby avoiding control chattering and unnecessary actuator cycling. The boost and relax principle are combined in P_{boost} which is negative for relax requests and positive for boost requests.

Figure 4.5: Working principle of the ship energy Management model.

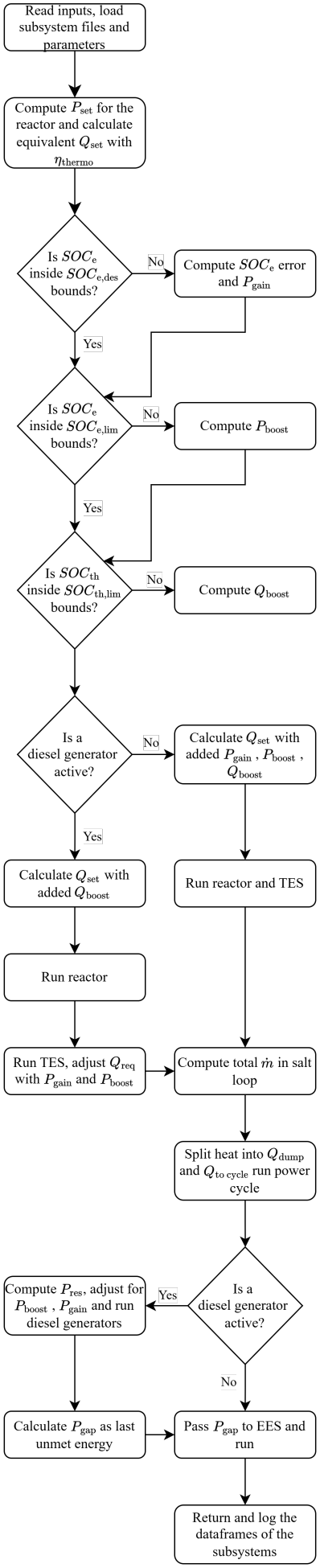

TES SOC is used only for outer-limit behaviour since TES mainly buffers reactor ramp-rate limitations. For the TES an abundance of energy is more important than a deficit since too much energy can be cooled away so the power cycle does not get too much heat. However, outer-limit boost and relax requests are there to make sure the TES does not operate close to its physical limits. The thresholds are set the same as for the EES and this control request is summarised in Q_{boost}.

The baseline electric-equivalent demand is the load demand, to which the management system adds or subtracts, like mentioned in Equation 4.25

- TES boost and relax request Q_{boost},
- battery boost and relax request P_{boost}, and
- the SOC-centring correction P_{gain}.

Q_{boost} will be converted to its electric equivalent before applying all requests to the setpoint. If the diesel generators are on, P_{boost} and P_{gain} will be requested from the generators and not be applied to the reactor. As discussed in subsection 2.1.1 the HTGR model will convert the electrical setpoint into the thermal power setpoint Q_{set} to be used in the model.

If the reactor saturates ($Q_{\text{reactor}} \simeq Q_{\text{nom}}$), overdrive is disabled for the next time step.

Given the resulting reactor output, the management system computes the thermal surplus and ramp deficit (ΔQ_{def},ΔQ_{sur}) like in Equation 4.30. Where the requested electrical power after the power cycle is converted with η_{thermo} to its thermal equivalent Q_{req}.

$$\Delta Q_{\text{def}} = Q_{\text{req}} - Q_{\text{reactor}}, \tag{4.30}$$

$$\Delta Q_{\text{sur}} = Q_{\text{reactor}} - Q_{\text{req}}. \tag{4.31}$$

Preliminary TES charge and discharge requests, $Q_{\text{c,req}}$ and $Q_{\text{d,req}}$, are then formed from these values and are subjected to:

- SOC-relax behaviour,
- SOC-centring bias (expressed in thermal units: $P_{\text{gain}}/\eta_{\text{thermo}}$),
- TES charge/discharge maxima,
- TES outer SOC limits.

These constraints are applied sequentially within each time step. The initial TES charge or discharge request is first modified by SOC-related bias terms, then limited by maximum charge and discharge power, and finally clipped to ensure that TES inventory bounds are not violated. This ensures that SOC control objectives influence TES behaviour without overriding physical limits.
Before sending these requests to the TES model, the management model checks the power-cycle (PC) ramp constraint (±5%/min). The combined effect of reactor ramping and TES action should not give the power cycle a too fast ramp, which would then directly be dumped. So Equation 4.32 should hold as well as the limit on maximum power that the power cycle could deliver (25 MW_e).

$$\Delta P_{\text{reactor}} + \eta_{\text{thermo}}\left(Q_{\text{d,req}} - Q_{\text{c,req}}\right) \leq \Delta P_{\text{pc,max}} \tag{4.32}$$

In this equation $\Delta P_{\text{pc,max}}$ is the maximum allowable PC ramp for this time step. If necessary, $Q_{\text{c,req}}$ and $Q_{\text{d,req}}$ are capped so that the power cycle does not go over its ramp or capacity limit due to TES action.

The capped heat flows are passed to the TES model, which enforces: heat-exchanger effectiveness limits, pinch-point constraints, temperature bands, molten-salt mass-flow limits, tank inventories, ambient losses, and transport delays like described in subsection 4.1.1. The TES returns actual flows $Q_{\text{c,real}}$ and $Q_{\text{d,real}}$ and updated internal states.

The management tool then computes the thermal power delivered to the PC by simply adding the heat in and output of the thermal system like in Equation 4.33.

$$Q_{\text{to cycle}} = Q_{\text{reactor}} - Q_{\text{c,req}} + Q_{\text{d,req}} \tag{4.33}$$

The corresponding gross electrical output using the PC efficiency map η_{thermo} is calculated. If the predicted net electrical output would exceed both the ship load and the battery charge capability, thermal dumping is applied.

$$Q_{\text{dump}} = \frac{P_{\text{excess}}}{\eta_{\text{thermo}}} \tag{4.34}$$

This ensures the electrical system is not overflown with energy. The adjusted power cycle input is fed into the power cycle model described in subsection 3.2.3 from which the resulting power output is calculated.

After the PC output is fixed, any residual power that is not met by the system is passed to the diesel plant under the condition that a diesel generator is on. If that is not the case the residual power request is sent directly to the EES.

$$P_{\text{res}} = P_{\text{load}} - P_{\text{pc,out}} \tag{4.35}$$

Diesel boost or relax behaviour P_{boost} applies only when diesels are already online and is otherwise already requested from the reactor. This makes the requested diesel generator output $P_{\text{res}} - P_{\text{boost}}$, which is fed into the diesel model like described in subsection 3.2.4. The diesel model returns actual diesel power output P_{DG}, which is logged for dump prediction in the next time step.

The battery is there to cover the last remaining mismatch, calculated with Equation 4.36.

$$P_{\text{gap}} = P_{\text{res}} - P_{\text{DG}} \tag{4.36}$$

A positive power is defined as power supplied to the ship grid, while a negative power corresponds to power absorbed by the storage system. This power request will be put into the EES model described in subsection 4.1.2 where it is subjected to the EES SOC and power limits. If SOC is below $\text{SOC}_{e,\text{min}}$ or above $\text{SOC}_{e,\text{max}}$, charging or discharging is forbidden and the unmet power is logged.

At the end of the step, the management logs all subsystem states to be used in the next time step. These are collected into the main dataframe for post-processing. The interaction of these subsystems and control strategies determines the required storage capacities, which are quantified in the next chapter.

5

Sizing Process of Hybrid ESS

This chapter discusses which combinations of ESS sizes are able to cover the desired load profile of the case study vessel. This will be explained by evaluating the objectives and constraints that the ESS must satisfy in order to meet the load demand of the case study vessel. In addition to aggregated performance metrics, the dynamic behaviour of a representative storage configuration is examined to assess physical realism. Adjusted load profiles will be created to represent different weather conditions and different combinations of ship operations. This will highlight the restrictions and capabilities of the hybrid energy storage system implemented with the HTGR and diesel generators.

5.1. Base Run

To compare the possible storage system combinations to a ship without energy storage capacity a base run is done without storage systems implemented. To ensure the system does meet the load demand the Ship Energy Management but also the diesel generator logic is adjusted. The diesel generators will always be enabled to produce power next to the reactor and will follow the load profile exactly to ensure the fast peaks are also met. This configuration represents a conservative reference case in which operational reliability is prioritised over efficiency. The SEM is changed as minimally as possible, by deleting the storage options, to ensure the systems operate in the same way as with the storage available.

Operating the vessel without energy storage requires at least one diesel generator to remain online at all times to guarantee fast load-following capability. Each diesel generator is constrained by a minimum stable operating load of 1.4 MW. When the ship demand falls below this level, generator output cannot be reduced further, even though the electrical power cannot be absorbed by the ship grid.

This behaviour is illustrated in Figure 5.1, which shows the persistent power margin resulting from minimum-load constraints. Integrating the generator operation at minimum load over the mission duration yields an electrical-equivalent energy of 317.8 MWh_e, corresponding to the fuel consumed while the generator is constrained to operate at its minimum stable output. This electrical-equivalent energy is not delivered to the ship grid and does not represent physical overproduction, but rather the fuel consumption associated with enforced idle or part-load diesel operation.

The operation of the two diesel generators is shown in Figure 5.2. As a consequence of these minimum-load constraints, the cumulative diesel fuel consumption over the mission amounts to 388.7 tonnes, despite a significant fraction of the generated energy not contributing useful electrical work. This highlights the inherent inefficiency of operating diesel generators under minimum-load conditions and provides a clear motivation for introducing energy storage to absorb curtailed generation and reduce fuel consumption.

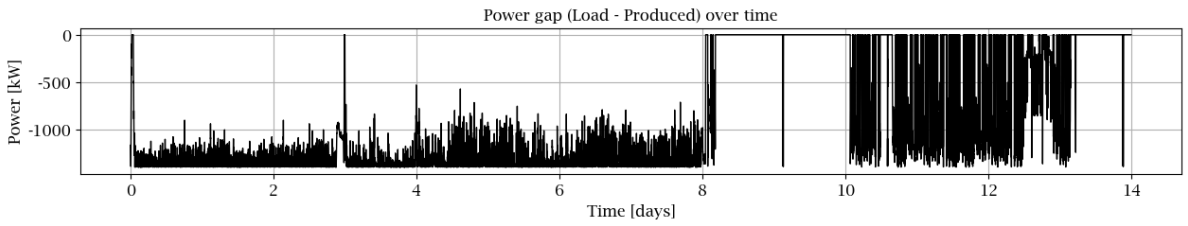

Figure 5.1: Power margin associated with minimum-load diesel generator operation during the base run.

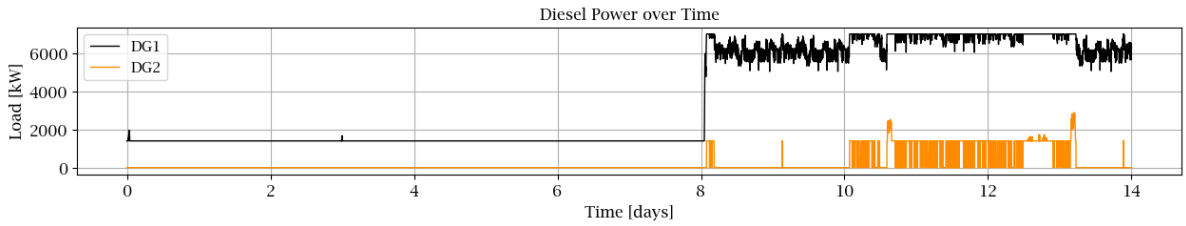

Figure 5.2: Diesel power per generator

The key results from the base run simulation can be found in Table 5.1. It should be noted that dumped energy and curtailed diesel energy originate from different mechanisms: dumped energy results from thermal-side power limitations of the reactor and power cycle, whereas the electrical-equivalent curtailed diesel energy is associated with fuel consumption enforced by minimum diesel load constraints.

Even though no storage is available in the system, the ramp rates between the reactor and the power cycle do differ. This is due to the changing efficiency in the turbine, the system power subtraction and the energy dump logic. The energy dump logic is the main cause of the higher apparent ramp rates. Because dumping is applied based on predicted power, the resulting turbine ramp rate can differ from the reactor ramp rate, although it never exceeds the imposed limit of 5% per minute.

Metric	Value	Unit
Dumped energy	17	MWh_e
Curtailed diesel generation	317.8	MWh_e
Fuel consumption	388.7	ton
Max reactor ramp up	+2.52	%/min
Max reactor ramp down	-1.03	%/min
Max power cycle ramp up	+4.22	%/min
Max power cycle ramp down	-5	%/min

Table 5.1: Key results for the base run simulation.

5.2. Storage Sizing

The main objective of this project is to ensure the reactor limitations interfere with ship operations as minimally as possible. This makes the primary criterion used to assess whether a storage combination of TES and EES is possible, the unmet power over the time of the load profile. Any unmet power during operation is considered a system failure. Next to this the total dumped power will be evaluated to see if there is not too much excess power produced, this will be compared with as well the base run as the other combination sizes of storage systems. Lastly the amount of diesel fuel used to meet the load will be evaluated next to the base run fuel usage, to see how much progress can be made by adding storage systems.

5.2.1. Performance metrics and feasibility criteria

The performance of a hybrid ESS configuration is evaluated using a set of system-level metrics that reflect both operational feasibility and overall efficiency. These metrics are chosen to align with the primary objective of this study: enabling the vessel to meet its electrical load demand while respecting the physical and operational constraints of the HTGR-based power system.

The most critical feasibility criterion is the absence of unmet load. Any storage configuration that results in non-zero unmet power at any point during the mission profile is classified as infeasible and excluded from further consideration. This criterion ensures that all retained configurations are capable of fully supporting vessel operation under the assumed conditions.

For feasible configurations, performance is further characterised using three aggregate metrics:

- **Dumped energy**, expressed in electrical equivalent energy, which quantifies the amount of excess energy that cannot be utilised or stored due to system constraints;
- **Diesel fuel consumption**, which reflects the extent to which auxiliary generation is required and serves as a proxy for emissions and operational cost;
- **Storage utilisation behaviour**, assessed indirectly through state-of-charge limits and, for selected configurations, explicitly through time-domain analysis.

Mass, volume, and cost are evaluated as secondary metrics to illustrate the physical and economic implications of different storage sizes, but are not used as optimisation objectives. Instead, they are intended to support design trade-off discussions, recognising that the relative importance of these factors is vessel-specific.

Finally, a representative time-domain analysis is used to verify that feasible storage configurations not only satisfy aggregate performance metrics, but also exhibit stable and physically realistic behaviour over the mission duration. Together, these criteria provide a consistent basis for identifying and interpreting viable hybrid ESS designs.

5.2.2. Feasible storage combinations

The combinations of system sizes that are considered and are able to meet the load profile are shown in Figure 5.3. Since the battery is installed to be the last line of defence for unmet load demand, it is not possible to have a system without it in combination with how the diesels are used when storage is included. The EES is considered within the range of 2 MWh_e to 10 MWh_e with steps of 0.5 MWh capacity and the thermal storage in the range of 0-10 MWh_{th} with the same steps.Initially, larger capacity ranges were considered, however the larger capacity options were discarded. This range of possible options is shown since it gives a few feasible options at the lowest end of both ranges (2 MWh_e/0 MWh_{th}). TES capacities are always expressed in MWh_{th}, while EES capacities are expressed in MWh_e. It should be noted that the two cannot be compared directly in terms of total deliverable energy.

In section 3.3 a storage size of 94.3 MWh_e was mentioned, however these storage capacities are lower. This large discrepancy arises because, once storage is introduced, the control system can adapt both reactor output and ESS operation to minimise load mismatches, which in turn reduces the storage capacity required from both TES and EES.

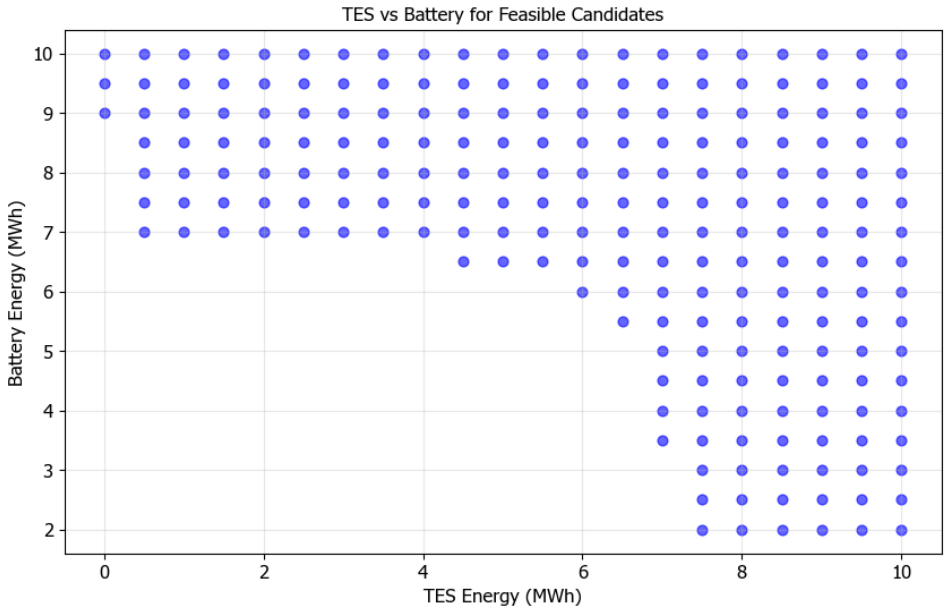

Figure 5.3: Possible combinations of storages to meet the load profile of the *Hidden Gem*.

Metric	Max value	Min value
Dumped energy [kWh]	1957	0
Fuel consumption [ton]	201.81	201.19

Table 5.2: Minimum and maximum values of fuel usage and dumped energy.

Figure 5.3 shows that the combinations of smaller storages are not able to meet the load profile. Out of the 357 tried combinations, 218 would be able to meet the load profile. To see the difference between the base run and the simulation with storages, Figure 5.4 shows the dumped energy and the total fuel consumption of the possible combinations.

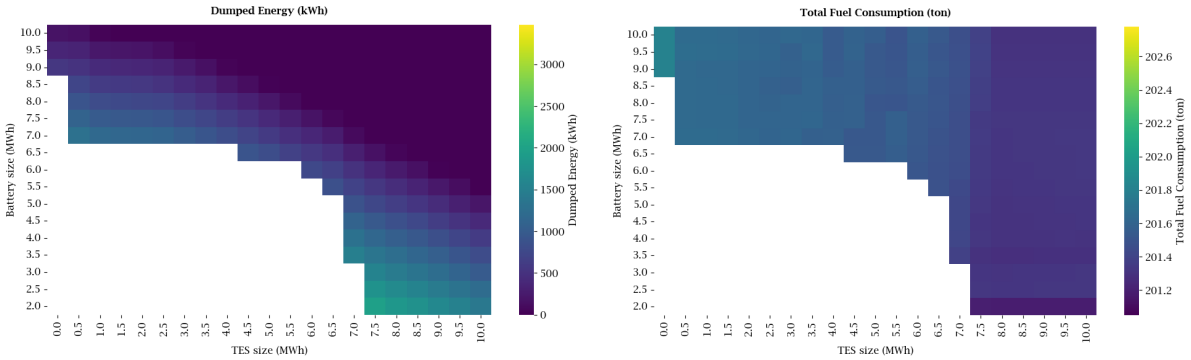

(a) Dumped energy of different storage combinations.

(b) Diesel fuel consumption of different storage combinations.

Figure 5.4: Dumped energy and diesel fuel consumption for the different storage sizing combinations covering the original load profile.

An important observation from these graphs is that the total amount of fuel used differs by less than 700 kilograms between the least and most fuel-intensive configurations. This is not even 0.5% of the total usage. The maximum dumped energy is almost 2 MWh where there are storage combinations that do not need to dump any energy.

From the possible combinations of storage systems the additions of mass and volume to the ship are important to take into account. Also the total cost of a storage system is evaluated. Which of these factors counts the heaviest is very dependant on the ship in question and there would not be one correct solution. Figure 5.5, 5.6, and 5.7 show the possible storage size combinations with their mass, volume and cost. For this calculation the numbers from Table 2.2 and 2.3 are used. From this it already becomes clear that electrical storage is more compact and lighter than TES, but comes at a higher cost.

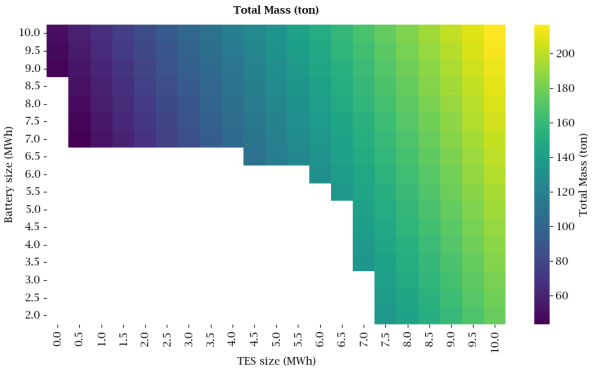

Figure 5.5: Mass for different combinations of storage system sizes.

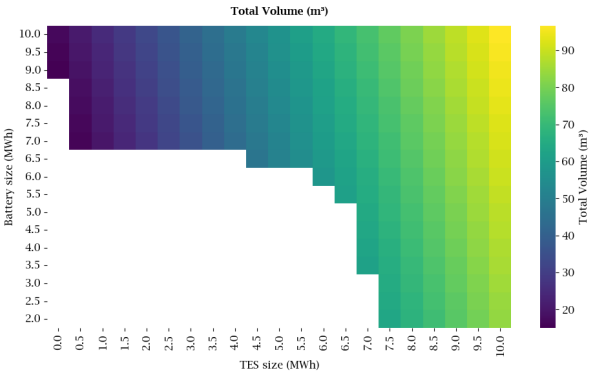

Figure 5.6: Volume for different combinations of storage system sizes.

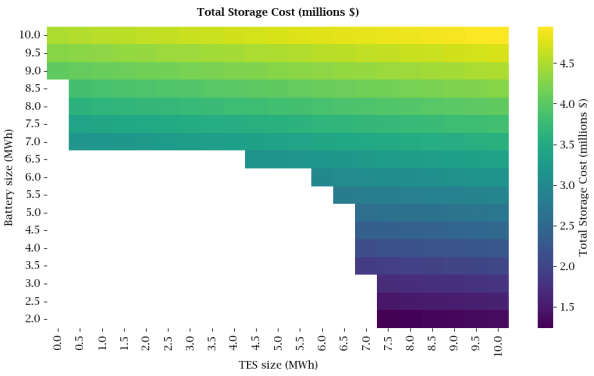

Figure 5.7: Cost for different combinations of storage system sizes.

5.2.3. Time-domain behaviour of the hybrid ESS

The sizing study presented in the previous part of the section identifies combinations of thermal and electrical energy storage that are capable of meeting the load demand without unmet power while respecting all subsystem constraints. While these aggregated performance metrics are essential for sizing, they do not directly reveal how the individual storage layers contribute during operation. In particular, differences between thermal and electrical storage are expected to manifest primarily in their temporal behaviour and frequency of activation rather than in consistently distinct power magnitudes. To assess the physical realism and stability of the control strategy, the time-domain behaviour of a representative hybrid ESS configuration is therefore examined.

A single storage configuration is selected from the feasible region identified in the previous subsec-

tion. The selected storage configuration consists of 7 MWh of thermal energy storage and 7 MWh of electrical energy storage. This configuration satisfies all operational constraints, results in negligible dumped energy, and avoids extreme values at the boundaries of the sizing space. It is thus representative of a practical hybrid ESS design rather than an optimised or limiting case. The results shown in this section correspond to the original 14-day load profile of the *Hidden Gem*.

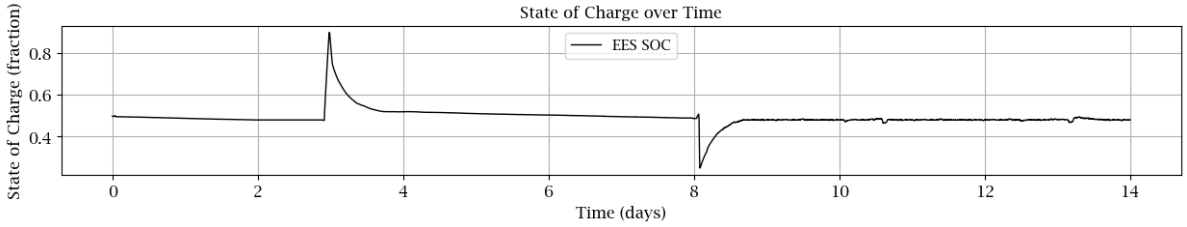

Figure 5.8: State of charge of the electrical energy storage (EES) over the 14-day mission profile for the selected hybrid ESS configuration.

Figure 5.8 shows the evolution of the electrical energy storage state of charge (SOC) over the mission. The EES exhibits frequent, short-duration charge and discharge events that coincide with fast load transients, manoeuvring actions, and residual mismatches that remain after the reactor, power cycle, TES, and diesel responses have been applied. This behaviour confirms the intended role of the battery as a fast-response buffer.

Despite the high-frequency cycling, the EES SOC remains well within its prescribed bounds throughout the mission. The SOC-centring and outer-limit control logic prevents long-term drift towards the minimum or maximum SOC limits, ensuring that sufficient headroom is preserved for both charging and discharging. This indicates that the battery is neither over-utilised nor required to deliver sustained energy, which is favourable for long-term durability.

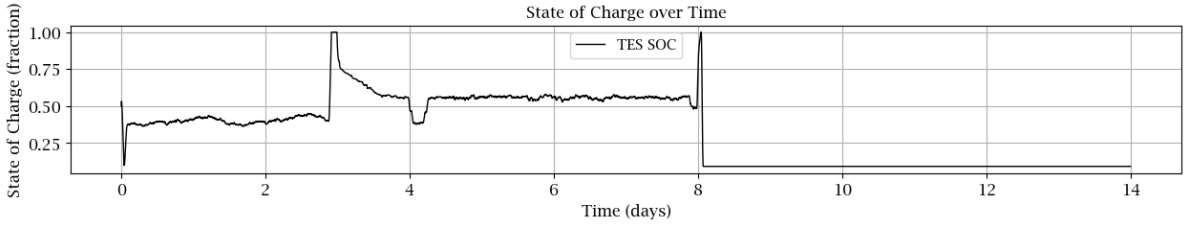

Figure 5.9: State of charge of the thermal energy storage (TES) over the 14-day mission profile for the selected hybrid ESS configuration.

Figure 5.9 presents the corresponding state of charge of the thermal energy storage. In contrast to the EES, the TES SOC evolves smoothly and on longer time scales. Charging occurs primarily during short periods of thermal surplus or limited reactor down-ramping capability, while discharging is observed during reactor ramp deficits or transient thermal shortfalls at the power-cycle inlet.

The absence of rapid oscillations and the infrequent activation of the TES demonstrate that the thermal storage is not exposed to high-frequency cycling. This behaviour is consistent with its intended function as a medium-timescale buffer that decouples reactor thermal inertia from power-cycle ramp constraints. The TES therefore contributes to reactor-friendly operation without being driven close to its inventory limits.
To relate the SOC trajectories to overall system operation, Figure 5.10 shows the ship load together with the reactor and power-cycle electrical output. The figure illustrates how the hybrid ESS enables the reactor to operate smoothly within its ramp-rate constraints while the power cycle delivers the required electrical power without violating its own ramp limitations.
Periods in which the reactor output cannot follow the load directly are compensated by coordinated TES and EES action, maintaining electrical power balance without unmet demand. This confirms that the storage systems act as effective intermediaries between the slowly responding nuclear system and the highly dynamic ship load.

Figure 5.11 and Figure 5.12 further clarify the division of roles between the two storage layers. The EES responds with sharp, high-power pulses of short duration, while the TES provides lower-frequency, event-

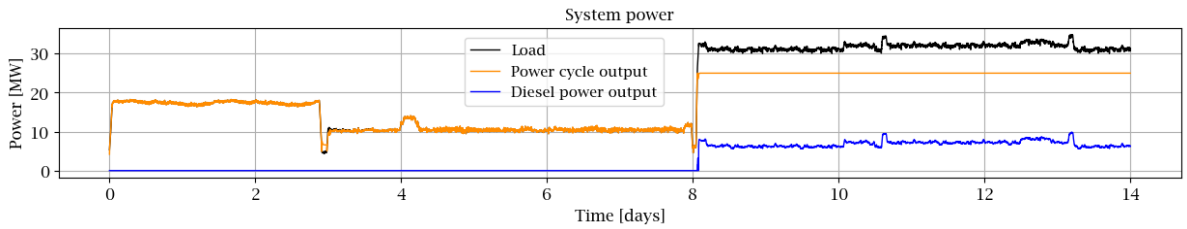

Figure 5.10: Electrical load demand, power-cycle output and diesel power output over time for the selected hybrid ESS configuration.

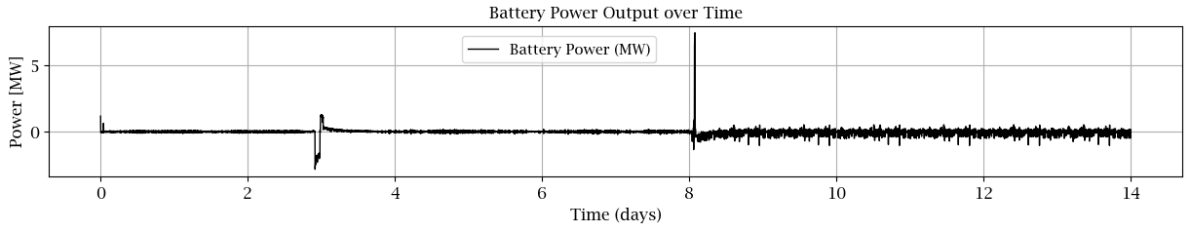

Figure 5.11: Power output of the electrical energy storage system over time for the selected hybrid ESS configuration.

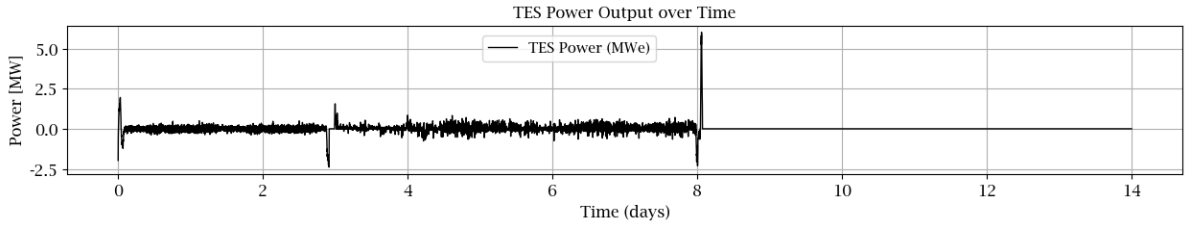

Figure 5.12: Power output of the thermal energy storage system over time for the selected hybrid ESS configuration.

driven thermal buffering during periods where reactor ramp-rate limitations become active. For extended periods of steady operation, particularly during sustained high-load phases, TES activity remains minimal as the reactor and power cycle operate close to their maximum output. In the initial phase of the mission, TES activity is more pronounced, indicating that thermal storage already absorbs a large fraction of reactor and power-cycle transients, thereby reducing the need for frequent intervention by the electrical energy storage. This separation of function aligns with the hierarchical control philosophy introduced in chapter 4.

Overall, the time-domain results demonstrate that the selected hybrid ESS configuration operates in a stable and physically consistent manner throughout all operational phases of the mission. Both storage systems remain within their allowable SOC windows, reactor and power-cycle constraints are respected, and no unmet load occurs. These results validate the control strategy and support the sizing conclusions drawn in this chapter by showing that feasible storage combinations also behave realistically in the time domain.

5.3. Adjusted Load Profiles

To simulate a heavier sea state the fluctuations of the load profile are exaggerated by a factor of five and three. Also a more favourable weather condition is looked into by adjusting the fluctuations of the load profile by a factor 0.5. These load profiles will be referred to as LPX, where X is its amplitude multiplier. Next to these adjusted amplitudes of the fluctuations a sinusoidally fluctuating load profile is created to simulate a daily fluctuating demand. These load profiles are shown in Figure 5.13. Each load profile is evaluated using the same performance metrics defined in subsection 5.2.1.

The operation of the ship has the biggest influence on its load profile. From section 3.1 it was already concluded that the mining operation demands the most from the ship's energy systems. During prolonged mining operations, the total power demand exceeds the maximum electrical output of the thermal power conversion system. As a result, both the reactor and power cycle operate continuously at full output, limiting the ability of the thermal side of the system to influence power distribution. Since building up the riser is not an operation that can realistically be shortened, the sailing period is shortened by almost 2.5 days. This time

of operation is added to the mining, giving the vessel the time to make an extra round and thus adding an extra peak where the vessel changes course. The adjusted load profile can be found in Figure 5.13e.

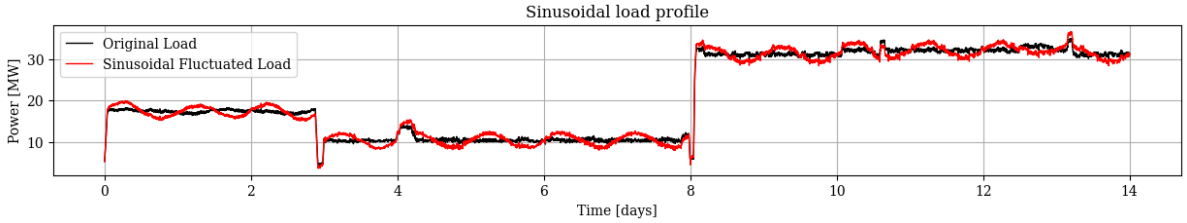

(a) Sinusoidal adjusted load profile.

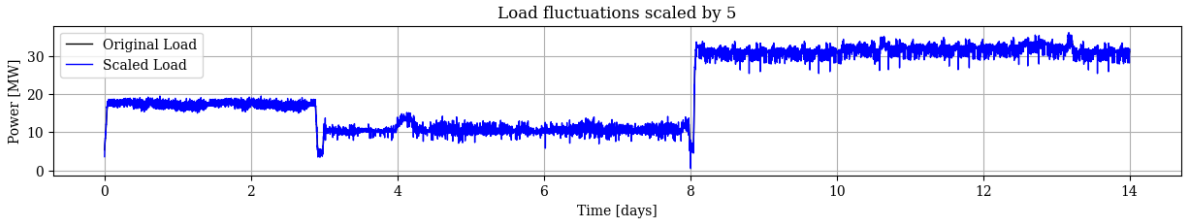

(b) Load profile with fluctuations five times bigger, later referred to as LP5.

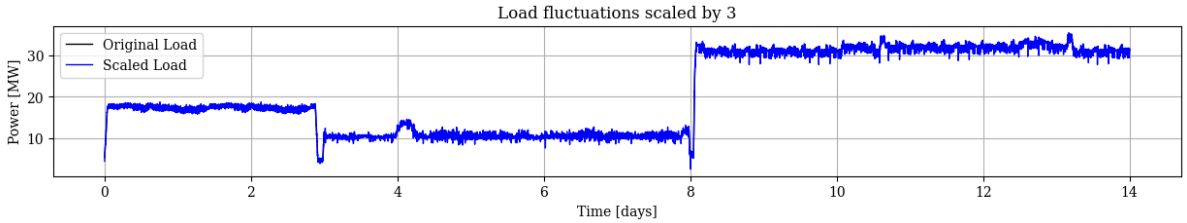

(c) Load profile with fluctuations three times bigger, later referred to as LP3.

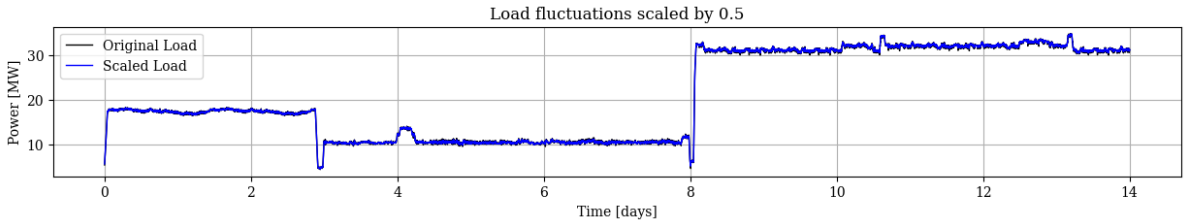

(d) Load profile with fluctuations two times smaller, later referred to as LP0.5.

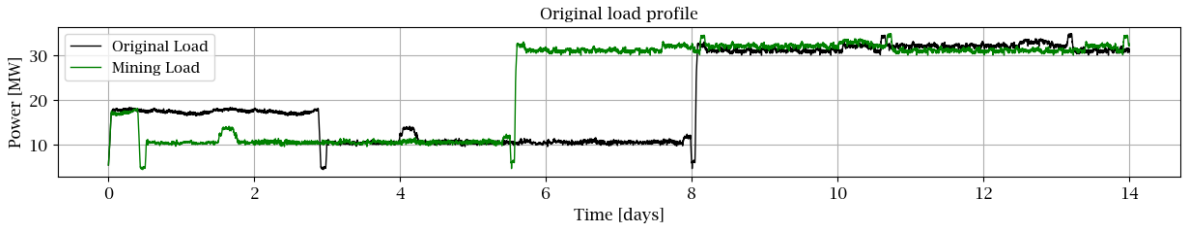

(e) Load profile with lengthened mining operation.

Figure 5.13: Overview of adjusted and original load profiles.

These adjusted load profiles will give different outcomes for the sizing of the energy storage system, section 5.2 elaborates on this process. This is due to the different characteristics of the load profile, which are summarised in Table 5.3. The same options of sizes of storage systems are tried with these new load profiles. Since the mass, volume and cost of the systems would not change with regard to the load profile, but rather with the energy storage capacity of the systems, only the dumped energy and the diesel fuel usage of the load profiles will be shown with some relevant values alongside. An important note is that the dumped energy will be expressed in its electrical equivalent to be comparable.

Table 5.3: Comparison of load profile characteristics across all load profile variants.

Metric	Original	Sinusoidal	LP5	LP3	LP0.5	Mining
Max load [MW]	34.8865	36.5285	36.1907	35.4989	34.8143	34.8865
Min load [MW]	4.3182	3.7065	0.4580	2.5074	4.4217	4.3182
Max ramp up [MW]	1.5503	1.5574	5.9397	3.5756	1.1734	1.5503
Max ramp down [MW]	-1.4968	-1.5039	-7.4338	-4.4653	-0.7547	-1.4968
Total energy [MWh]	7035.5252	7035.5252	7036.3540	7035.9396	7035.4216	7868.4231

5.3.1. Sinusoidal load profile

Applying the different sizes of storage to the sinusoidal load profile results in 178 possible storage combinations. To cover this load profile in general more electrical storage is needed, but mainly the storages need to become bigger. This is due to the higher peaks in the load profile and the slightly rougher ramp rates compared to the original load profile. The main difference is that due to the sinusoidal load the peaks stay higher for longer time, so the ESS do not have the opportunity to charge in between.

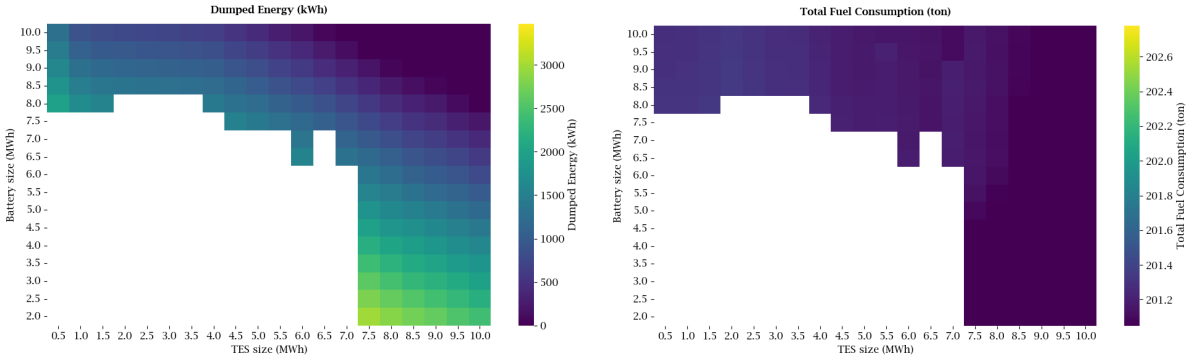

(a) Dumped energy of different storage combinations with the sinusoidal load profile.

(b) Diesel fuel consumption of different storage combinations with the sinusoidal load profile.

Figure 5.14: Dumped energy and diesel fuel consumption for the different storage sizing combinations covering the sinusoidal load profile.

The figures in Figure 5.14 show the 178 possible storage combinations alongside their dumped energy and diesel fuel usage. The maximum and minimum values of these graph are quantified in Table 5.4. The maximum dumped energy is higher than with the original load profile, which also comes from the higher peaks and the slightly higher ramp rates.

Metric	Max value	Min value
Dumped energy [kWh]	2984	0
Fuel consumption [ton]	201.35	201.01

Table 5.4: Minimum and maximum values of fuel usage and dumped energy.

5.3.2. Heavy fluctuation load profile

In the heavy fluctuated load profile the amplitude of the fluctuations is five times as high as in the original load profile to simulate heavier weather conditions. This also brings higher peaks and lower troughs with it alongside heavier ramps. This brings the total amount of possible combinations of storage sizing to 231 candidates. This is more then the sinusoidal load profile case, since with these heavy fluctuations there is also time to charge the ESS at a fast rate during operation.

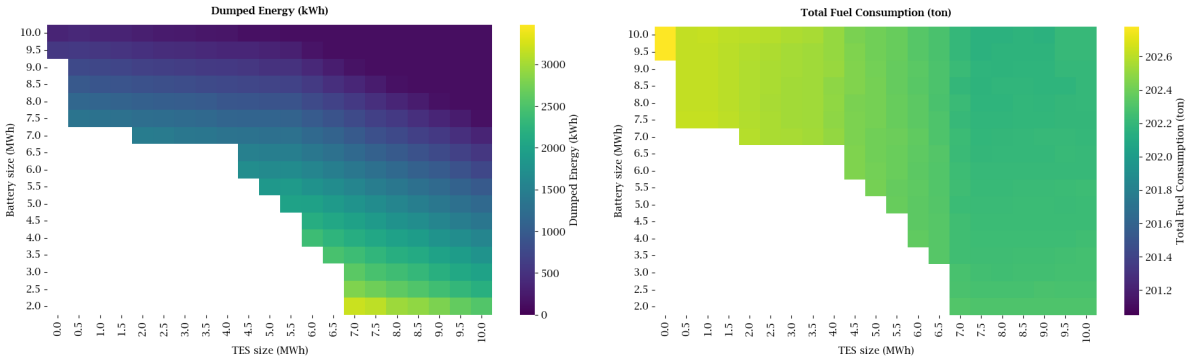

(a) Dumped energy of different storage combinations with the Heavy fluctuation load profile.

(b) Diesel fuel consumption of different storage combinations with the Heavy fluctuation load profile.

Figure 5.15: Dumped energy and diesel fuel consumption for the different storage sizing combinations covering the Heavy fluctuation load profile.

The heavier fluctuating load profile has a somewhat higher fuel consumption floating around 202.5 ton of fuel, with very low margins between the lowest and the highest as can be seen in Table 5.5. The total dumped energy is fluctuating less, however an option without any energy dumping is not possible within the range of storages evaluated.

Metric	Max value	Min value
Dumped energy [kWh]	3197	128.14
Fuel consumption [ton]	202.79	202.16

Table 5.5: Minimum and maximum values of fuel usage and dumped energy.

5.3.3. Mild fluctuation load profile

With slightly less fluctuations, amplitude times 3 instead of 5, there are 225 ESS candidates that can meet the load profile. The range of dumped energy is lower and the total fuel consumption drops as expected.

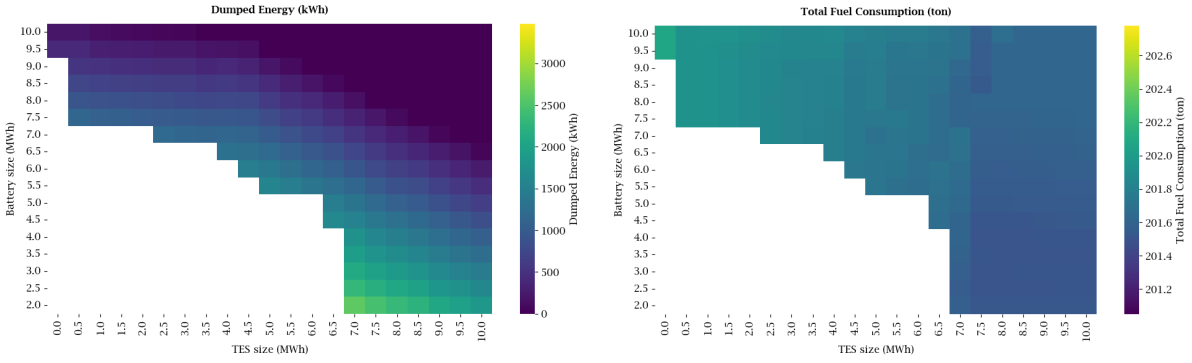

(a) Dumped energy of different storage combinations with the mild fluctuation load profile.

(b) Diesel fuel consumption of different storage combinations with the mild fluctuation load profile.

Figure 5.16: Dumped energy and diesel fuel consumption for the different storage sizing combinations covering the mild fluctuation load profile.

The total fuel usage drops more towards the original and the sinusoidal load profile and also here does not differ a lot between the storage sizing options with this load profile. The dumped energy is overall lower and with a big enough storage can reach zero dumped power.

Metric	Max value	Min value
Dumped energy [kWh]	2618	0
Fuel consumption [ton]	202.07	201.50

Table 5.6: Minimum and maximum values of fuel usage and dumped energy.

5.3.4. Less fluctuation load profile

With half the amplitude of fluctuations compared to the original load profile it is to be expected that the dumped power and fuel consumption drop and there are more possible combinations of storage systems.

However, with 221 possible storage combinations this is only just more then for the original load profile. On the edge of the possible storages a few options come forward, most likely due to slight computational differences only. This means that the fluctuations in the original load profile were already on the low side, with less fluctuation the fuel usage and dumped energy drop only slightly.

Metric	Max value	Min value
Dumped energy [kWh]	1844	0
Fuel consumption [ton]	201.46	200.90

Table 5.7: Minimum and maximum values of fuel usage and dumped energy.

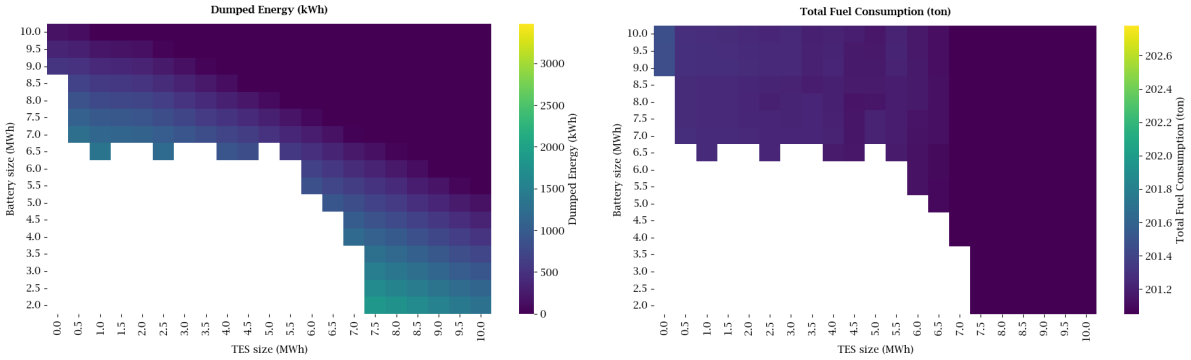

(a) Dumped energy of different storage combinations with the Less fluctuation load profile.

(b) Diesel fuel consumption of different storage combinations with the Less fluctuation load profile.

Figure 5.17: Dumped energy and diesel fuel consumption for the different storage sizing combinations covering the Less fluctuation load profile.

5.3.5. Mining load profile

Testing the load profile with a longer mining operation is not that much comparable with the other load profiles. However, as expected the fuel consumption rises. 218 ESS combination candidates are able to meet the load profile, this is due to the fact that extended mining operation, which is also the most demanding operation, is always supported by the diesel generators. This makes that the same limiting peaks of the original load profile are still in this load profile, during the switching of operations.

Metric	Max value	Min value
Dumped energy [kWh]	1750	0
Fuel consumption [ton]	280.29	279.73

Table 5.8: Minimum and maximum values of fuel usage and dumped energy.

Even though the importance of electric energy storage becomes higher intuitively, since the power cycle power output is at its maximum for a long period of time and thus the thermal storage is not useful, the use of the diesel generators makes that extra storage is not needed.

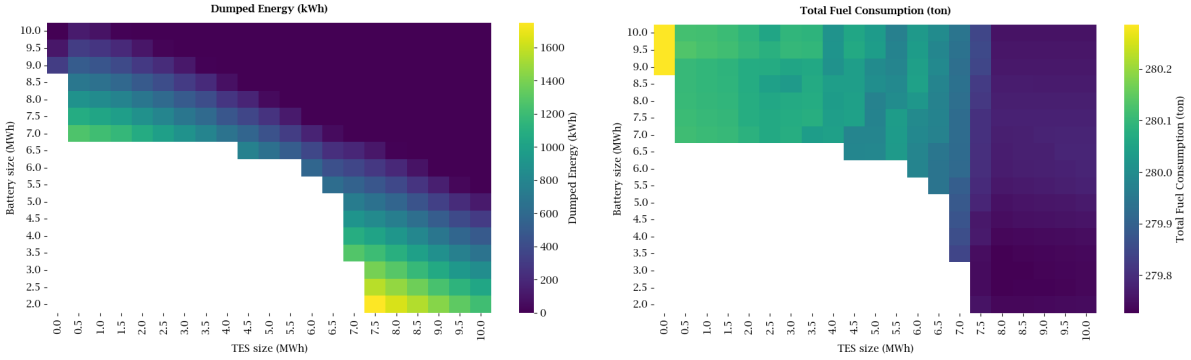

(a) Dumped energy of different storage combinations with the extra mining load profile.

(b) Diesel fuel consumption of different storage combinations with the extra mining load profile.

Figure 5.18: Dumped energy and diesel fuel consumption for the different storage sizing combinations covering the extra mining load profile.

5.4. Performance Evaluation

When comparing the simulations including storage to the base run described in section 5.1, several changes in operational behaviour become apparent. The base run reveals the limitations of operating the vessel using only the HTGR and diesel generators without any ESS: continuous diesel generator operation at the average load of 1.4 MW, sustained curtailed energy generation due to minimum diesel load, and 17 MWh of dumped energy, electrical equivalent. This configuration results in 388.7 tonnes of fuel consumption and an average electrical-equivalent power margin of nearly 1 MW associated with minimum diesel load operation due to the combined effects of reactor constraints, turbine efficiency variations, and minimum diesel load requirements.

Across all feasible storage combinations, the simulations show that no unmet load occurs. The amount of dumped energy decreases significantly: even the smallest feasible ESS sizes reduce dumping compared to the base run, and many larger combinations eliminate dumping entirely. Fuel consumption also decreases compared to the base case, with the total reduction approaching 50%. Variations between different feasible storage configurations remain small, with a spread of less than 700 kg of diesel (under 0.5%). This small spread is the result of the control framework used, in which diesel generators are disabled whenever possible in favour of reactor operation and ESS usage. Larger thermal storage capacities reduce diesel operation a little, since the diesels engage later in the operational sequence.

The simulations also demonstrate that ESS capacity moderates extreme ramp rates. Storage systems absorb fast positive and negative load changes, resulting in the possibility for smoother turbine and reactor behaviour. This limits cycling within the power conversion system and supports stable thermal-to-mechanical operation under variable conditions. Overall, relative to the base run, the storage-enabled simulations demonstrate:

- an 85–100% reduction in dumped energy across all feasible configurations for the original load profile;
- almost a 50% reduction in diesel fuel usage;
- greater operational flexibility during fast fluctuations or abrupt operational mode changes;
- elimination of electrical-equivalent power margins associated with minimum diesel load operation.

The adjusted load profiles provide additional insight into how operational conditions influence storage behaviour. While all profiles permit feasible storage combinations without unmet load, the magnitude and temporal structure of fluctuations determine which ESS sizes are viable.

Profiles with higher variability, such as LP5 and LP3, impose steeper ramp requirements and larger amplitude deviations. These profiles require larger EES capacities to handle fast changes in demand, while TES supports longer imbalances between reactor output and electrical load. LP5 provides deeper troughs enabling rapid ESS recharge, whereas the sinusoidal profile offers almost no recharge opportunity during prolonged peaks, which broadens the range of feasible ESS combinations.

The sinusoidal profile introduces prolonged periods of elevated load. Under these conditions, the limiting factor is sustained demand rather than ramp rate, and opportunities for ESS recharging are limited. Feasible combinations therefore shift towards larger overall ESS capacities, particularly for electrical storage.

The LP0.5 case, with reduced fluctuation amplitude, shows lower dumped energy and slightly reduced fuel consumption. The reactor and thermal cycle follow the load more closely, reducing the frequency of ESS intervention. The set of feasible ESS combinations remains similar to that of the original profile.

During the longer mining operation, the vessel operates at or near maximum power for extended periods. Under these conditions, the reactor and power cycle remain at full output, reducing opportunities for TES charging. Feasible combinations therefore depend mainly on EES power capacity to cover short transients and manoeuvring peaks.

The mass, volume, and cost of the ESS configurations have also been evaluated. The operational profile remains the primary factor in determining feasible sizing combinations, but physical and economic constraints may influence the final system selection. In retrofitted systems, spatial limitations are likely to restrict TES volume, whereas a new-build vessel may offer more flexibility. EES components can be distributed more easily throughout the ship, although overall cost must also be considered.

6

Discussion and Conclusion

This chapter interprets the results of the sizing study and evaluates their implications for the integration of hybrid energy storage with an HTGR-powered vessel. The discussion relates the observed behaviours to the underlying reactor physics, the operational characteristics of the storage systems, and the structure of the load profiles. Where appropriate, it also reflects on the modelling assumptions and limitations outlined in section 1.6, acknowledging that several system-level simplifications—such as lumped-parameter reactor dynamics, idealised battery behaviour, and deterministic load variations—may influence the quantitative outcomes. These limitations do not undermine the qualitative findings but should be considered when applying the insights to future, higher-fidelity design studies.

6.1. Discussion

The results indicate that integrating hybrid thermal and electrical energy storage substantially improves the operational flexibility of the *Hidden Gem* if it were to be converted to an HTGR-powered vessel. While the HTGR can sustain a stable power output, its limited ramping capability requires complementary systems to manage the rapid and variable loads typical of deep-sea mining operations. The ESS fulfils this role by supporting manoeuvrability, moderating rapid load fluctuations, and reducing dependence on continuous diesel operation.

A key outcome of the study is that the characteristics of the load profile directly influence how TES and EES must be sized. Highly fluctuating profiles, such as LP5 and LP3, generate short-duration, high-frequency variations that exceed the HTGR's permissible ramp rate. Under these conditions, the separation of function between the storage types becomes evident: the EES supports fast transients, while the TES manages medium-duration discrepancies between reactor output and demand. The deep troughs in these profiles also provide frequent opportunities for recharging, allowing a broader range of ESS combinations to remain feasible.

By contrast, the sinusoidal profile emphasises the importance of sustained energy availability. Here, the challenge is not rapid change but prolonged high-load periods during which storage cannot recharge effectively. The storage requirement shifts towards larger total energy capacity, particularly for the EES, while TES contributes less due to limited surplus thermal power.

The LP0.5 profile demonstrates that under mild variability, the reactor and thermal cycle can follow the load more effectively, reducing the role of the ESS. This suggests that for vessels with inherently stable operational patterns, storage serves primarily as a resilience measure rather than a continuously active subsystem.

The extended mining scenario introduces a distinct operating regime in which the vessel remains near maximum power for long durations. In this case, TES provides little benefit, as no surplus thermal power is available for charging. The EES therefore becomes the primary storage technology required to manage transient peaks and manoeuvres. This illustrates the dependence of storage utility on operational context rather than solely on technology characteristics.

These observations are consistent with findings in other nuclear–storage hybrid studies, where TES typically addresses slow variations and EES manages rapid transients. They highlight the need for storage sizing approaches that incorporate temporal load structure, rather than depending only on peak or average values.

Beyond operational behaviour, the system-level considerations are significant. TES must be located close to the reactor and power cycle to minimise thermal losses and transport delays, which constrains ship layout. EES placement is more flexible, enabling distributed installation throughout the vessel. Economically, EES

generally has higher energy density but also higher cost, whereas TES is more voluminous but potentially less expensive. In retrofit scenarios, spatial constraints may favour EES; new-build vessels may accommodate larger TES volumes.

In addition to these performance considerations, several practical challenges must be acknowledged. Lithium-ion batteries introduce safety risks related to thermal runaway, gas release, and fire suppression complexity, which may affect their integration in confined marine environments. Thermal storage systems, particularly molten salts, require careful management of freezing margins and insulation performance, while their mass and volume can influence ship stability and layout. Both storage types also introduce regulatory and classification implications, as they interact with the vessel's electrical and thermal safety architecture. These constraints do not diminish the value of hybrid ESS integration but highlight the need for detailed engineering and safety assessments during practical implementation.

The modelling also assumes perfect availability of the diesel generators. In practice, maritime diesel generators can experience unplanned outages, which would increase the reliance on the ESS and potentially tighten sizing requirements.

The modelling framework used in this study contains several simplifications. Lumped-parameter representations neglect spatial thermal gradients and detailed neutronic feedback; battery ageing and TES stratification dynamics are not included; and sea-state variability is represented deterministically rather than stochastically. Addressing these limitations through high-fidelity modelling, improved control strategies, and expanded techno-economic optimisation would further strengthen future analyses.

Overall, the discussion highlights that effective integration of hybrid ESS in HTGR-powered vessels requires an operationally informed design approach. The interplay between ramp rates, fluctuation duration, recharge opportunities, and spatial constraints determines the suitability of different storage configurations and should guide future design decisions.

6.2. Conclusion

This study set out to determine how a hybrid thermal and electrical energy storage system could be sized and integrated to enable an HTGR to meet the variable power demands of a deep-sea mining vessel. The findings show that a combination of TES and EES provides the operational flexibility required to compensate for the intrinsic ramp-rate limitations of the HTGR and the dynamic load characteristics of the Hidden Gem.

Integrating energy storage leads to marked performance improvements compared with a baseline configuration relying solely on the HTGR and diesel generators. All feasible storage configurations meet the full load profile without unmet demand, whilst dumped energy can be reduced by up to 100% and diesel consumption by almost 50% compared to the base run scenario. In addition, the storage systems mitigate ramp-rate mismatches, thereby reducing thermal and mechanical cycling within the power conversion chain and improving overall operational robustness.

The study also shows that the characteristics of the load profile strongly influence the appropriate balance between TES and EES capacities. Fast fluctuations require greater electrical storage capability, while TES primarily buffers medium-duration thermal imbalances. Under sustained high-load operation, TES becomes less influential, and the EES provides the main support during short transients. Conversely, milder or more stable load profiles reduce the reliance on both storage types, emphasising the need for an ESS sizing methodology that reflects the vessel's operational mission.

These findings highlight that there is no universal storage solution; instead, the optimal configuration depends on fluctuation magnitude, the duration of power peaks, recharge opportunities, and the operational regime. The work provides a structured basis for evaluating hybrid ESS integration within maritime nuclear propulsion.

The research has inherent limitations. While the hybrid ESS concept offers clear operational advantages, its practical deployment must also account for installation constraints, safety requirements, and regulatory approval processes. Lithium-ion storage requires robust fire mitigation measures; TES installations must ensure adequate freezing protection and structural integration; and both technologies demand compliance with evolving maritime nuclear safety standards. These factors will influence the final system design and should be addressed in parallel with future technical optimisation.

Even though the electrical storage would be able to handle all sorts of fluctuations, the use of thermal storage bring lower cost and easy integration and thus should be considered during the design.

Simplifications in thermal-hydraulic, neutronic, and electrochemical modelling may affect the precision of the results, and operational uncertainties such as weather-induced variability were represented determin-

istically rather than probabilistically. Future work should incorporate higher-fidelity modelling, ageing mechanisms, stochastic operational scenarios, refined control strategies, and techno-economic optimisation of storage sizing.

In conclusion, this study demonstrates that hybrid thermal and electrical storage systems enable HTGR-powered vessels to operate safely, efficiently, and flexibly under highly variable power demands. The insights gained form a strong foundation for future marine nuclear system designs and underline the potential of HTGR–ESS hybrid architectures in advancing low-emission maritime propulsion.

Answers to the Research Questions

Main Research Question:

How can a hybrid energy storage system be sized, configured, and integrated with a high-temperature gas-cooled reactor to enable safe, efficient, and economically viable operation of a nuclear-powered vessel under dynamically varying maritime load conditions?

This thesis demonstrates that a hybrid combination of thermal energy storage (TES) and electrical energy storage (EES) can effectively compensate for the intrinsic ramp-rate limitations of an HTGR, enabling it to operate safely and efficiently under the highly variable power demands of a deep-sea mining vessel. Possible sizing depends strongly on the temporal characteristics of the load profile, with TES and EES fulfilling fundamentally different but complementary roles. The hybrid ESS enables full load coverage without unmet demand, eliminates dumping for some feasible configurations, and significantly reduces diesel usage. The following sub-questions summarise the detailed findings.

1. How can a dynamic model of ship load profiles and HTGR operational constraints be developed to quantify power mismatches and inform hybrid ESS sizing requirements?

A dynamic system model was developed that couples the HTGR, intermediate molten-salt loop, power cycle, diesel generators, and storage subsystems through a unified energy-management framework. The HTGR was modelled using lumped-parameter physics, including thermal inertia, ramp-rate limits of ±5%/min, xenon-related down-ramp restrictions, and setpoint filtering via exponential moving averages to simulate realistic thermal response. Load-dependent thermodynamic efficiency and turbine ramp limits were included in the power cycle, while diesel dispatch followed a fuel-optimal strategy with headroom and dead-band logic.

Using the 14-day operational load profile of the *Hidden Gem*, the model quantified where the reactor and power cycle fall short—principally during steep transitions and during high-load mining operations. The baseline mismatch of 108.6 MWh provided the initial sizing reference for storage, while the detailed temporal mismatch profile allowed identification of whether deficits stemmed from power ramps, sustained high loads, or mode transitions. This model therefore forms the foundation for determining the minimum and feasible storage capacities.

2. Which technical and operational characteristics of hybrid ESS components are required for a feasible system design in HTGR-powered maritime applications?

The required ESS characteristics arise directly from the reactor and load behaviour. TES must be able to buffer medium-duration thermal imbalances, operate within HTGR-compatible temperature windows (290–565 °C), endure cyclic charge/discharge conditions, and respect heat-exchanger effectiveness, pinch constraints, and mass-flow limits.

The EES must have high power capability to handle fast load spikes, respond instantaneously to power imbalance, operate within specified SOC windows (10–90%), and reliably deliver or absorb power within charge–discharge limits of the battery. Together, TES and EES must maintain HTGR stability by smoothing both the thermal and electrical sides of the system, ensuring that reactor ramp rates and turbine constraints are never violated.

3. How can thermal and electrical storage subsystems be managed in a hybrid ESS while maintaining HTGR safety and operational stability?

This is achieved through the hierarchical Ship Energy Management model developed in the model. The management:

- computes a smoothed reactor setpoint using EMA filtering,

- allocates thermal surplus/deficit to TES while enforcing heat-exchanger, mass-flow, and temperature constraints,
- dispatches the EES to handle fast transients and final mismatches,
- engages the diesel plant only when HTGR+TES+EES cannot fulfil the load or the reactor reaches saturation,
- manages TES and EES SOC via centring and outer-limit control,
- ensures turbine ramp-rate compliance by adjusting TES charge/discharge requests.

This coordinated control ensures that the HTGR operates within safe thermal margins at all times and that neither storage subsystem is pushed to unsafe operating states.

4. Which sizes of hybrid ESS can balance performance, safety, and cost?

A parameter sweep over TES and EES capacities between 0–10 MWh_{th} (TES) and 2–10 MWh_e (EES) was performed to explore feasible configurations. Feasibility was defined by the absence of unmet load, acceptable SOC behaviour, and compliance with HTGR and turbine ramp constraints. Performance metrics included dumped energy, diesel consumption, and ability to manage transients.

The sweep revealed 233 feasible configurations for the original load profile. Mass–volume–cost estimates derived from literature were overlaid on the feasible region, allowing identification of trade-offs between system compactness, cost, and performance. While no single combination is universally optimal for all load profiles, the sweep-based approach provides a clear method for determining cost-effective and operationally robust ESS sizes.

5. What is the most effective configuration of different storage layers for maritime nuclear propulsion, based on load demand and operational constraints in the selected case study?

The most effective configuration is a hybrid system in which:

- **EES** provides fast-response power for short-duration spikes and manoeuvring transients,
- **TES** provides medium-duration thermal buffering to protect the HTGR from ramp-rate and thermal inertia limitations,
- **Diesel generators** serve only as a last-resort backup during extended high-load mining operations.

For the *Hidden Gem*, the results show that moderate TES capacities (3–7 MWh thermal equivalent) combined with moderate EES capacities (5–8 MWh) form a reliable operational envelope, offering zero unmet load, minimal dumping, and significant diesel reduction compared to having no storage installed without overdoing the total mass, volume and cost. Heavily fluctuating profiles require greater EES power capability, while long high-load intervals prioritise storage energy capacity in general. Extended mining phases reduce the utility of TES, shifting importance toward the EES.

Overall, the optimal configuration depends on the vessel's operational regime, but the study confirms that a balanced hybrid system—dominated by electrical storage for fast transients and supported by thermal storage for reactor-friendly load shifting—is the most effective architecture for HTGR-powered maritime propulsion.

6.3. Recommendations

Based on the modelling results, sizing study, and performance evaluation, several recommendations can be made to guide future development of hybrid HTGR–ESS propulsion systems.

Technical and Design Recommendations

Across all load profiles, the battery consistently acts as the critical final layer of power support, particularly during steep manoeuvring ramps and mining operations. Future system designs should therefore prioritise electrical storage for fast transients by ensuring sufficient EES power capability, even when TES is present, and by considering distributed battery placement to optimise integration with the ship layout.

Thermal storage should be used primarily for ramp smoothing rather than continuous power support. TES proves most effective in profiles with medium-duration fluctuations or reactor ramp-rate constraints, while during sustained high-load mining operations it contributes minimally. The TES should therefore be sized for ramp-rate moderation and reactor stability rather than long-duration energy shifting. When adjusting this, a less limited turbine would ensure the TES can support the ramping of the reactor even better. The effective output of the turbine for this study was limited at 25 MW_e with a maximum ramp rate of 5% per minute. Increasing these metrics would enable the TES to increase the ramp flexibility of the system and remain more useful at higher ship loads.

Spatial and integration constraints should be addressed early in the design process. TES requires proximity to the reactor and power cycle to avoid heat losses and excessive transport delay, whereas EES offers more flexibility. Early integration studies should evaluate ship layout, available volume, and mass distribution to avoid late-stage design conflicts. This would limit the amount of possible storage combinations and make it easier to weigh the pros and cons of a storage combination.

Future work should also advance the fidelity of subsystem models. Detailed thermo-hydraulic modelling of the molten-salt loop, battery ageing and thermal behaviour, and more realistic TES stratification should be incorporated, as these refinements will improve accuracy during transients and long-duration cycling leading to a better informed storage decision.

Operational and Methodological Recommendations

Improved control strategies with predictive or adaptive elements should be developed. The deterministic SOC control method used here performs well, but more advanced control—such as model predictive control—could optimise charge/discharge behaviour under highly variable operating conditions, especially for sinusoidal or prolonged high-load cases. This would also bring the model more towards reality, since the crew of a ship does know what operations they are going to be performing.

Analysis should be extended to probabilistic weather and operational scenarios. Load variability in this study was introduced through deterministic scaling. Incorporating stochastic sea-state effects, uncertain operational cycles, and probabilistic transient peaks would yield more robust sizing recommendations.

Techno-economic optimisation including lifecycle considerations would be an improvement. The present study evaluates mass, volume, and cost only basically by using static metrics. Future research should consider full lifecycle costs, maintenance, battery degradation, TES insulation performance, and the economic implications of port access and safety requirements.

Finally, regulatory pathways and classification requirements for HTGR–ESS integration should be investigated. Because thermal and electrical storage will form part of the vessel's auxiliary and potentially safety-critical systems, early collaboration with classification societies is essential to ensure that storage integration does not compromise nuclear safety case development, but enhances the safety and redundancy of the total system.

These recommendations highlight clear development pathways for hybrid nuclear–storage propulsion systems and strengthen the basis for future research and implementation in advanced maritime applications.

Bibliography

[1] European Maritime Safety Agency. *Potential Use of Nuclear Power for Shipping*. Tech. rep. EMSA/Nuclear-2024-4837444. Technical Report. EMSA, 2024. URL: www.emsa.europa.eu.

[2] Jin Iwatsuki et al. *Overview of high temperature gas-cooled reactor*. Jan. 2021, pp. 1–16. DOI: 10.1016/b978-0-12-821031-4.00001-4. URL: https://doi.org/10.1016/b978-0-12-821031-4.00001-4.

[3] Piyush Sabharwall, Shannon M. Bragg-Sitton, and Carl Stoots. "Challenges in the development of high temperature reactors". In: *Energy Conversion and Management* 74 (May 2013), pp. 574–581. DOI: 10.1016/j.enconman.2013.02.021. URL: https://doi.org/10.1016/j.enconman.2013.02.021.

[4] International Atomic Energy Agency. *High Temperature Gas Cooled Reactor Test Module Core Physics Benchmarks Part 2*. Tech. rep. TE-1382 Part 2. IAEA, 2007. URL: https://www-pub.iaea.org/MTCD/publications/PDF/te_1382_web/TE_1382_Part2.pdf.

[5] X-energy. *TRISO-X Pebble Fuel Qualification Methodology, Revision 2*. https://www.nrc.gov/docs/ML2124/ML21246A289.pdf. ML21246A289. U.S. Nuclear Regulatory Commission, 2021.

[6] Paolo Balestra et al. "Modular high temperature gas reactor core modeling with RELAP5-3D/PHISICS – Optimization schemes for load following". In: *Nuclear Engineering and Design* 362 (2020), p. 110526. DOI: 10.1016/j.nucengdes.2020.110526.

[7] X.-L. Yan et al. "Evaluation of high temperature gas reactor for demanding cogeneration load follow". In: *Journal of Nuclear Science and Technology* 49.1 (2012), pp. 121–132. DOI: 10.1080/18811248.2011.636564.

[8] Alexey Lokhov. *Technical and Economic Aspects of Load Following with Nuclear Power Plants*. Technical Report. Paris: Nuclear Energy Agency, Organisation for Economic Co-operation and Development (OECD/NEA), 2011. DOI: 10.1787/29e7df00-en. URL: https://www.oecd.org/en/publications/technical-and-economic-aspects-of-load-following-with-nuclear-power-plants_29e7df00-en.html.

[9] Charles Forsberg. "Separating Nuclear Reactors from the Power Block with Heat Storage to Improve Economics with Dispatchable Heat and Electricity". In: *Nuclear Technology* 208.4 (Aug. 2021), pp. 688–710. DOI: 10.1080/00295450.2021.1947121. URL: https://doi.org/10.1080/00295450.2021.1947121.

[10] U.S. Department of Energy. *Hybrid Energy Systems: Opportunities for coordinated research*. Tech. rep. DOE/GO-102021-5447. 2021. URL: https://www.nrel.gov/docs/fy21osti/77503.pdf.

[11] John Carlton, R Smart, and V Jenkins. "The nuclear propulsion of merchant ships: aspects of risk and regulation". In: (2010).

[12] Halvor Schøyen and Kenn Steger-Jensen. "Nuclear propulsion in ocean merchant shipping: The role of historical experiments to gain insight into possible future applications". In: *Journal of Cleaner Production* 169 (2017). Experimentation for climate change solutions, pp. 152–160. ISSN: 0959-6526. DOI: https://doi.org/10.1016/j.jclepro.2017.05.163. URL: https://www.sciencedirect.com/science/article/pii/S0959652617311150.

[13] Luciano Ondir Freire and Delvonei Alves De Andrade. "Historic survey on nuclear merchant ships". In: *Nuclear Engineering and Design* 293 (Aug. 2015), pp. 176–186. DOI: 10.1016/j.nucengdes.2015.07.031. URL: https://doi.org/10.1016/j.nucengdes.2015.07.031.

[14] Phan Anh Duong, JungJi Won, and Hokeun Kang. "Nuclear propulsion in cargo ship: A Pathway to the future of emission-free shipping?" In: *Han-guk marin enjinieoring hakoeji* 48.6 (Dec. 2024), pp. 392–401. DOI: 10.5916/jamet.2024.48.6.392. URL: https://doi.org/10.5916/jamet.2024.48.6.392.

[15] S.E. Hirdaris et al. "Considerations on the potential use of Nuclear Small Modular Reactor (SMR) technology for merchant marine propulsion". In: *Ocean Engineering* 79 (2014), pp. 101–130. ISSN: 0029-8018. DOI: https://doi.org/10.1016/j.oceaneng.2013.10.015. URL: https://www.sciencedirect.com/science/article/pii/S0029801813003843.

[16] Vaclav Novotny et al. *Energy storage options for future nuclear systems*. Tech. rep. Idaho National Laboratory, Apr. 2024, p. 2. URL: https://www.energy.gov/sites/default/files/2024-05/Energy%20Storage%20Options%20for%20Future%20Nuclear%20Systems_Vaclav%20Novotny.pdf.

[17] Fletcher Carlson and Jane H. Davidson. "Nuclear Power coupled with thermal Energy Storage: Impact of technical performance on economics in an exemplary electricity grid". In: *ASME Open Journal of Engineering* 1 (Jan. 2022). DOI: 10.1115/1.4053419. URL: https://doi.org/10.1115/1.4053419.

[18] Elisabetta Ferrero. *Nuclear-powered deep-sea mining vessel ; Functional integration and reliability analysis of the power generation and conversion systems*.

[19] J. Tominga. "Primary Coolant Systems". In: *Structural Alloys for Nuclear Energy Applications*. Accessed: 2025-09-12. Elsevier, 2018, p. 51. DOI: 10.1016/B978-0-08-100314-5.00003-8. URL: https://www.sciencedirect.com/science/article/pii/B9780081003145000038.

[20] Steve Thomas. "The Pebble Bed Modular Reactor: An obituary". In: *Energy Policy* 39.5 (Mar. 2011), pp. 2431–2440. DOI: 10.1016/j.enpol.2011.01.066. URL: https://doi.org/10.1016/j.enpol.2011.01.066.

[21] Rainer Moormann. "A Safety Re-Evaluation of the AVR Pebble Bed Reactor Operation and Its Consequences for Future HTR Concepts". In: *Proceedings of the Fourth International Topical Meeting on High Temperature Reactor Technology (HTR2008)*. Vol. 2. Washington, D.C., USA: American Society of Mechanical Engineers (ASME), 2008, pp. 265–274. DOI: 10.1115/HTR2008-58336. URL: https://doi.org/10.1115/HTR2008-58336.

[22] *Pebble Bed Reactor*. Mar. 2012. URL: https://catatanstudi.wordpress.com/unduhan-2/unduhan.

[23] Javier Ortensi and Abderrafi M. Ougouag. *Improved Prediction of the Temperature Feedback in TRISO-Fueled Reactors*. Technical Report INL/EXT-09-16494. Idaho Falls, Idaho: Idaho National Laboratory, Aug. 2009. URL: https://inldigitallibrary.inl.gov/sites/sti/sti/4336183.pdf.

[24] J. M. Beck and L. F. Pincock. *High Temperature Gas-Cooled Reactors: Lessons Learned Applicable to the Next Generation Nuclear Plant*. Tech. rep. INL/EXT-10-19329, Revision 1. Idaho Falls, Idaho, USA: Idaho National Laboratory, Apr. 2011. URL: https://inldigitallibrary.inl.gov/sites/sti/sti/4682662.pdf.

[25] Zuoyi Zhang et al. "The Shandong Shidao Bay 200 MWe High-Temperature Gas-Cooled Reactor Pebble-BED Module (HTR-PM) Demonstration Power Plant: an engineering and Technological innovation". In: *Engineering* 2.1 (Mar. 2016), pp. 112–118. DOI: 10.1016/j.eng.2016.01.020. URL: https://doi.org/10.1016/j.eng.2016.01.020.

[26] D. Gosset. "Absorber materials for Generation IV reactors". In: *Structural Materials for Generation IV Nuclear Reactors*. Ed. by Pascal Yvon. Woodhead Publishing / Elsevier, 2017, pp. 533–567. DOI: 10.1016/B978-0-08-100906-2.00015-X.

[27] Seddon Atkinson, Dzianis Litskevich, and Bruno Merk. "Small modular high temperature reactor optimisation part 2: Reactivity control for prismatic core high temperature small modular reactor, including fixed burnable poisons, spectrum hardening and control rods". In: *Progress in Nuclear Energy* 111 (2019), pp. 1–13. DOI: 10.1016/j.pnucene.2018.11.001.

[28] Zhibo Zhang and Jin Jiang. "On load-following operations of small modular reactors". In: *Progress in Nuclear Energy* 173 (May 2024), p. 105274. DOI: 10.1016/j.pnucene.2024.105274. URL: https://doi.org/10.1016/j.pnucene.2024.105274.

[29] Nicholas Dunkle and Ondřej Chvala. "Effect of xenon removal rate on load following in high power thermal spectrum Molten-Salt Reactors (MSRs)". In: *Nuclear Engineering and Design* 409 (2023), p. 112329. DOI: 10.1016/j.nucengdes.2023.112329.

[30] Haisheng Chen et al. "Progress in electrical energy storage system: A critical review". In: *Progress in Natural Science Materials International* 19.3 (Jan. 2009), pp. 291–312. DOI: 10.1016/j.pnsc.2008.07.014. URL: https://doi.org/10.1016/j.pnsc.2008.07.014.

[31] Richard A. Dunlap. *Supercapacitors and superconductors*. Jan. 2020, pp. 229–251. DOI: 10.1007/978-3-031-02521-1\{_}8. URL: https://doi.org/10.1007/978-3-031-02521-1_8.

[32] H Ibrahim, A Ilinca, and J Perron. "Energy storage systems—Characteristics and comparisons". In: *Renewable and Sustainable Energy Reviews* 12.5 (May 2007), pp. 1221–1250. DOI: 10.1016/j.rser.2007.01.023. URL: https://doi.org/10.1016/j.rser.2007.01.023.

[33] Ioannis Hadjipaschalis, Andreas Poullikkas, and Venizelos Efthimiou. “Overview of current and future energy storage technologies for electric power applications”. In: *Renewable and Sustainable Energy Reviews* 13.6-7 (Nov. 2008), pp. 1513–1522. DOI: 10.1016/j.rser.2008.09.028. URL: https://doi.org/10.1016/j.rser.2008.09.028.

[34] Wenxu Shang et al. “Insight into the self-discharge suppression of electrochemical capacitors: Progress and challenges”. In: *Advanced Powder Materials* 2.1 (July 2022), p. 100075. DOI: 10.1016/j.apmate.2022.100075. URL: https://doi.org/10.1016/j.apmate.2022.100075.

[35] U.S. Department of Energy. *Grid Energy Storage*. Tech. rep. Accessed: 2025-09-24. Office of Electricity Delivery and Energy Reliability, 2013. URL: https://www.energy.gov/oe/articles/grid-energy-storage-december-2013.

[36] Weijia Yuan. *Development of SMES Systems*. Jan. 2011, pp. 25–37. DOI: 10.1007/978-0-85729-742-6\{_}3. URL: https://doi.org/10.1007/978-0-85729-742-6_3.

[37] Xing Luo et al. “Overview of current development in electrical energy storage technologies and the application potential in power system operation”. In: *Applied Energy* 137 (Oct. 2014), pp. 511–536. DOI: 10.1016/j.apenergy.2014.09.081. URL: https://doi.org/10.1016/j.apenergy.2014.09.081.

[38] Peter J. Hall and Euan J. Bain. “Energy-storage technologies and electricity generation”. In: *Energy Policy* 36.12 (Oct. 2008), pp. 4352–4355. DOI: 10.1016/j.enpol.2008.09.037. URL: https://doi.org/10.1016/j.enpol.2008.09.037.

[39] Marc Beaudin et al. “Energy storage for mitigating the variability of renewable electricity sources: An updated review”. In: *Energy Sustainable Development/Energy for sustainable development* 14.4 (Nov. 2010), pp. 302–314. DOI: 10.1016/j.esd.2010.09.007. URL: https://doi.org/10.1016/j.esd.2010.09.007.

[40] Furquan Nadeem et al. “Comparative review of energy storage systems, their roles, and impacts on future power systems”. In: *IEEE Access* 7 (Dec. 2018), pp. 4555–4585. DOI: 10.1109/access.2018.2888497. URL: https://doi.org/10.1109/access.2018.2888497.

[41] S. Koohi-Fayegh and M.A. Rosen. “A review of energy storage types, applications and recent developments”. In: *Journal of Energy Storage* 27 (Nov. 2019), p. 101047. DOI: 10.1016/j.est.2019.101047. URL: https://doi.org/10.1016/j.est.2019.101047.

[42] Andrea Coraddu et al. *Energy storage on ships*. Jan. 2022, pp. 197–232. DOI: 10.1016/b978-0-12-824471-5.00012-8. URL: https://doi.org/10.1016/b978-0-12-824471-5.00012-8.

[43] Solomon Evro et al. “Navigating Battery Choices: A comparative study of Lithium iron phosphate and Nickel manganese cobalt battery technologies”. In: *Deleted Journal* (Oct. 2024), p. 100007. DOI: 10.1016/j.fub.2024.100007. URL: https://doi.org/10.1016/j.fub.2024.100007.

[44] Gebrekidan Gebresilassie Eshetu et al. “Production of high-energy Li-ion batteries comprising silicon-containing anodes and insertion-type cathodes”. In: *Nature Communications* 12.1 (Sept. 2021). DOI: 10.1038/s41467-021-25334-8. URL: https://www.nature.com/articles/s41467-021-25334-8?utm.

[45] Zhi-Wei Gao et al. “Development and Commercial Application of Lithium-Ion batteries in electric vehicles: a review”. In: *Processes* 13.3 (Mar. 2025), p. 756. DOI: 10.3390/pr13030756. URL: https://doi.org/10.3390/pr13030756.

[46] Giovanni Lucà Trombetta et al. “Lithium-Ion Batteries On Board: A review on their integration for enabling the energy transition in shipping industry”. In: *Energies* 17.5 (Feb. 2024), p. 1019. DOI: 10.3390/en17051019. URL: https://doi.org/10.3390/en17051019.

[47] Trung Nguyen and Robert F. Savinell. “Flow batteries”. In: *The Electrochemical Society Interface* 19.3 (Jan. 2010), pp. 54–56. DOI: 10.1149/2.f06103if. URL: https://doi.org/10.1149/2.f06103if.

[48] Farshad Boorboor Ajdari et al. “Silicon Solid State battery: the Solid-State compatibility, particle size, and carbon compositing for high energy density”. In: *Advanced Functional Materials* 34.30 (Apr. 2024). DOI: 10.1002/adfm.202314822. URL: https://doi.org/10.1002/adfm.202314822.

[49] Ioan Sarbu and Calin Sebarchievici. “A comprehensive review of thermal energy storage”. In: *Sustainability* 10.1 (Jan. 2018), p. 191. DOI: 10.3390/su10010191. URL: https://doi.org/10.3390/su10010191.

[50] Rami M. Saeed et al. “Mapping thermal energy storage technologies with advanced nuclear reactors”. In: *Energy Conversion and Management* 267 (June 2022), p. 115872. DOI: 10.1016/j.enconman.2022.115872. URL: https://doi.org/10.1016/j.enconman.2022.115872.

[51] G. Angelini, A. Lucchini, and G. Manzolini. “Comparison of thermocline molten salt storage performances to commercial two-tank configuration”. In: *Energy Procedia* 49 (Jan. 2014), pp. 694–704. DOI: 10.1016/j.egypro.2014.03.075. URL: https://doi.org/10.1016/j.egypro.2014.03.075.

[52] Ana Borisova and Dimityr Popov. “An option for the integration of solar photovoltaics into small nuclear power plant with thermal energy storage”. In: *Sustainable Energy Technologies and Assessments* 18 (Nov. 2016), pp. 119–126. DOI: 10.1016/j.seta.2016.10.002. URL: https://doi.org/10.1016/j.seta.2016.10.002.

[53] Konor Frick, J. Michael Doster, and Shannon Bragg-Sitton. “Design and operation of a sensible heat peaking unit for small modular reactors”. In: *Nuclear Technology* 205.3 (Aug. 2018), pp. 415–441. DOI: 10.1080/00295450.2018.1491181. URL: https://doi.org/10.1080/00295450.2018.1491181.

[54] Wolf-Dieter Steinmann and Markus Eck. “Buffer storage for direct steam generation”. In: *Solar Energy* 80.10 (July 2005), pp. 1277–1282. DOI: 10.1016/j.solener.2005.05.013. URL: https://doi.org/10.1016/j.solener.2005.05.013.

[55] Kyunghwa Kim et al. “Analysis of a Supercapacitor/Battery hybrid power system for a bulk carrier”. In: *Applied Sciences* 9.8 (Apr. 2019), p. 1547. DOI: 10.3390/app9081547. URL: https://doi.org/10.3390/app9081547.

[56] Dina A. Elalfy et al. “Comprehensive review of energy storage systems technologies, objectives, challenges, and future trends”. In: *Energy Strategy Reviews* 54 (July 2024), p. 101482. DOI: 10.1016/j.esr.2024.101482. URL: https://doi.org/10.1016/j.esr.2024.101482.

[57] BM Bhagwan. *ABS ADVISORY ON HYBRID ELECTRIC POWER SYSTEMS*. Tech. rep. 2021. URL: https://ww2.eagle.org/content/dam/eagle/advisories-and-debriefs/ABS_Hybrid_Advisory_17033.pdf.

[58] Hao Fan. *Exploring the Relationship Between Lithium-ion Battery Mass and Energy Density*. Sept. 2025. URL: https://www.large-battery.com/blog/lithium-ion-battery-weight-and-density-explained-guide.

[59] Abraham Alem Kebede et al. “A comprehensive review of stationary energy storage devices for large scale renewable energy sources grid integration”. In: *Renewable and Sustainable Energy Reviews* 159 (Feb. 2022), p. 112213. DOI: 10.1016/j.rser.2022.112213. URL: https://doi.org/10.1016/j.rser.2022.112213.

[60] Subin Antony Jose et al. “Solid-State Lithium Batteries: Advances, challenges, and future perspectives”. In: *Batteries* 11.3 (Feb. 2025), p. 90. DOI: 10.3390/batteries11030090. URL: https://doi.org/10.3390/batteries11030090.

[61] Thomas Bauer, Christian Odenthal, and Alexander Bonk. “Molten salt storage for power generation”. In: *Chemie Ingenieur Technik* 93.4 (Feb. 2021), pp. 534–546. DOI: 10.1002/cite.202000137. URL: https://doi.org/10.1002/cite.202000137.

[62] Nikolaos Stathopoulos et al. “Packed Bed Thermocline Thermal Energy Storage for Medium-Temperature Concentrating Solar Systems Numerical and Experimental study”. In: *SCIRP* (May 2023). DOI: 10.4236/jpee.2023.115001. URL: https://doi.org/10.4236/jpee.2023.115001.

[63] Abdullah Mohammed AlShahrani et al. “Study on development and testing of low-carbon Firebrick battery for reject heat storage”. In: *Case Studies in Thermal Engineering* 74 (Aug. 2025), p. 106865. DOI: 10.1016/j.csite.2025.106865. URL: https://doi.org/10.1016/j.csite.2025.106865.

[64] Vilayanur Viswanathan et al. *Energy Storage Grand Challenge Cost and Performance Assessment 2022*. Tech. rep. PNNL-33283. Pacific Northwest National Laboratory and Mustang Prairie Energy, Aug. 2022. URL: https://www.energy.gov/sites/default/files/2022-09/2022%20Grid%20Energy%20Storage%20Technology%20Cost%20and%20Performance%20Assessment.pdf.

[65] Qian. *how much does a solid state battery cost? A Deep Dive into Pricing & Future Trends*. Feb. 2025. URL: https://vibms.com/how-much-does-a-solid-state-battery-cost/#:~:text=Solid%20state%20battery%20costs%20currently,expenditures%20for%20new%20manufacturing%20lines..

[66] Terrafore Technology. *Developing Cost-Effective Thermal Energy Storage products and Technologies*. URL: https://terraforetechnologies.com/.

[67] William Driscoll. *Firebrick thermal energy storage could reach 170 GW in the U.S. by 2050*. Sept. 2024. URL: https://pv-magazine-usa.com/2024/09/19/firebrick-thermal-energy-storage-could-reach-170-gw-in-the-u-s-by-2050.

[68] University of Strathclyde. *Thermal storage results*. URL: https://www.esru.strath.ac.uk/EandE/Web_sites/15-16/Industrial_Energy_Autonomy/thermal-storage-results.html.

[69] American Bureau of Shipping. *Requirements for use of lithium-ion batteries in the marine and offshore industries*. Tech. rep. 2024. URL: https://maritimecyprus.com/wp-content/uploads/2024/04/ABS-RequirementsforUseofLithium-ionBatteries.pdf.

[70] Kunwer Sachdev. *What is Depth of Discharge (DOD) in Lithium battery*. Feb. 2025. URL: https://suvastika.com/what-is-depth-of-discharge-dod-in-lithium-battery/#:~:text=Typical%20DoD%20Range:,reduce%20their%20lifespan%20over%20time..

[71] Rami M. Saeed et al. *Use cases and model development of thermal storage coupling for advanced nuclear reactors*. Tech. rep. Idaho National Laboratory, June 2022. URL: https://inldigitallibrary.inl.gov/sites/sti/sti/Sort_61403.pdf.

[72] International Atomic Energy Agency. *Design of Auxiliary Systems and Supporting Systems for Nuclear Power Plants*. Tech. rep. SSG-62. IAEA, 2021. URL: https://www.iaea.org/publications/13523/design-of-auxiliary-systems-and-supporting-systems-for-nuclear-power-plants.

[73] International Atomic Energy Agency. *Safety Classification of Structures, Systems and Components in Nuclear Power Plants*. Tech. rep. SSG-30. IAEA, 2014. URL: https://www.iaea.org/publications/8930/safety-classification-of-structures-systems-and-components-in-nuclear-power-plants.

[74] International Atomic Energy Agency. *Design of Electrical Power Systems for Nuclear Power Plants*. Tech. rep. SSG-34. IAEA, 2016. URL: https://www.iaea.org/publications/10697/design-of-electrical-power-systems-for-nuclear-power-plants.

[75] International Atomic Energy Agency. *The Fukushima Daiichi Accident: Report by the Director General*. Tech. rep. IAEA, 2015. URL: https://www.iaea.org/publications/10962/the-fukushima-daiichi-accident.

[76] International Maritime Organization. *Code of Safety for Nuclear Merchant Ships*. Tech. rep. IMO, 1981. URL: https://wwwcdn.imo.org/localresources/en/KnowledgeCentre/IndexofIMOResolutions/AssemblyDocuments/A.491(12).pdf.

[77] Andrew Yarwood. *IMO agrees major revision of safety code for Nuclear-Powered ships*. Aug. 2025. URL: https://www.brookesbell.com/news-and-knowledge/article/imo-agrees-major-revision-of-safety-code-for-nuclear-powered-ships-159536.

[78] Safety4sea. *IMO agrees to revision of regulations for nuclear-powered ships*. Tech. rep. June 2025. URL: https://safety4sea.com/imo-agrees-to-revision-of-regulations-for-nuclear-powered-ships/.

[79] DNV. *Rules for Classification: Ships, Part 6 Chapter 2 – Additional Class Notations*. 2025. URL: https://www.dnv.com/rules-standards/.

[80] American Bureau of Shipping. *Requirements for Use of Lithium-ion Batteries and Hybrid Power Systems*. 2024. URL: https://ww2.eagle.org/en/rules-and-guides.html.

[81] Lloyd's Register. *Rules and Regulations for the Classification of Ships – Machinery and Systems*. 2025. URL: https://www.lr.org/en/rules-and-regulations/.

[82] American Bureau of Shipping. *Guidance Notes on Thermal Analysis of Vessels with Tanks for Liquefied Gas*. 2019. URL: https://ww2.eagle.org/content/dam/eagle/rules-and-guides/current/design_and_analysis/309_gn_thermalanalysisofvessels/thermal-analysis-gn-sept19.pdf.

[83] Peicheng Shi et al. "Research progress on thermal runaway warning methods and fire extinguishing technologies for Lithium-Ion batteries". In: *World Electric Vehicle Journal* 16.2 (Feb. 2025), p. 81. DOI: 10.3390/wevj16020081. URL: https://doi.org/10.3390/wevj16020081.

[84] Byoungchul Kwon, Alexandra Schraiber, and Judith A. Jeevarajan. "Evaluating Fire and Smoke Risks with Lithium-Ion Cells, Modules, and Batteries". In: *ACS Energy Letters* 9.11 (2024), pp. 5319–5328. DOI: 10.1021/acsenergylett.4c02480. URL: https://doi.org/10.1021/acsenergylett.4c02480.

[85] Nathaniel G. Sauer, Benjamin Gaudet, and Adam Barowy. "Experimental investigation of explosion hazard from lithium-ion battery thermal runaway effluent gas". In: *Fuel* 378 (Aug. 2024), p. 132818. DOI: 10.1016/j.fuel.2024.132818. URL: https://doi.org/10.1016/j.fuel.2024.132818.

[86] NFPA. *National Fire Protection Association report*. Tech. rep. Aug. 2022, pp. 1–42. URL: https://docinfofiles.nfpa.org/files/AboutTheCodes/68/68_F2022_EXL_AAA_SRReport.pdf.

[87] Yasmine Lalau et al. “Latent Thermal Energy Storage System for Heat Recovery between 120 and 150 °C: Material Stability and Corrosion”. In: *Energies* 17.4 (Feb. 2024), p. 787. DOI: 10.3390/en17040787. URL: https://doi.org/10.3390/en17040787.

[88] Luisa F. Cabeza et al. “Thermal energy storage using phase change materials in High-Temperature Industrial applications: Multi-Criteria selection of the adequate material”. In: *Materials* 17.8 (Apr. 2024), p. 1878. DOI: 10.3390/ma17081878. URL: https://doi.org/10.3390/ma17081878.

[89] Rahul Bidiyasar, Rohitash Kumar, and Narendra Jakhar. “State-of-the-art review of mitigation techniques and performance enhancement methods of phase change materials for thermal energy storage technology”. In: *Environmental Science and Pollution Research* (Mar. 2025). DOI: 10.1007/s11356-025-36189-7. URL: https://doi.org/10.1007/s11356-025-36189-7.

[90] Lorenzo Ciappi, Pouriya Niknam, and Adriano Sciacovelli. “Application of flat plate latent heat thermal energy storage for waste heat recovery and energy flexibility in maritime sector”. In: *34th International Conference on Efficiency, Cost, Optimization, Simulation and Environmental Impact of Energy Systems (ECOS 2021)* (Jan. 2023). DOI: 10.52202/069564-0211. URL: https://doi.org/10.52202/069564-0211.

[91] Keith E. Holbert. “A review of maritime nuclear reactor systems”. In: *Journal of Nuclear Engineering* 6.1 (Feb. 2025), p. 5. DOI: 10.3390/jne6010005. URL: https://doi.org/10.3390/jne6010005.

[92] Vedran Mrzljak et al. “Efficiencies and losses comparison of three steam turbines – from conventional, nuclear and marine power plant”. In: *Faculty of Engineering, University of Rijeka, Rijeka, Croatia* (2021). URL: https://stumejournals.com/journals/mtm/2021/1/10.

[93] Eleftherios Dedes et al. “Possible power train concepts for nuclear powered merchant ships”. In: June 2011. DOI: 10.13140/RG.2.1.1620.6165. URL: https://www.researchgate.net/publication/277865742_Possible_power_train_concepts_for_nuclear_powered_merchant_ships.

[94] Marcin Kolodziejski and Iwona Michalska-Pozoga. “Battery energy storage systems in ships’ Hybrid/-Electric propulsion systems”. In: *Energies* 16.3 (Jan. 2023), p. 1122. DOI: 10.3390/en16031122. URL: https://doi.org/10.3390/en16031122.

[95] Wärtsilä. “The new Shuttle Tanker”. In: (2017). URL: https://www.wartsila.com/insights/article/the-new-shuttle-tanker.

[96] Francesco Baldi et al. *A preliminary study on the application of thermal storage to merchant ships*. Tech. rep. 2015, pp. 000–000. URL: https://publications.lib.chalmers.se/records/fulltext/215155/local_215155.pdf.

[97] F. Catapano et al. “Development and experimental testing of an integrated prototype based on Stirling, ORC and a latent thermal energy storage system for waste heat recovery in naval application”. In: *Applied Energy* 311 (Feb. 2022), p. 118673. DOI: 10.1016/j.apenergy.2022.118673. URL: https://doi.org/10.1016/j.apenergy.2022.118673.

[98] Justin Coleman, Eric Dufek, and Shannon Bragg-Sitton. *An Evaluation of Energy Storage Options for Nuclear Power*. Tech. rep. INL/EXT-17-42420. Idaho National Laboratory, June 2017.

[99] International Atomic Energy Agency. *Industrial applications of nuclear energy*. International Atomic Energy Agency, 2017. URL: https://www-pub.iaea.org/MTCD/Publications/PDF/P1772_web.pdf.

[100] Muhammad Faizan et al. “Thermal energy storage integration with nuclear power: A critical review”. In: *Journal of Energy Storage* 96 (June 2024), p. 112577. DOI: 10.1016/j.est.2024.112577. URL: https://doi.org/10.1016/j.est.2024.112577.

[101] Rob Hovsapian et al. “Grid-Scale Ternary-Pumped Thermal Electricity Storage for Flexible Operation of Nuclear Power Generation under High Penetration of Renewable Energy Sources”. In: *Energies* 14.13 (June 2021), p. 3858. DOI: 10.3390/en14133858. URL: https://doi.org/10.3390/en14133858.

[102] Seunghwan Oh, Jeong Ik Lee, and KAIST Department of Nuclear & Quantum Engineering. *Performance analysis of thermal energy storage system for nuclear power plant application*. Tech. rep. Department of Nuclear & Quantum Engineering, KAIST, Oct. 2021. URL: https://www.kns.org/files/pre_paper/46/21A-293-%EC%98%A4%EC%8A%B9%ED%99%98.pdf.

[103] Santiago Andrade Aparicio and John Parsons. *Exploring a suitable business model for nuclear batteries | MIT Climate Portal*. Mar. 2023. URL: https://climate.mit.edu/posts/exploring-suitable-business-model-nuclear-batteries.

[104] World Nuclear Organisation. *Electricity and energy Storage - World Nuclear Association*. Dec. 2022. URL: https://world-nuclear.org/information-library/current-and-future-generation/electricity-and-energy-storage.

[105] Yvotte Brits et al. "A control approach investigation of the Xe-100 plant to perform load following within the operational range of 100 – 25 – 100%". In: *Nuclear Engineering and Design* 329 (Dec. 2017), pp. 12–19. DOI: 10.1016/j.nucengdes.2017.11.041. URL: https://doi.org/10.1016/j.nucengdes.2017.11.041.

[106] Zhiee Jhia Ooi et al. *Modeling of a Generic Pebble Bed High-temperature Gas-cooled Reactor (PB-HTGR) with SAM*. Tech. rep. ANL/NSE-22/59. Argonne National Laboratory, 2022.

[107] Aidan Rigby, Ben Lidley, and Daniel Mark Mikkelson. *Transient Modelling of HTGR Thermal Load Follow in Modelica*. Tech. rep. Idaho National Laboratory, June 2023. URL: http://www.inl.gov.

[108] Industrial Nitrates. *Thermo-Solar Salts - Industrial Nitrates*. June 2024. URL: https://sqmindustrialchemicals.com/thermo-solar-salts/.

[109] W. M. Kays and A. L. London. *Compact heat exchangers*. Tech. rep. Stanford University, 1984.

[110] M. Subramanian. *Heat Exchangers - Effectiveness-NTU Method*. Tech. rep. Department of Chemical Engineering SSN College of Engineering, Aug. 2019, pp. 1–33. URL: https://msubbu.in/ln/ht/HT-Lecture-19-HeatExchangers-Effectiveness.pdf.

[111] Md. Zahurul Haq. *HX: Effective NTU Method*. Tech. rep. Bangladesh University of Engineering & Technology (BUET), 2021. URL: https://zahurul.buet.ac.bd/ME307/ME307_HeatExchangerNTUmethod.pdf.

[112] Kaijun Jiang et al. "Design and dynamic simulation of flue gas-molten salt heat exchanger in flexible operation coal-fired power plant". In: *Journal of Energy Storage* 93 (June 2024), p. 112227. DOI: 10.1016/j.est.2024.112227. URL: https://doi.org/10.1016/j.est.2024.112227.

[113] Piyush Sabharwall et al. "Advanced heat exchanger development for molten salts". In: *Nuclear Engineering and Design* 280 (Oct. 2014), pp. 42–56. DOI: 10.1016/j.nucengdes.2014.09.026. URL: https://doi.org/10.1016/j.nucengdes.2014.09.026.

[114] Chunyang Zheng, Keyong Cheng, and Dongjiang Han. "High-Temperature Molten Salt Heat Exchanger Technology: Research Advances, Challenges, and Future Perspectives". In: *Energies* 18.12 (June 2025), p. 3195. DOI: 10.3390/en18123195. URL: https://doi.org/10.3390/en18123195.

[115] Sinan Karakurt and Ümit Güneş. *PERFORMANCE ANALYSIS OF a STEAM TURBINE POWER PLANT AT PART LOAD CONDITIONS*. Tech. rep. 2. Naval Architecture and Maritime Faculty, Yildiz Technical University, Mar. 2017, pp. 1121–1128.

[116] R. Chacartegui et al. *PERFORMANCE ANALYSIS OF a 565 MW STEAM POWER PLANT*. Tech. rep. Thermal Power Group (GMTS) and Escuela Técnica Superior de Ingenieros, 2011.

[117] M Petrovic et al. "Off-design flow analysis of low-pressure steam turbines". In: *Proceedings of the Institution of Mechanical Engineers, Part A: Journal of Power and Energy*. 211 (1997), pp. 215–224. DOI: 10.1243/0957650971537123.

[118] Mohammad Ali Motamed and Lars O. Nord. "Assessment of Organic Rankine Cycle Part-Load Performance as Gas Turbine Bottoming Cycle with Variable Area Nozzle Turbine Technology". In: *Energies* 14.23 (Nov. 2021), p. 7916. DOI: 10.3390/en14237916. URL: https://doi.org/10.3390/en14237916.

[119] U.S.NRC. *U.S. EPR FINAL SAFETY ANALYSIS REPORT*. Tech. rep. U.S.NRC, 2012, pp. 10.2-1-10.2–3. URL: https://www.nrc.gov/docs/ML1326/ML13261A551.html.

[120] Giovanni Barone et al. "How to achieve energy efficiency and sustainability of large ships: a new tool to optimize the operation of on-board diesel generators". In: *Energy* 282 (July 2023), p. 128288. DOI: 10.1016/j.energy.2023.128288. URL: https://doi.org/10.1016/j.energy.2023.128288.

[121] A. Caraballo et al. "Molten Salts for Sensible Thermal Energy Storage: A Review and an Energy Performance Analysis." In: *Energies* 14(4).1197 (2021). DOI: 10.3390/en14041197. URL: https://www.mdpi.com/1996-1073/14/4/1197#metrics.

[122] Cristiana Brasil Maia et al. "A comprehensive review of solar tower CSP systems using TES and molten salts". In: *International Journal of Ambient Energy* 44.1 (2023), pp. 1733–1747. DOI: 10.1080/01430750.2023.2185814. eprint: https://doi.org/10.1080/01430750.2023.2185814. URL: https://doi.org/10.1080/01430750.2023.2185814.

[123] Francesco Sciatti et al. “A comprehensive overview of lithium-ion batteries for electric vehicles: Materials, performance, safety, recycling, and emerging technologies”. In: *Journal of Energy Storage* 144 (Dec. 2025), p. 119694. DOI: 10.1016/j.est.2025.119694. URL: https://doi.org/10.1016/j.est.2025.119694.